SELECTING AND MODIFYING SMECTITES AND LAYERED DOUBLE HYDROXIDES

TO BIND FUMONISIN B$_1$, OCHRATOXIN A, ZEARALENONE, AND DEOXYNIVALENOL

A Dissertation

by

CHUN-CHUN HSU

Submitted to the Office of Graduate and Professional Studies of
Texas A&M University
in partial fulfillment of the requirements for the degree of

DOCTOR OF PHILOSOPHY

| | |
|---|---|
| Chair of Committee, | Youjun Deng |
| Committee Members, | Paul Schwab |
| | Terry Gentry |
| | Timothy Phillips |
| Head of Department, | David Baltensperger |

May 2018

Major Subject: Soil Science

ABSTRACT


Aflatoxins (AF), fumonisins (FB), ochratoxin A (OTA), deoxynivalenol (DON), and zearalenone (ZEN) are the five major groups of agriculturally important mycotoxins produced by molds *Fusarium*, *Aspergillus*, and *Penicillium*. They are naturally occurring mycotoxins and frequently found in corn, wheat, barley, oat, tree nuts, rice, peanut, sorghum, hay, fruits, and other crops. Contamination of food and feedstuff by mycotoxins is a worldwide problem and unavoidable despite significant progress in preventing the growth of the fungi, developing more resistant crops, and implementing biological control measurements. Preventing the health risks and economic losses from mycotoxin contamination are crucial issues. Using clays or similar products as binders of the mycotoxins is an attractive strategy for managing the mycotoxins. However, such a material has not been discovered for fumonisin $B_1$ ($FB_1$), OTA, DON, or ZEN. The objectives of this research were to (1) select and modify natural smectites to optimize their binding efficiency for $FB_1$, OTA, DON, and ZEN and (2) synthesize layered double hydroxides (LDHs) to bind $FB_1$.


Six smectites with different layer charged densities were chosen in this research to evaluate their adsorption capacities for OTA, DON, and ZEN. The interlayer cation in smectites was replaced with different hydration energy and valences to change the space between the hydrated cations and thus match the size of the targeted mycotoxins. The surface hydrophobicity of the smectite was increased by intercalating a cationic surfactant to enhance the adsorption capacities of ZEN and OTA which had low water solubility. The effects of the ionic form of $FB_1$ were studied on smectite and synthesized anionic adsorbent, layered double hydroxide, under various pH values.


Despite ZEN and $AFB_1$ shared high similarities in several aspects, the size-matching theory observed in $AB_1$ between adsorbed molecules and smectites was not applicable to ZEN. The determinative factor of ZEN adsorption was the hydrophobicity of the adsorbent, which can be indicated by the charge density of smectites and $Z^2/r$ value of exchange cations. Lacking highly negative

surface charge carbonyl oxygen and less planar structure of ZEN made the hydrophobic interaction between carbonyl oxygen and smectite more difficult than $AFB_1$. Water-soluble DON showed inverse responses to exchange cation and layer charge density of smectite on adsorption compared to hydrophobic ZEN. Low OTA adsorption at neutral pH of the aqueous solution was attributed to its ionic form.

$FB_1$ can be adsorbed onto interlayer of smectite at low pH and exhibited a decrease in affinity with pH increased. Estimation of chemical species of $FB_1$ at various pH can help predict the adsorption behavior of $FB_1$ based on the ionic form of FB1 and charge type of adsorbent. Although $FB_1$ existed mainly as the anionic form at pH 7, isothermal adsorption suggested adsorption of $FB_1$ was still observed.

The charge density of Mg/Al LDHs significantly affected the $FB_1$ adsorption capacity through varied the amount of adsorbing site. The $FB_1$ adsorption on Mg/Al LDHs was primarily driven by the electrostatic interactions between the anionic part of $FB_1$ and the positive charge sites on LDHs. Anion exchange of $NO_3^-$ or $CO_3^{2-}$ by $FB_1$ was the dominant adsorption mechanism. However, increase in the amount of anionic $FB_1$ by raising the solution pH did not increase the adsorption capacity as the competition between anionic $FB_1$ and $OH^-$ for adsorbing site was observed.

ACKNOWLEDGMENTS

I would like to express my most sincere and profound gratitude to my advisor, Dr. Youjun Deng, for his support, guidance, and encouragement throughout my graduate study at Texas A&M University. I am also grateful to my committee members, Dr. Paul Schwab, Dr. Terry Gentry, and Dr. Timothy Phillips, for their comments and suggestions during this research, along with Dr. Natalie Johnson for serving as a substitute for my dissertation defense and offering inspiring discussion. Dr. Paul Schwab also provided guidance and unlimited access to atomic absorption spectroscopy.

My appreciation is due to Dr. Joseph M. Awika for allowing me to use his HPLC, to Mr. Timothy Rogers for performing the elemental analysis, to Dr. Sin-Hong Lin and Dr. Lin Xu for carrying out the ion chromatography analysis.

A special thanks also goes to the following individuals in the Soil Mineralogy Group for their constant academic support and invaluable assistance during these years: Dr. Joe B. Dixon, Dr. Ana L. Barrientos Velázquez, Dr. Luke Morgan, Dr. Sabrina Alam, Bidemi Fashina, Jason Paul, Dr. Chao Hu, Dr. Fangqun Gan, Dr. Hongli Huang, and Dr. Yuan Ding. I also appreciate Sewwandi Rathnayake for her kindness and encouragement. I would like to extend my gratitude to the department faculty and staff for their assistance.

I gratefully acknowledge my friends for their friendship making my time at Texas A&M University a great experience. I would like to give special thanks to Dr. Peter Yu and his family for generous support, encouragement, and companionship.

Lastly, I am deeply indebted to my parents and my family for their emotional and financial support. I also wish to express my deep appreciation to my boyfriend, Dr. Andrew F Chen, and my dog, Poki, for their warmest comfort and support.

CONTRIBUTORS AND FUNDING SOURCES

TABLE OF CONTENTS

LIST OF FIGURES

x

LIST OF TABLES

# 1.   INTRODUCTION AND LITERATURE REVIEW

Mycotoxins are a group of secondary metabolites produced by fungal species such as *Aspergillus*, *Fusarium*, and *Penicillium*. More than 300 mycotoxins have been isolated and structurally characterized. A small number of them are carcinogenic (Cole and Cox, 1981). According to the Food and Agriculture Organization of the United Nations, twenty-five percent of the world's food crops are affected by mycotoxin-producing fungi, and nearly one billion tons of foodstuffs loss due to mycotoxin occurs every year (Mannon and Johnson, 1985; Bryden, 2007; Neme and Mohammed, 2017). Ingestion of mycotoxin-contaminated grains or their products can cause illnesses or reduced growth in animals and humans. Avoiding consumption of contaminated commodities is an effective measure to reduce exposure of mycotoxins. Yet, individuals in some developing countries or poor communities are facing the higher risk of mycotoxin exposure due to poverty and lacking alternatives.

## 1.1   Five major groups of mycotoxins and their toxicities

The five major agriculturally important mycotoxins are aflatoxins, deoxynivalenol, fumonisins, ochratoxins, and zearalenone (Table 1.1).

Aflatoxins are hepatotoxic, immunotoxic and carcinogenic. Among about 20 aflatoxin compounds, aflatoxin $B_1$ (AFB$_1$) is the most toxic and potent carcinogenic (Figure 1.1) (Sweeney and Dobson, 1998). The designated term AFB$_1$ was as due to its emitting blue fluorescence when irradiated with UV light. AFB$_1$ (molecular weight= 312.27 g/mol) has slightly solubility in water (0.03 mg/mL) and has a melting point at 268 °C. It's unstable to extreme pH (pH<3 and pH>10) and the lactone ring is susceptible to alkaline hydrolysis (IARC, 1993). The International Agency of Research on Cancer (IARC) classified AFB$_1$ as a Group 1 human carcinogen (IARC, 1993), and the primary target organ is liver. The metabolite of AFB$_1$ in liver was demonstrated to bind guanine and form

Table 1.1. Five agriculturally important mycotoxins and their main producing fungi and affected crops.

| Mycotoxin | Main producing fungi | Main affected crop |
|---|---|---|
| Aflatoxins | *Aspergillus* flavus <br> *A.* parasiticus | maize, nuts, rice, wheat |
| Fumonisins | *Fusarium* verticillioides <br> *F.* proliferatum | maize, maize products |
| Ochratoxin A | *A.* ochraceus <br> *Penicillium* verrucosum | cereal, coffee, dried vine fruit |
| Deoxynivalenol | *F.* graminearum <br> *F.* culmorum | maize, wheat |
| Zearalenone | *F.* graminearum <br> *F.* culmorum | maize, wheat |

$AFB_1$-guanine, a DNA adduct, which was contributed to liver cancer (Autrup et al., 1983; Essigmann et al., 1977).

$AFB_1$ is found in a variety of foods and feeds. The common infected food commodities are maize, sorghum, nuts, and peanut. Exposure of $AFB_1$ to animals and humans causes liver toxicity, damage, and cancer. The occurrence of $AFB_1$ is unavoidable due to drought, heat, insect, and improper storage and transportation conditions. Aflatoxins were noticed in the 1960s because an outbreak of fatal disease caused more than 100,000 turkey deaths in England (Heathcote and Hibbert, 1978). The disease was known as turkey X disease and resulted from the contamination of animal feed by fungi *Aspergillus flavus*. The pathological effects of $AFB_1$ include hepatotoxicity, hemorrhage on kidney and intestinal tract, and carcinogenesis on liver (Council for Agricultural Science and Technology (CAST), 2003). The reaction after exposure of $AFB_1$ varies with age, dose, species, and length of exposure. Individuals continuously exposed to $AFB_1$ contaminated foods may cause acute aflatoxicosis.

Deoxynivalenol (DON) (Figure 1.2) is the most common trichothecene which is produced by strains of *Fusarium* including *F. graminearum* and *F. culmorum* (Richard, 2007). DON has a
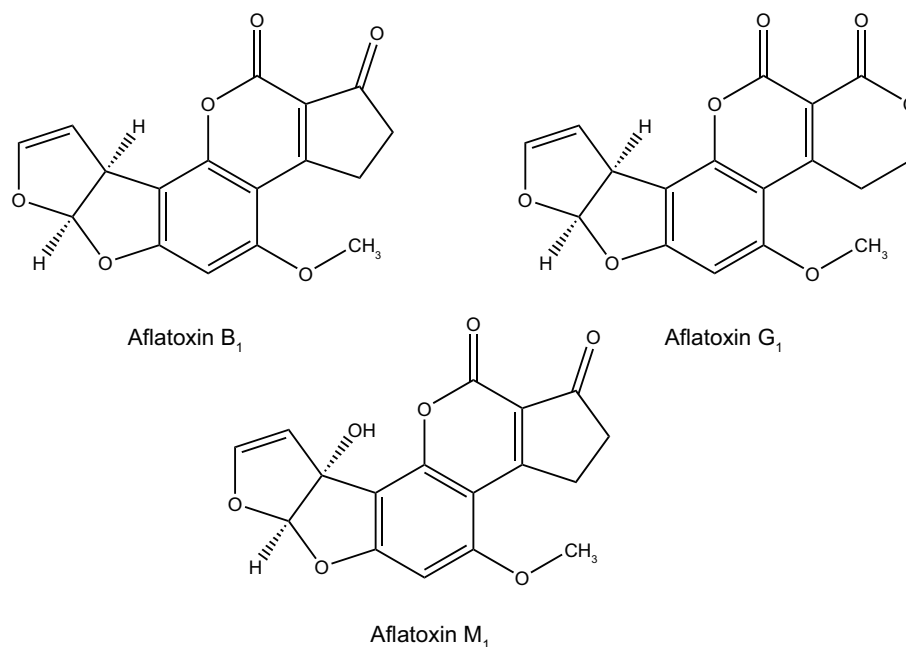
Figure 1.1. Selected structures of aflatoxins.

relatively smaller molecular weight of 296.32 g/mol. It commonly crystalizes as a white needle with a melting point of 151 °C and water solubility of 11 mg/mL (Sigma-Aldrich, 2016). It is also soluble in various organic solvents including ethanol, methanol, ethyl acetate, and chloroform (IARC, 1993). Major infected plants by DON are maize, wheat, oats, and barley. *Fusarium* can be transported by wind or animals from infected crops to healthy crops. Improper storage condition, such as high moisture, also increases the risk of occurrence of DON (Richard, 2007). DON is known as vomitoxin due to its most commonly known vomiting reaction after consumption. Some frequent acute symptoms of toxicity by consuming deoxynivalenol are vomiting, diarrhea, nausea, abdominal pain, weight loss, and severe dermatitis hemorrhage(Council for Agricultural Science and Technology (CAST), 2003; Richard, 2007; Avantaggiato et al., 2004). Ruminants appear to have a higher tolerance to DON than monogastric animals since rumen microbes can degrade DON (King et al., 1984; Razzazi-Fazeli et al., 2000).

Fumonisins are a group of *Fusarium* mycotoxins produced mainly by *Fusarium verticillioides*

3
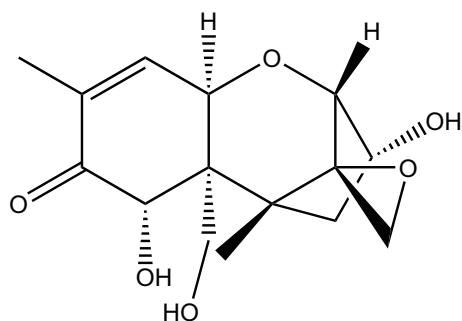
Figure 1.2. Structure of deoxynivalenol.

and *F. proliferatum* (Richard, 2007; Gelderblom et al., 1988). Fumonisins were found and isolated by Gelderblom et al. in 1988 by culturing *Fusarium moniliforme* (strain MRC 826) on corn. Nearly at the same time, Bezuidenhout et al. (1988) elucidated the structures of fumonisin $A_1$, $A_2$, $B_1$, and $B_2$ by using mass spectrometry and ^{1}H and ^{13}C NMR spectroscopy. Fumonisin $B_1$ ($FB_1$) is the most common, harmful, toxic, and thoroughly studied fumonisin among at least 28 identified different fumonisins (Figure 1.3). $FB_1$ (molecular weight= 721.84 g/mol) is a white hygroscopic powder, its solubility in water is greater than 20 mg/mL (IARC, 2002). The molecule has 10 chiral centers (Figure 1.4), providing 1,024 different stereochemical structures (Momany and Dombrink-Kurtzman, 2001; ApSimon et al., 1994). The NMR data indicates that, in aqueous solution, fumonisin $B_1$ adopts a linear configuration rather than globular one. Some reports suggested that the structure with the lowest energy is a cage-like or compact structure (Momany and Dombrink-Kurtzman, 2001). A decrease in toxicity of deamination products of $FB_1$ indicated that the amino group plays an important role in its toxicity (Lemke et al., 2001). The $FB_1$ affects several organs such as liver, kidney, brain, and lung. Its adverse effects include porcine pulmonary edema, equine leukoencephalomalacia, and hepatocarcinogenic in rats (Council for Agricultural Science and Technology (CAST), 2003; Gelderblom et al., 1988; Marasas et al., 1988; Voss et al., 2007). Several studies have shown esophageal cancer is correlated with fumonisins occurrence (Thiel et al., 1992; Yoshizawa et al., 1994; Marasas et al., 1984). Fumonisin $B_1$ is classified as a Group 2B carcinogen (possibly carcinogenic to humans) according to the International Agency for
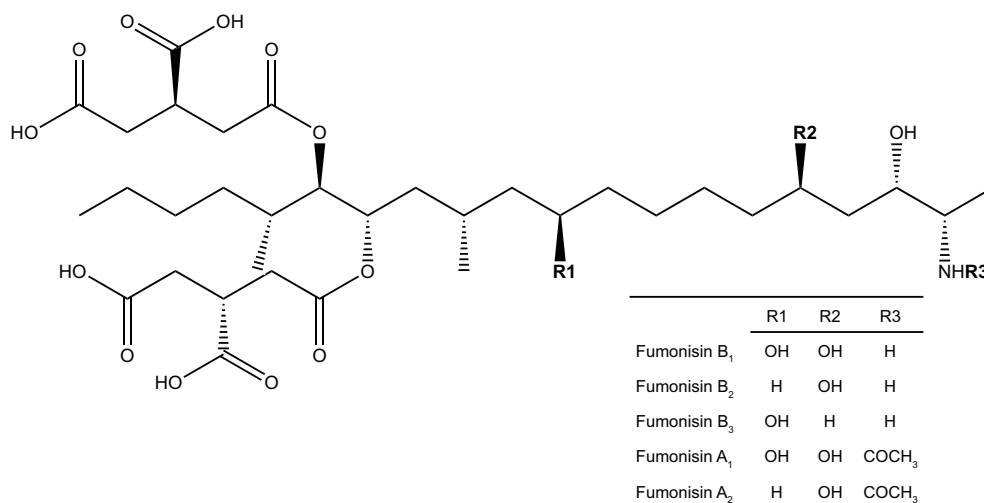
Figure 1.3. Selected structures of fumonisins.

|  | R1 | R2 | R3 |
|---|---|---|---|
| Fumonisin B₁ | OH | OH | H |
| Fumonisin B₂ | H | OH | H |
| Fumonisin B₃ | OH | H | H |
| Fumonisin A₁ | OH | OH | COCH₃ |
| Fumonisin A₂ | H | OH | COCH₃ |
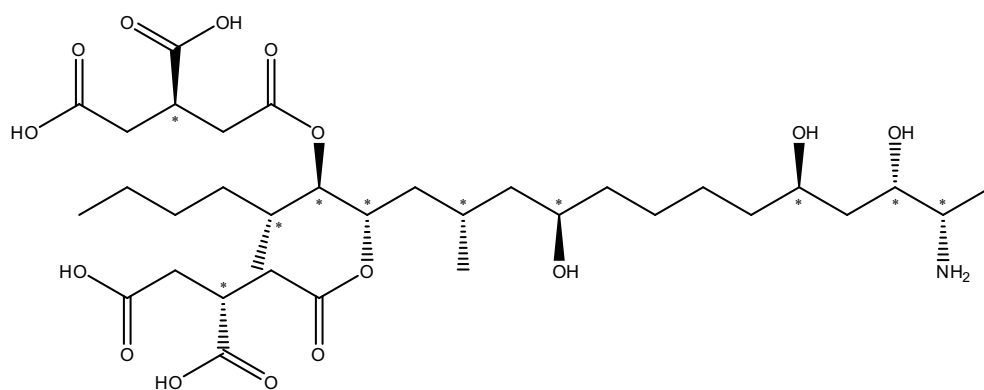


Figure 1.4. Structure of Fumonisin B$_1$ with potential stereocenters (*).

Research on Cancer (IARC) since 2003 (IARC, 1993).

Ochratoxins are produced mainly by *Aspergillus ochraceus* and *Penicillium verrucosum* and cause several significant health effects in animals. Ochratoxin A (OTA) (Figure 1.5) is the major toxin of this group and is nephrotoxic and nephrocarcinogenic. The OTA has a molecular weight of 403.82 g/mol. It is soluble in water (solubility 1 mg/mL) and moderately soluble in organic solvents when it exists as a free acid. It fluoresces intensely in acid (green fluorescence) and alkaline (blue fluores-

| | R1 | R2 |
|---|---|---|
| Ochratoxin A | H | Cl |
| Ochratoxin B | H | H |
| Ochratoxin C | C$_2$H$_5$ | Cl |
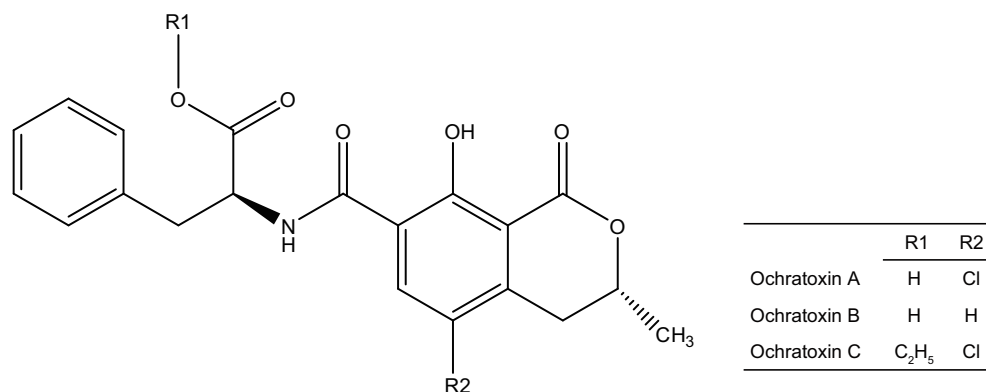
Figure 1.5. Selected structures of ochratoxins.

cence) solution when irradiated with UV light. The OTA can be partially degraded under cooking conditions and completely degraded by treating with an excess of sodium hypochlorite solution (IARC, 1993). OTA has have been found in a wide range of commodities, such as cereal grains, coffee, wine, cheese, and dried vine fruits(Clark and Snedeker, 2006; Kurtbay et al., 2008). OTA is usually produced in storage or drying process favor the growth of mold. The nephrotoxic effects of consuming OTA are a primary disease in swine. Damage of glomerulus and proximal convoluted tubule were observed in pigs (Krogh, 1977). Ochratoxin A is a kidney toxin. It can also induce liver damage in high concentration. The IARC classified OTA as a Group 2B carcinogen (possibly carcinogenic to humans) (IARC, 1993). The symptoms of ochratoxicosis include increased water intake and urination, immunosuppression, growth retardation, feed efficiency reduction, a decrease of laying and hatching rate, and birth defects (Council for Agricultural Science and Technology (CAST), 2003; Richard, 2007; Duarte et al., 2011; Xiao et al., 1996).

Zearalenone (ZEN) (Figure 1.6) is an endocrine disrupting mycotoxin produced mainly by *Fusarium graminearum* and *F. culmorum*. It may commonly co-exist with other mycotoxins produced by *Fusarium*, such as deoxynivalenol. The ZEN (molecular weight= 318.37 g/mol) is poorly water soluble (0.02 mg/mL) at 25°C, heat stable up to 120°C, and hydrolysis stable in neutral or acid buffer solutions (IARC, 1993). Most often zearalenone is found in maize, wheat, barley,
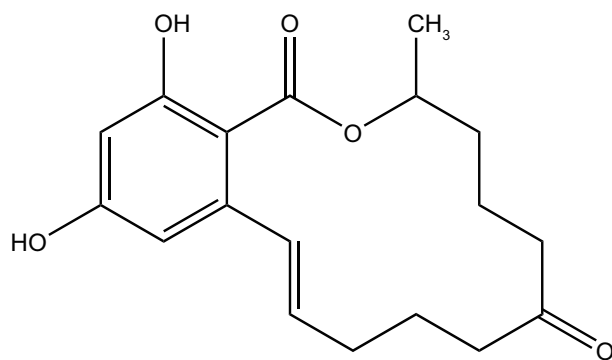
Figure 1.6. Structures of zearalenone.

and sorghum (Kuiper-Goodman et al., 1987). This phenolic resorcylic acid lactone with potent estrogen can cause estrogenic syndrome and precocious development in various animals, particularly young pigs. Precocious pubertal changes induced by zearalenone have also been observed in children (Council for Agricultural Science and Technology (CAST), 2003; Massart et al., 2008; Massart and Saggese, 2010). Swine are the most significantly affected animals and more sensitive to ZEN than poultry, cattle, and other animals. Reproductive effects on swine are one of the major negative effects of ZEN. The lactones on ZEN is chemically similar to 17β-estradiol, a hormone produced in the ovary. This similar structure results in its competition with 17β-estradiol to bind to estrogen receptors. Estrogen receptors binding by ZEN can disrupt hormonal control and cause strong estrogenic effects. Effects of ingestion ZEN by sows include premature puberty, increased number of stillbirths, and ovarian cysts (Council for Agricultural Science and Technology (CAST), 2003; Richard, 2007; Hussein and Brasel, 2001).

## 1.2    Decontamination and detoxification of mycotoxins

The strategies to avoid mycotoxicosis can be divided into pre- and post- harvest measures and into physical, chemical, and biological methods. Preventing the growth of the fungi, developing more resistant crops, and implementing biocontrol technologies are pre-harvest strategies aim to reduce mycotoxin- producing fungi proliferation during cultivation. After harvest, crops can be contam-

inated by mycotoxins as a result of improper handling and processing (grinding and mixing) and environmental factors (temperature, humidity, and mechanical damage). Due to various biological and abiotic stresses, such as drought, heat, insects, humidity stresses, and improper storage condition, the occurrence of the mycotoxins appeared to be unavoidable. As the last defending mechanism in preventing the adverse effects of the mycotoxin to humans and animals, decontamination and detoxification for mycotoxin through either adsorption or degradation contaminated crops become more critical.

Decontamination by biological methods include fermentation procedures with microorganism have been proposed but have not yet been used in practice on a large scale (Huwig et al., 2001). Various physical methods for the decontamination of *Fusarium* mycotoxin-contaminated grain commodities have been investigated, including density segregation of maize and wheat, food processing practices such as cleaning, milling and baking (Sydenham et al., 1994). Physical removal is a common preliminary decontamination procedure. Removing fine particulate material from corn can reduce $FB_1$ contamination. Due to the thermostability of $FB_1$, heat treatments and drying process did not reduce the $FB_1$ concentration. The ammonia treatment at atmospheric pressure is also ineffective for $FB_1$ detoxification (Galvano et al., 1997). Chemically, some mycotoxins can be destroyed with calcium hydroxide monoethylamine or ozone (Huwig et al., 2001). Studies also suggest that calcium hydroxide is highly effective in removing $FB_1$ (Huwig et al., 2001; Galvano et al., 1997; Sydenham et al., 1995). Galvano *et al.* showed that activate carbon exhibited a high in vitro affinity for $FB_1$ and adsorption abilities (Galvano et al., 1997).

## 1.3  Common measures for mycotoxin decontamination/detoxification

### 1.3.1  Pre-harvest

In most cases, crops can be infected and contaminated by fungi before and after harvest under condition favored the fungi to thrive and produce mycotoxins. However, some mycotoxin-produced

fungi, such as *Fusaria* species, infect the crops in the field and produce mycotoxins mostly during cultivation. Thus pre-harvest practices are more important as a preventive strategy to mitigate the growth of mycotoxin-produced fungi. With proper cultivation practices, the occurrence of mycotoxin and the potential health risk and economic losses can be controlled.

Abiotic stresses involving drought, heat, and damage of the crop lead susceptible crops to be infected by *Aspergillus* (Hill et al., 1983). For example, a drought stress in the last 4 to 6 weeks prior to harvest of groundnut leads to an increase of soil temperature and a decrease of kernel moisture which accelerates aflatoxin production. Sufficient irrigation can effectively reduce aflatoxin formation at the pre-harvest stage (Keenan and Savage, 1994). To reduce the risk of mold contamination, removal of fungal infected agricultural waste from previous crop residues is an effective and straightforward measure. The Codex Alimentarius Commission (Codex) (2003) suggested a good crop rotation practice of avoiding planting crops susceptible to certain fungi species in two consecutive years. For example, potato, clover and alfalfa, and other vegetables which are not targeted host of *Fusarium* species are suggested crops in rotation.

Appropriate use of fungicides, pesticides, and insecticides could minimize or prevent fungal or insect infection and subsequently mycotoxin contamination. The application of fungicides, cyproconazole, prochloraz, tebuconazole, and azoxystrobin, significantly reduce the *Fusarium* head blight and DON content in wheat (Haidukowski et al., 2005). However, an increase of mycotoxin contamination level was observed in other fungicide application studies: a mixture of tebuconazole and triadimenol, fungicide Matador, reduced *Fusarium* head blight but a 16-fold increase of nivalenol (NIV) was observed in harvest grain (Gareis and Ceynowa, 1994). Thus, use of fungicides and pesticides became undesirable due to economic, environmental, and food safety concerns.

Various strategies have been proposed through biocontrol, such as breeding mycotoxin resistant crops and developing bio-competitive agents. Inheritance of resistance in crosses by incorporated

mycotoxin resistant inbreds into the breeding program has been developed. The results also indicated breeding for resistance to *Aspergillus* ear rot and aflatoxin formation is effective (Walker and White, 2001; Hamblin and White, 2000; Campbell and White, 1995). Another strategy to limit mycotoxin contamination of crops is the use of atoxigenic fungi, which are non-mycotoxin producing strains. The atoxigenic fungi can compete for limited resources and reduce or impede development of mycotoxin-producing strains (Bhatnagar et al., 2004; Cleveland et al., 2003; Dorner et al., 1999; Bhatnagar et al., 1993). Inoculating of atoxigenic *Aspergillus flavus* and *Aspergillus parasiticus* into soil significantly reduced (up to 99.9%) aflatoxin contamination (Dorner et al., 1998). A commercial biocontrol agent, Afla-Guard, was developed by the Agricultural Research Service of United States Department of Agriculture (USDA ARS) to control aflatoxin formation in corn and peanuts.

### 1.3.2  Post-harvest

After harvest, crops infected with mycotoxin-producing fungi in field can be further contaminated with mycotoxins under poor storage condition. Some simple and traditional practices such as sorting, cleaning, and milling can effectively reduce mycotoxin level in the final products. Contaminated grain can be sorted in the first processing stage of post-harvest according to their appearance, color, or gravity (Tibola et al., 2016; Afolabi et al., 2006). Lovett et al. (1975) reported an over 93% reduction of total patulin concentration by trimming of the rotten tissue from apple in a laboratory study. The DON concentration in flour can also be reduced by 80% by cleaning raw wheat grain with industrial millers and 40% by traditional grain millstone, respectively (Lesnik et al., 2008). These studies demonstrated the possibility of significant removal of mycotoxins by sorting, cleaning, or trimming before the further process was feasible.

Biological and abiotic degradation of mycotoxins is a strategy that has shown the ability to ameliorate their toxicity. Several studies have shown that the structural rings of OTA and ZEN can be cleaved by microorganisms such as fungi and yeast (Schatzmayr et al., 2006; Vekiru et al., 2010;

Schatzmayr et al., 2003). Degradation of aflatoxin $B_1$ by bacteria, *Rhodococcus erythropolis* and *Mycobacterium fluoranthenivorans*, was observed through a cascade of enzyme reactions over time (Shih and Marth, 1975; Hormisch et al., 2004). Chemical deactivation is another method used to decontaminated mycotoxins. A traditional food preparation process, nixtamalization, originated from Mexico allows mycotoxin contaminated maize or other grains immersed and cooked in an alkaline solution of limewater. These processes have been proven to dramatically reduce fumonisins and aflatoxins concentration (Torres et al., 2001; Humpf and Voss, 2004; de la Campa et al., 2004).

Irradiation is one technology used to eliminate or reduce the number of molds and their spores in harvested crops and control the occurrence of mycotoxins. Numerous reports evaluated the effects of gamma-irradiation on microbial flora and the amount of produced mycotoxin (Afifi et al., 2003; Rustom, 1997; Calado et al., 2014). An irradiation dose of 6 kGy on chilies successfully reduced fungal load by 5 orders of magnitude (Iqbal et al., 2013). Another chemical method oxidation uses oxidizing agents such as $H_2O_2$, $O_3$, or bleach (sodium hypochlorite) to destroy mycotoxins. McKenzie et al. (1997, 1998) showed $AFB_1$ and $AFG_1$ in aqueous solution were rapidly degraded with 2% weight $O_3$ treatment in 5 min. Their study demonstrated the reduced toxicity to young turkey poults when the contaminated corn was treated with $O_3$.

## 1.4 Successes of bentonite clays in reducing bioavailability in animal feeding trials and human clinical trials

### 1.4.1 Successful trials of using bentonite as aflatoxin binders

Deliberate consumption of clay, as known as geophagy, is a practice of ancient medicine used all around the world for centuries to heal ailments such as diarrhea, skin wound, and supplying mineral nutrients (Ferrell Jr., 2008; Abrahams, 2012; Ghadiri et al., 2015). Incorporation of clay minerals into feed and food to decrease absorption, bioavailability, and carcinogenicity of aflatoxin is an effective and low-cost measure. Silicate products are one of the most widely studied mycotoxin

adsorbents. Natural aluminosilicates-rich materials such as bentonite clays and zeolites are the most widely studied mycotoxin adsorption agents. Zeolites have the three-dimensional framework structure containing channels that provide vacant spaces and exhibit as molecular sieves allowing various cation, molecules, and water to move in and out (Dixon et al., 2002). Zeolites showed high affinity for $AFB_1$ in the bovine ruminal fluid, removed approximately 92% of added $AFB_1$ (Spotti et al., 2005). Clinoptilolite, a natural zeolite, is capable of reducing the deleterious effects of aflatoxins (Parlat et al., 1999).

Bentonite clays are used in animal feed primarily as an anticaking agent with a maximum 2 % (wt) dose limit. A commercial bentonite branded as Novasil (NS) clay was used as an additive in animal feeds and was capable of binding aflatoxins. Several clay additives as mycotoxin binders were evaluated *in vivo* and *in vitro*, and NS was the best aflatoxin adsorbent (up to 0.4 mol $AFB_1$/kg) among the tested 13 additives (Marroquín-Cardona et al., 2009). Consuming NS clays up to 3.0 g/day in two weeks was confirmed to be safe through a clinical trial (Wang et al., 2005). Further human clinical trial indicated that NS clay reduced $AFB_1$-albumin adduct in blood and $AFM_1$ in urine (Wang et al., 2008).

One early study reported up to 100 % $AFB_1$ adsorption by adding 2 % (w/v) bentonite into a 50 mL pH 6.5 buffer solution containing 400 μg $AFB_1$ (Masimango et al., 1978). Based on this result, many bentonites have been evaluated as binders to detoxify or reduce the bioavailability of mycotoxins. Swine fed with different amounts of bentonites in the diet containing 800 ppb of $AFB_1$ showed improvements in average daily gain, average daily feed intake, and clinical chemistry indicator (Lindemann et al., 1993).

The aflatoxin adsorption efficiency and selectivity by smectite, the major mineral in bentonite clays, are mainly determined by the environment of the adsorption domains in the interlayer (Barrientos-Velazquez et al., 2016; Deng et al., 2010, 2012). Deng et al. (2012) elucidated the

12

relationship between adsorbed aflatoxin $B_1$ and their adsorption sites on smectite and the adsorption mechanism. They proposed a size matching hypothesis which describes the smectite's adsorption capacity and selectivity for aflatoxin $B_1$ can be enhanced by matching the adsorption domain size and polarity to those of an aflatoxin $B_1$ molecule. The non-polar domains in smectite interlayer were the places can be occupied by adsorbed aflatoxin $B_1$. The polar domains in the interlayer were occupied by the exchange cations. Consequently, smectites with divalent cations saturated interlayer could induce higher affinity and higher adsorption capacity for aflatoxin $B_1$ as they yield greater non-polar domains than monovalent cations. Barrientos-Velázquez et al. (2016) investigated the effects of the layer charge origin, octahedral cation composition, and layer charge density on smectite's selectivity and adsorption capacity for aflatoxin $B_1$. They found that the non-polar adsorption sites are decreased when charge density is increased, which cause the reduction of $AFB_1$ adsorption by the smectites. They also demonstrated that $AFB_1$ adsorption capacity on high charge density smectites can be improved after reducing the charge density of smctites through the Hofmann-Klemen effect. The Hofmann-Klemen effect was proposed in 1950 by Hofmann and Klemen, who advocated the migration of interlayer $Li^+$ into vacant octahedral sites until the octahedral charge was balanced (Hofmann and Klemen, 1950).

### 1.4.2   Studies of using clay or similar materials as binders for other mycotoxins

When montmorillonite was added in a concentration of 0.5 % (w/w) to rat diets containing 5 mg DON per kg bodyweight, the cytotoxicity and genotoxicity were reduced (Abdel-Wahhab et al., 2015). Bentonite can adsorb 0.03 µg/kg OTA from red wine, 2.37 µg/kg from white wine, and 19.4 µg/kg from synthetic OTA solution (Var et al., 2008; Kurtbay et al., 2008). However, Bhatti et al. (2016) failed to show alleviation of deleterious effects of OTA (1mg/kg in feed) in broiler chicks by incorporating bentonite at 3.7, 7.5, and 15 g/kg levels. A similar negative result was reported in a pig feeding test with maize infected by *F. graminearum* naturally (Williams et al., 1994). In this study, bentonite with a ratio of 20 or 50 g bentonite per kg of maize was added in pig feeds contaminated with ZEN (3 mg/kg) and nivalenol (NIV) (11.5 mg/kg). Bentonite was

ineffective in overcoming either the oestrogenic or depressed performance effects induced by the two mycotoxins. The concentration of mycotoxins was extremely high in this study and bentonite might still be effective at lower mycotoxin concentration.

## 1.5   Objective of study

Both laboratorial adsorption of aflatoxin and animal and human trials with clays have suggested that smectite can be used to detoxify aflatoxin. The overall objective of this study is to test if natural or modified clay minerals or similar materials can be used to detoxify the other four groups of mycotoxins.

# 2.  SELECTING AND MODIFYING SMECTITES TO BIND OCHRATOXIN A, ZEARALENONE, AND DEOXYNIVALENOL

## 2.1  Introduction

Aflatoxins (AF), fumonisins, ochratoxin A (OTA), deoxynivalenol (DON), and zearalenone (ZEN) are the five major groups of agriculturally important mycotoxins (Table 2.1). These mycotoxins are produced by fungal species *Fusarium*, *Aspergillus*, and *Penicillium*(Sweeney and Dobson, 1998). More than 300 mycotoxins have been isolated and structurally characterized. Scientific attention is mainly focused on those most common, harmful, and carcinogenic ones. The contamination of food and feedstuff by mycotoxins is a worldwide problem for corn, wheat, barley, oat, tree nuts, rice, peanut, sorghum, hay, fruits, and other crops. Crops can be infected by multiple mycotoxins because fungi are usually able to produce several mycotoxins and various fungal species can infect a crop (Atalla et al., 2003). The Food and Agriculture Organization (FAO) of the United Nations estimates that 25% of the world's food crops are affected by mycotoxin-producing fungi and that nearly one billion tons of foodstuffs are lost due to mycotoxins every year.

ZEN and $AFB_1$ molecules have similarities in many aspects: they have similar molecular weights and low water solubilities; they have only C, O, H in their structures, have two carbonyl groups, and aromatic rings (Table 2.1). They may share similar requirements for their adsorbents. The carbonyl groups in $AFB_1$ play an important role in the interaction between smectite and $AFB_1$. Under the dry condition, adsorbed $AFB_1$ and smectite interacted by ion-dipole interaction and coordination between the exchangeable cations and carbonyl groups in the interlayer. Under the humid condition, water molecules are involved and the H-bonding between the hydration shell of exchangeable cations and carbonyl groups was the dominant bonding force (Deng et al., 2010).

The critical mineralogical factors in controlling ZEN adsorption are unclear. Based on the re-

ported high adsorption capacity of many smectites for aflatoxins, and the similarity in molecular weight, functional groups, and polarity between ZEN and AFs, it is possible that they may share similar requirements on their adsorbing materials. Thus, the objectives of this study are 1) to seek clay minerals to detoxify/decontaminate ZEN, DON, and OTA and 2) to deduce the determining chemical and mineralogical factors in controlling the adsorption of the mycotoxins. These four mycotoxins have very different structures, polarities, and solubilities. The specific aims of the study are: 1) to examine the effects of charge density and types of the interlayer cation of smectite on the adsorption, 2) to examine if the mycotoxins can go into the interlayer of smectite, and 3) to reveal the bonding mechanism between ZEN and smectite.

## 2.2 Materials and methods

The goal of detoxifying mycotoxins through the use of clays was pursued by modifying natural smectite to change the size and polarity of the adsorbing domains on smectites and reveal the controlling chemical and mineralogical mycotoxin adsorption factors of smectites.
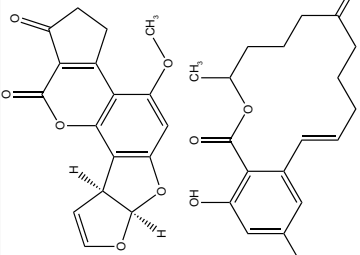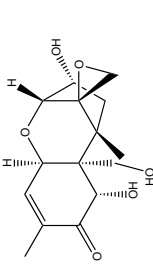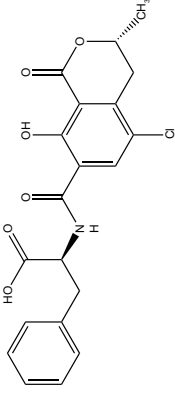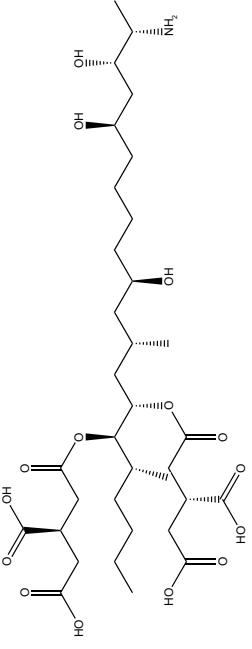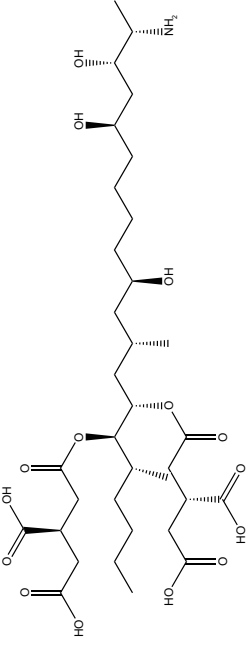
### 2.2.1 Preparation of smectites with different charge densities

#### 2.2.1.1 Size fractionation

Six smectites 1MS, 5OK, 7AZ, 8TX, 37GR, and 6TX coded after their origins of Mississippi, Oklahoma, Arizona, Texas, Greece, and Gonzales, respectively, were analyzed in this study. These six smectites were air-dried, ground, passed through 2 mm sieve, and carbonate minerals and organic matters removed with pH 5 sodium acetate buffer solution. From these smectites, clays with the particle size smaller than 2 μm were collected to conduct the adsorption experiment by sedimentation based on Stoke's Law (Deng and Tenorio Arvide, 2011).

The clay fractions were collected as suspension and the interlayer was saturated with $Na^+$ after size fractionation by flocculated the clay suspension with NaCl. These $Na^+$ saturated smectites were treated with 0.5 M $CaCl_2$ as described in Chapter 2.2.2 to obtain Ca-smectites (Ca-6TX, Ca-8TX, Ca-1MS, Ca-37GR, Ca-5OK, and Ca-7AZ). Dispersions with smectite content of 2 mg/mL were

Table 2.1. Structure and molecular property of $AFB_1$, ZEN, DON, OTA, and $FB_1$.

| Mycotoxin | Structure | Molecular weight ($g\ mol^{-1}$) | Solubility ($mg\ mL^{-1}$) | pKa |
|---|---|---|---|---|
| Aflatoxin $B_1$ |  | 312.27 | 0.03[a] | N/A |
| Zearalenone |  | 318.37 | 0.02[b] | 7.62[b] |
| Deoxynivalenol |  | 296.32 | 11[c] | 11.9[c] |
| Ochratoxin A |  | 403.82 | 1[d] | $pKa_1$ 3.5[d] $pKa_2$ 7.0[d] |
| Fumonisin $B_1$ |  | 721.84 | 25[e] | N/A |

[a]IARC (1993); [b]Lemke et al. (1998); [c]Sigma-Aldrich (2016); [d]Marković et al. (2017); [e]IARC (2002).

17

prepared with deionized water for each of Ca-smectite. Different treatments and further experiments were applied with these homogeneous smectite dispersions instead of dry clay powders.

### 2.2.1.2  *Cation exchange capacity (CEC) determination*

The determination of cation exchange capacity was conducted with three steps: saturation of clays with $CaCl_2$, replacement of the $Ca^{2+}$ with $MgCl_2$, and quantification of the amount of replaced $Ca^{2+}$. An adequate amount of clay suspension was saturated with 0.5 M $CaCl_2$ three times to ensure complete saturation. Before replacing the interlayer $Ca^{2+}$ with $MgCl_2$, clays were washed with 0.005 M $CaCl_2$ three times to avoid replacing $Ca^{2+}$ by $H^+$. The $Ca^{2+}$ in Ca-saturated clays were then replaced by washing with 0.5 M $MgCl_2$ four times, and all supernatant were collected during these washing procedures.

## 2.2.2  Exchanging interlayer cations on 37GR with Li, K, Cs, Mg, Ca, Sr, and Ba

After size fractionation, clay fraction of bentonite 37GR was saturated with Na during flocculation. To evaluate the exchange cation effects on mycotoxin adsorption, four divalent cations, Mg, Ca, Sr, Ba, and three monovalent cations, Li, K, Cs, were selected to replace Na in the interlayer of smectite sample 37GR. An adequate amount of clay suspension containing approximately 100 mg of clay was used in each cation saturation. Each of 10 mL of 1M LiCl, CsCl, or KCl, or 0.5 M of $MgCl_2$, $CaCl_2$, $SrCl_2$, or $BaCl_2$ solutions was mixed with the smectite in a 50 mL centrifuge tube. The tubes were then shaken for 15 minutes and centrifuged at 2,000 rpm (769 g) for 10 minutes. The clear supernatants were discarded with care, and the saturation procedures were repeated in total of 3 times to ensure the clays were fully saturated with targeted cations. The excess electrolytes in the suspensions were washed out twice with deionized water. The smectites were dispersed in about 5 mL of deionized water. An adequate amount of these smectite dispersions were transferred into 15-mL centrifuge tubes and diluted with deionized water to achieve 2 mg/mL of smectite dispersions for later experiments.

18

### 2.2.3 Reducing charge density of a high CEC smectite

#### 2.2.3.1 Layer charge density reduction

The layer charge reduction of smectites was achieved by incorporating $Li^+$ into vacant octahedral sites of smectite based on Hofmann & Klemen effects (Jaynes and Bigham, 1987; Jaynes et al., 1992; Lim and Jackson, 1986). To test the effect of the charge density on mycotoxin adsorption, the smectite 5OK with a high CEC of 136.6 cmol(+)/kg was chosen for this treatment.

Seven different Li/Na molar ratio solutions were prepared with mixed solutions of LiCl and NaCl. To conduct the charge reduction test, smectite dispersions containing 50 mg of smectite were mixed with the corresponding Li/Na ratio solution three times as described in first saturation step in cation exchange capacity (CEC) determination (Chapter 2.2.1.2) and then washed with deionized water twice. The seven smectites with different Li/Na ratios after the treatments were transferred into glass beakers and oven-dried at 90°C, and then heated at 250°C for 12 hours. This high temperature allowed the $Li^+$ to migrate from interlayer into the vacant octahedral sites of smectite. After heating, about 25 mL of 1:1 ethanol:water mixture was used to disperse the aggregated smectites in each beaker with the assistance of an ultrasonic cleaner.

These charge reduced smectites were then saturated with Ba in the interlayer as described in first saturation step in cation exchange capacity (CEC) determination (Chapter 2.2.1.2) with a 0.5 M $BaCl_2$ as the exchanging cation. The smectites were washed with deionized water twice after saturation, and then the concentration of smectite in suspension were calculated. A 2 mg/mL of smectite dispersion was prepared with deionized water for each of the charge-reduced smectites and used in later adsorption experiment.

*2.2.3.2    The CEC and charge density calculation of charge reduced 37GR*

These Ba saturated, charge reduced smectites were digested with hydrofluoric acid (HF) and aqua regia to break down the layer structure and to release the octahedral Li into the digestion solution. The original smectite without charge reduction treatment was also digested as a control. Each smectite dispersion containing approximately 10 mg of smectite were transferred into pre-weighed 50-mL centrifuge tubes in duplicate. Fresh prepared 0.6 mL aqua regia and 0.9 mL HF were pipetted into each tube and mixed thoroughly. The smectite and acids mixtures were shaken gently on an orbital shaker at 200 rpm for 24 hours. The digestion solution was brought to 15-mL mark with the saturated boric acid solution and shaken for additional 24 hours to dissolve any precipitated cation fluoride compounds. Then the mixture was diluted 1:1 with 15mL 0.05 M NaCl solution addition to preventing ionization of Li atoms during the atomic emission analysis. The weights of the tubes with mixtures were recorded before quantification of Li. Standard $Li^+$ solutions were prepared with same digestion solutions.

### 2.2.4    Mycotoxin adsorption experiments

*2.2.4.1    Adsorption of mycotoxins by natural smectites with different charge densities and modified smectites with reduced charge densities*

Mycotoxins, ZEN, DON, and OTA, were purchased from Sigma-Aldrich Inc. and 1000 mg/L mycotoxin stock solutions were prepared. Ten mg of each mycotoxin powder was dissolved in 10 mL of acetonitrile. The mycotoxin stock solutions were stored at 4°C and wrapped with aluminum foils. The 4 mg/L working solutions were diluted from each of the 1000 mg/L stock solutions with deionized water.

The adsorption of mycotoxins by natural smectites with different charge densities and smectites with reduced charge densities were followed the same procedures. To each 15mL centrifuge tube (Nalgene Falcon) containing 5 mL of 4 mg/L mycotoxin solution, 50 μL of clay suspension from

Section 2.2.1.1 and Section 2.2.3.1 containing 0.1 mg of smectite was added. The mixtures were shaken overnight at 200 rpm on a rotary shaker. The clear supernatant was obtained after the tubes were centrifuged at 4500 rpm for 57 min. Quantification of each mycotoxin in the clear supernatant was described in Chapter 2.2.7 and 2.2.8. The adsorption experiments were conducted in triplicate.

### 2.2.4.2 *Adsorption of mycotoxins on smectite 37GR with different exchanging cations*

The adsorption was followed the procedure described in Section 2.2.4.1. Each 5 mL of 4 mg/L mycotoxin solution was mixed with 0.1 mg of smectite from Section 2.2.2. After overnight shaken at 200 rpm and centrifuged, clear supernatant was collected for further quantification. All experiments were conducted in triplicate.

### 2.2.4.3 *Zearalenone adsorption isotherm*

Several mathematical methods have been developed to describe the different kinds of adsorption processes. The most widely used are isotherms, in which the amount of adsorbed chemicals is plotted against the equilibrium concentration of the compound in the solution at a constant temperature. Thus, to describe the relationship between the amount of adsorbed ZEN on smectites and the concentration of ZEN in solution at equilibrium, adsorption isotherms were used. The wavelength for DON quantification by UV-spectrophotometer was short (219 nm), and thus, interference from reagents and clay resulted in a high detection error. Therefore, the adsorption isotherm experiments were conducted with ZEN only due to its higher adsorption capacity than OTA and less quantification interference than DON. The experimental adsorption data were calculated with the standard Langmuir, exponential Langmuir, and modified Langmuir equation (QKLM) and fitted better with the modified Langmuir equation. These equations were:

Langmuir equation:

$$q = Q_{max}(\frac{KC}{1 + KC})$$

exponential Langmuir equation:

$$q = Q_{max}\left(\frac{KC^n}{1 + KC^n}\right)$$

modified Langmuir equation:

$$q = Q_{max}\left[\frac{Ke^{(-2bq)}C}{1 + Ke^{(-2bq)}C}\right]$$

where the q is the amount of adsorbed mycotoxin, $Q_{max}$ is the maximum adsorption capacity, C is the equilibrium concentration of mycotoxin in solution, K is the distribution constant, n is an exponential parameter, and b is an energy-dependent affinity parameter.

The adsorption isotherms were conducted following the procedures by Kannewischer et al. (2006). An aliquot of the stock solution was diluted with deionized water to prepared 8 mg/L working solution. A total volume of 5 mL of ZEN solution with various concentration was added into 15 mL centrifuge tubes. Then 50 μL of Li-, Na-, K-, Cs-, Mg-, Ca-, Sr-, or Ba-37GR smectite dispersion (as described in Section 2.2.2) was added into the tube. The centrifuge tubes were shaken overnight at 200 rpm on a rotary shaker at room temperature and then centrifuged at 4500 rpm for 57 min. The clear supernatant was collected for quantification. This study was conducted in triplicate and then averaged.

### 2.2.5   Synthesis of zearalenone-smectite complexes

To investigate if the ZEN were adsorbed into interlayer by smectites and the bonding mechanism, ZEN-smectite complexes were prepared. A 15 mg/L ZEN working solution was prepared by diluting the 1000 mg/L ZEN stock solution with deionized water. To synthesize ZEN-smectite complex, 50 mL of the K-smectite dispersion containing 15 mg of acidified smectite was mixed with 100 mL of 15 mg/L ZEN solution in 250-mL centrifuge bottle and shaken for 24 h at 200 rpm. After

centrifuging at 3000 rpm for 20 min and decanting the supernatant, the settled smectite was re-dispersed in 50 mL of deionized water and mixed with another 100 mL of 15 mg/L ZEN solution. The large volume of ZEN-smectite mixture was reduced by centrifugation.

To address possible desorption of ZEN during sample preparation, this ZEN-Smectite complex was divided into three parts and transferred to three 15-mL centrifuge tubes. One part was marked as "ZEN-K-Sm without wash" and stored at 4°C for later XRD analysis, the other part was washed twice with deionized water (10 mL each time) and marked as "ZEN-K-Sm with wash", and the last part was used to prepare Cu-saturated ZEN-Smectite complex. The centrifuge bottle weight was recorded, and the supernatant was stored during all the procedures for further adsorbed and desorbed ZEN quantification.

### 2.2.5.1  Cu saturation of zearalenone-smectite complex

To test whether the exchange cation can affect the bonding strength, the interlayer $K^+$ in the ZEN-K-Smectite complex was then replaced with $Cu^{2+}$. To prevent precipitation of Cu hydroxide compounds, the smectite was acidified by mixing 15 mg of K-smectite with ten mL of 1mM HCl. This step was carried out before the synthesis of the ZEN-Smectite complex to minimize the loss of smectite during experiment. A 0.1 M $CuCl_2$ prepared in 1 mM HCl was used to keep the low pH. Ten mL of 0.1 M $CuCl_2$ was added into a 15 mL centrifuge tube containing 10 mg of ZEN-K-Sm complex. The tube was shaken for 1 h at 200 rpm, and centrifuged at 3000rpm for 20 min. This treatment was repeated one more time with another 10 mL of 0.1 M $CuCl_2$. The supernatant in both treatments was collected for quantification of desorbed ZEN.

### 2.2.5.2  Variable-temperature X-ray diffraction

To investigate if ZEN adsorption occurred in the interlayer of smectite, the basal spacing of ZEN-smectite complexes were determined at various temperatures. The three ZEN-smectite complexes,

ZEN-K-Sm without wash, ZEN-K-Sm with wash, and ZEN-Cu-Sm, were re-dispersed on a vortex mixer and air dried on the polished side of silicon plates (0.407 mm×130 mm×150mm) cut from a (100) silicon wafer (University Wafers, Boston, Massachusetts, USA). Each silicon plate was placed on top of a ceramic sample holder of a reactor chamber XRK 900 (Anton Paar GmbH, Graz, Austria). The XRD pattern of the sample at elevated temperatures up to 200°C was recorded at every 25°C interval on a D8 Bruker Advance X-Ray diffractometer (Bruker, Madison, WI). A CuK$\alpha$ radiation source and an energy dispersive Sol-X detector were used for the XRD analysis. The diffractometer was operated at 40kV and 40 mA with a step size of 0.05° and a dwell time of 3 s per step. Each XRD pattern was recorded 20 min after the temperature of the sample holder reached the target temperature, and a heating rate of 0.1°C/s was used during the heating. The XRD patterns of a K-smectite (37GR) at elevated temperatures were also recorded to monitor the collapse of smectite under the same heating treatment.

### 2.2.5.3 *Fourier-transform infrared spectroscopic analysis*

Each ZEN-smectite complex was air dried as a film on a 25 mm×2 mm ZnS window (ClearTran, International Crystal Labs, Garfield, New Jersey, USA) for FTIR study. The FTIR spectra were recorded in the transmission mode with a resolution of 2 cm$^{-1}$ and 32 scans using a Spectrum 100 Fourier transform infrared spectrometer (Perkin-Elmer). To reach nearly 0 % humidity, the chamber was purged with dry $N_2$ gas for at least 10 min before recording the IR spectra. For nearly 100 % humidity, a piece of wet Kimwipe tissue was kept between the sample window and a blank window sealed with a rubber ring. Spectra were also recorded at room humidity.

### 2.2.6 Modification of smectites with surfactant BDTDA

The clay used for this study was a bentonite from Gonzales, Texas. After size fractionation, the <2 μm clay fraction was collected for modification. During the size fractionation, the clay suspension was collected and flocculated by shaking with 0.5 M $CaCl_2$ solution for three times to ensure

the clay was saturated with $Ca^{2+}$. Excess salts on the collected clay were removed by washed with deionized water and dialyzed against deionized water until the electric conductivity value was nearly equal to the value of fresh deionized water. This $Ca^{2+}$ saturated clay was referred to Ca-6TX in this study, and the cation exchange capacity (CEC) was 81.2 cmol/kg.

A cationic surfactant, benzyldimethyltetradecyl ammonium (BDTDA) chloride, was purchased from Fluka Chemical Company. The BDTDA is a quaternary ammonium compound with a formula $CH_3(CH_2)_{13}N^+(CH_3)_2CH_2C_6H_5$ (Figure 2.1). In brief, the BDTDA treated smectite, BDTDA-6TX, was synthesized by mixing an amount of BDTDA equal to the CEC of Ca-6TX with the clay and shaking and washing (Boyd et al., 1988). One hundred mL of 0.04 M BDTDA solution was mixed with 50 mL of Ca-6TX clay suspension containing 5 g Ca-6TX sample in a 250-mL centrifuge bottle. The suspension was shaken overnight. The synthesized BDTDA-6TX sample was collected after centrifuging, decanting the supernatant, and washing with deionized water three times. This organo-clay was freeze-dried and stored in a glass bottle at room temperature. An adequate amount of BDTDA-6TX was dispersed in deionized water to make 2 mg/mL of clay suspensions for later experiments.
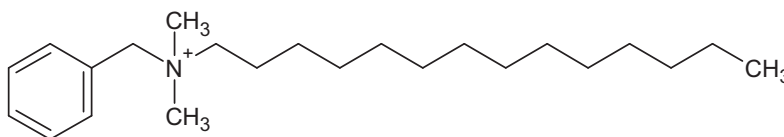
Figure 2.1. Ideal structure of benzyldimethyltetradecyl ammonium (BDTDA).

### 2.2.7 Quantification of ochratoxin A and deoxynivalenol with UV/visible spectrophotometer

The DON and OTA concentrations in the supernatant were measured using Beckman Coulter DU800 UV/visible-spectrophotometer at 219 nm and 333 nm wavelength, respectively. After the absorbance of the solution obtained from UV/visible-spectrophotometer, the concentration of DON and OTA can be calculated with the equation:

$$C = \frac{ABS \times M.W. \times 1000 \times C.F.}{\varepsilon}$$

where C is the mass concentration (μg/mL), ABS is absorbance at $\lambda_{max}$, M.W. is molecular weight of the mycotoxin, C.F. is correction factor (after calibrating the UV-VIS spectrophotometer with $K_2Cr_2O_7$, C.F.= 1.00), and $\varepsilon$ is molar absorptivity (extinction coefficient), $\varepsilon$ =6400 for DON (Krska et al., 2004) and $\varepsilon$ =6640 for OTA (Bauer and Gareis, 1987).

### 2.2.8 Quantification of zearalenone with high-performance liquid chromatography (HPLC)

ZEN was quantified by reversed-phase HPLC with an Agilent Technologies 1200 Series (Agilent Technologies, Santa Clara, CA) pump and a fluorescence detector. The separation was carried out on a C18 analytical column with a particle size of 2.6 μm, a pore diameter of 100 Å, and dimensions of 100×4.6 mm (Phenomenex, Torrance, CA). The remaining ZEN in solution after adsorption experiment was determined by HPLC (Liao et al., 2009) with its ability to exhibit fluorescence. The mobile phase was a mixture of acetonitrile:water (50:50, v/v). Injection volume was 50 μL with a 1.0 mL/min flow rate. Fluorescence detection was performed by setting wavelengths at 274 nm (excitation) and 440 nm (emission). With these parameters, the retention time was 5.4 min (Figure 2.2). A 50 μg/mL certified ZEN standard solution (Sigma-Aldrich Inc., St. Louis, MO) was injected with 0.4, 0.8, 1.6, 2.4, 3.2, 4.0, 4.8, 5.6, 6.4, 7.2, 8.0 μL to obtain respective peak areas. A standard curve was prepared by plotting the concentrations of the standard solution against the corresponding peak areas (Figure 2.3). With the regression equation from the standard
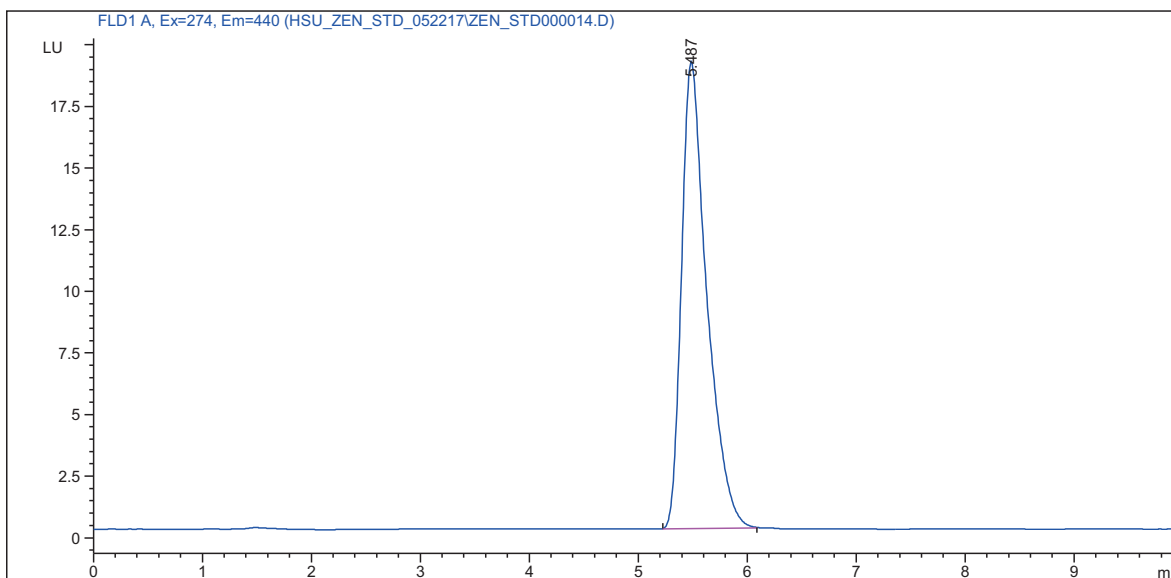
Figure 2.2. An example of HPLC chromatogram of pure zearalenone standard solution.

curve, the ZEN concentration can be calculated with the obtained HPLC peak areas. All samples were filtered through 0.2 μm pore size membrane filters before injected.

### 2.2.9    Molecular simulations

To evaluate the interaction sites on ZEN with smectite, the molecular geometry optimization of ZEN molecule for electrostatic potential calculation was performed with Density Functional Theory (DFT) at the PCM/ B3LYP/ DGDZVP level of theory (Becke, 1993; Lee et al., 1988; Miertus et al., 1981) using Gaussian Inc. software (Frisch et al., 1995). The distribution of Mulliken atomic charge was computed after the ZEN was optimized. The surface electrostatic potential of ZEN was mapped by using VEGA ZZ software (Pedretti et al., 2004). Similar simulation has been conducted for $AFB_1$ (Deng and Szczerba, 2011), and therefore, the properties of ZEN were compared with $AFB_1$.
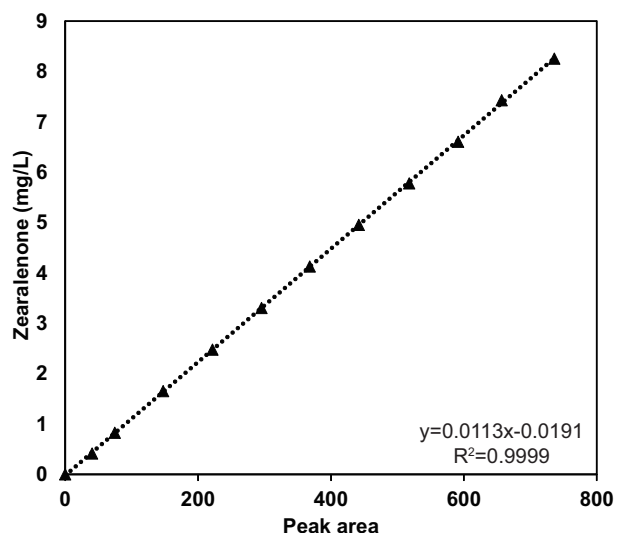
Figure 2.3. Standard curve of zearalenone analyzed by HPLC.

## 2.3 Results and discussion

### 2.3.1 Effects of layer charge density of smectite on mycotoxin adsorption

#### 2.3.1.1 Natural smectites with different charge densities

Figure 2.4 (left) shows the three mycotoxins adsorption on smectites with different cation exchange capacities, which are indications of charge densities. On average, OTA showed lower adsorption capacities than DON and ZEN among all the smectites. The smectite showed highest adsorption for each mycotoxin was 37GR at 0.02 mol/kg for OTA, 37GR at 0.05 mol/kg for DON, and 1MS at 0.06 mol/kg for ZEN, respectively (Table 2.2). These adsorption values of ZEN, OTA, and DON on these smectites were one order of magnitude lower than $AFB_1$ adsorption capacity (more than 0.6 mol/kg) (Deng et al., 2012). Such large differences indicated that the smectites had low affinity or adsorption capacities for these mycotoxins.

For ZEN, the highest adsorption capacity was observed in 1MS smectite with CEC value at 107.7 cmol/kg. 6TX and 8TX had lowest adsorption capacity (less than half of the highest) followed by 7AZ. The better CEC range for ZEN adsorption seemed to be between 107 and 136 cmol/kg.
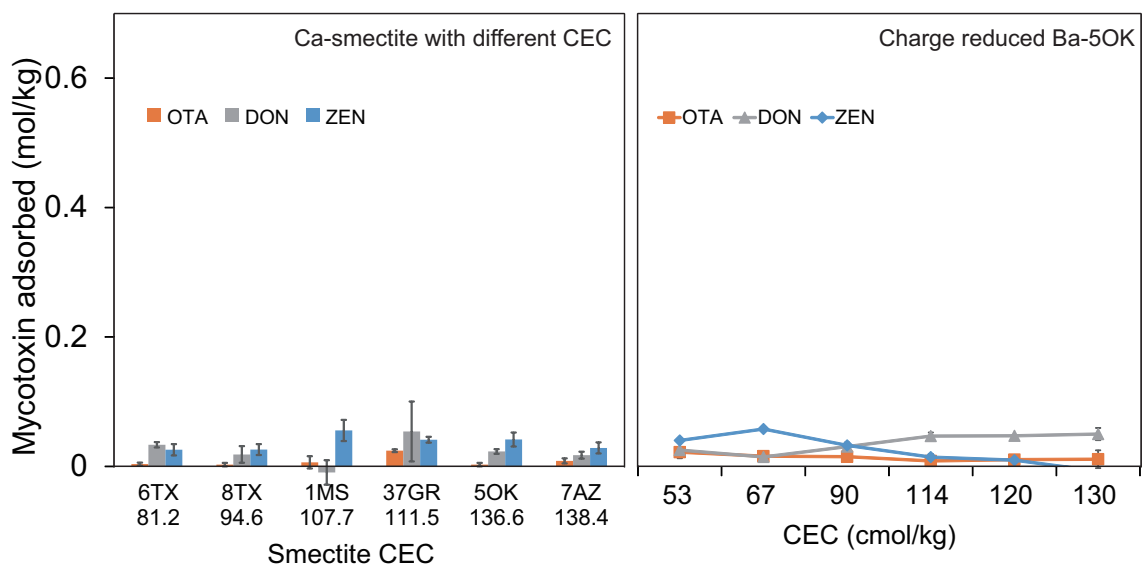
Figure 2.4. Zearalenone (ZEN), deoxynivalenol (DON), and ochratoxin A (OTA) adsorptions on different CEC Ca-smectites (left) and a charge-reduced Ba-smectite (right).

However, smectites with CEC values between 94 and 112 cmol/kg or charge density between 0.34 and 0.40 charge/ half cell were observed the best for $AFB_1$ adsorption($Q_{max}$ =0.51-0.63 mol/kg for Ca-saturated smectite) (Deng et al., 2012).

Although these six smectites did not sequestrate OTA well, the sample 37GR exhibited the highest adsorption capacity (Table 2.2). The adsorption capacities for DON ranged from 0 to 0.054 mol/kg, which did not show a trend with CEC. The quantification of DON concentration was derived from the absorbance with UV-spectrophotometer at 219 nm wavelength. Higher absorbance error from reagent and small particles like smectite were observed at short wavelength. Thus, the instrument error in quantification method accounted for the negative value and large variation.

### 2.3.1.2    *Smectites with reduced charge densities by the Hofmann-Klemen effect*

After incorporating $Li^+$ into the octahedral sheet, the CEC of 5OK reduced from 136.6 to 53 cmol/kg with increasing Li/Na ratio. The three mycotoxins had different responses to the charge

Table 2.2. Chemical properties of smectites and their adsorption capacity on mycotoxins.

| Smectite | CEC (cmol/kg) | Layer charge (charge/half unit cell) | OTA | DON | ZEN |
|---|---|---|---|---|---|
| | | | average adsorption level (mol/kg) | | |
| 6TX | 81.2 | 0.29 | $0.004 \pm 0.023$ | $0.034 \pm 0.004$ | $0.026 \pm 0.009$ |
| 8TX | 94.6 | 0.34 | $0.003 \pm 0.003$ | $0.018 \pm 0.013$ | $0.026 \pm 0.008$ |
| 1MS | 107.7 | 0.39 | $0.006 \pm 0.010$ | $-0.010 \pm 0.019$ | $0.056 \pm 0.016$ |
| 37GR | 111.5 | 0.40 | $0.024 \pm 0.002$ | $0.054 \pm 0.046$ | $0.041 \pm 0.005$ |
| 5OK | 136.6 | 0.49 | $0.003 \pm 0.003$ | $0.023 \pm 0.004$ | $0.042 \pm 0.011$ |
| 7AZ | 138.4 | 0.50 | $0.008 \pm 0.004$ | $0.017 \pm 0.005$ | $0.029 \pm 0.009$ |

density from these natural smectites with different charge density (Figure 2.4, right). The OTA adsorption had no significant difference when the CEC of the smectite reduced from 130 to 114 cmol/kg but significantly increased ($p<0.05$) to highest adsorption capacity (0.021 mol/kg) when CEC decreased from 114 to 53 cmol/kg. DON adsorption had no significant fluctuation with CEC reduction in higher CEC range (130 to 114 cmol/kg) but significantly decreased to 0.013 mol/kg ($p<0.01$) when the CEC further reduced to lower value (67 cmol/kg). The lowest ZEN adsorption was observed when the CEC was 130 cmol/kg and then increased to 0.06 mol/kg with the CEC reduction ($p<0.01$). The ZEN adsorption was calculated by subtracting residual ZEN concentration from blank concentration, thus, a negative value was imaginable when the adsorption was negligible.

Enhanced $AFB_1$ adsorption was achieved when charge density of smectite 5OK was reduced (Barrientos-Velazquez et al., 2016). A high CEC smectite showed relatively lower adsorption capacity (0.3 mol/kg) and low affinity for $AfB_1$ compared to those on lower CEC smectites. As the CEC was reduced from 137 to 86 cmol/kg, an increment of more than twice of $AFB_1$ adsorption capacity (0.8 mol/kg) was observed. Although there are some fluctuations in OTA adsorption with CEC reduction, an optimal CEC of 67 cmol/kg or lower was required to reach the highest OTA adsorption capacity. The results of charge reducing indicated that the adsorption capacity of ZEN was slightly enhanced by reducing charge density while DON adsorption seemed to exhibit an inverse trend. Reducing cation exchange capacity increased the nonpolar domain size of smectite and decrease the number of exchange cations and the associated water in their hydration shells in the interlayer space (Deng et al., 2012). This can indirectly explain the decreased of DON (water solubility=11 mg $mL^{-1}$) adsorption and increased of ZEN (water solubility=0.02 mg $mL^{-1}$) adsorption with CEC decreasing. The above adsorption of ZEN, OTA, and DON on smectites suggested that the layer charge density did not exert the same effect on these mycotoxins as it did on $AFB_1$.

### 2.3.2 Effects of the type of exchange cation on ZEN, OTA, and DON adsorption on smectite

Even though the overall adsorption of ZEN, OTA, and DON on the smectite were low compared to the adsorption of $AFB_1$, single point adsorption indicated the interlayer exchange cation affected the adsorption capacities of OTA, DON, and ZEN. The smectite with monovalent interlayer cations showed significant higher adsorption capacities ($p< 0.05$ for OTA, $p< 0.01$ for DON and ZEN) than smectite with divalent interlayer cations, which were 3 times enhancement in ZEN and OTA and more than 10 times enhancement in DON (Figure 2.5).
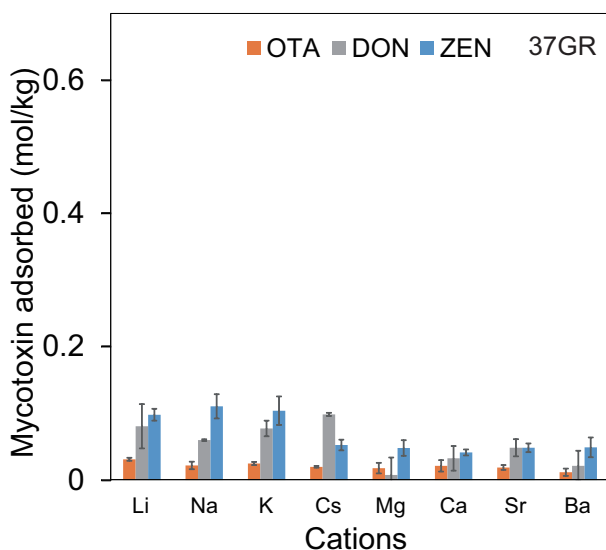


Figure 2.5. Zearalenone, deoxynivalenol, and OTA adsorption on smectite saturated with different cations.

The DON molecule is highly water soluble. Changing the interlayer cations from divalent to monovalent enhanced the adsorption of DON more than 10 times. Interlayer cations balance the negative charge in 2:1 layer smectites in which water was usually involved as in the hydration shell of cations. With fixed amount of negative charge on the smectite, the number of monovalent cation was higher than divalent cation on smectite since more cations were needed to balance the nega-
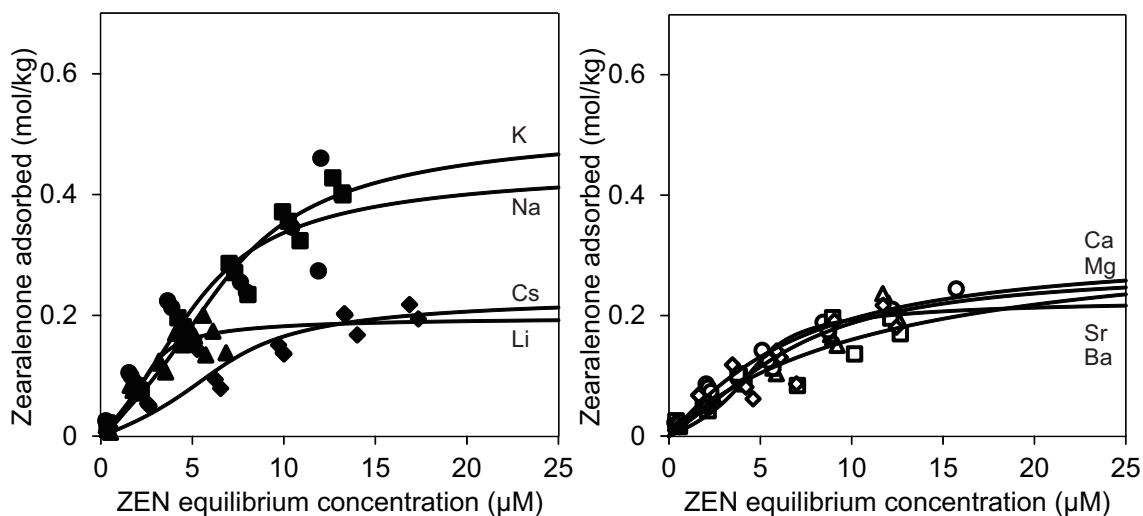
Figure 2.6. Zearalenone adsorption isotherms of 37GR smectite saturated with different cations.

tive charge, resulting in more water with monovalent cation than divalent cation in their hydration shells. A hydrophilic compound DON was expected to be adsorbed in a water-rich environment. Higher adsorption of DON on smectites with monovalent cations was observed.

### 2.3.3 Isothermal adsorption of zearalenone by smectite saturated with Li, Na, K, Cs, Mg, Ca, Sr, and Ba

Adsorption isotherm experiments were conducted with ZEN only (Figure 2.6). The adsorption isotherm fit parameters were shown in Table 2.3 and demonstrate that K-smectite is able to adsorb 0.53 mol ZEN/kg adsorbent, whereas Na-, Sr-, Ca-, Mg-, Cs-, Ba-, and Li-smectite were able to adsorb 0.45, 0.34, 0.31, 0.29, 0.24, 0.23, and 0.20 mol ZEN/kg adsorbent, respectively. According to the adsorption fitting model, smectite with different exchange cation had a 2.6-fold difference in adsorption capacity ($Q_{max}$) and up to a 2.4-fold difference in affinity ($K_d$). The effects of exchange cation on $AFB_1$ adsorption were investigated and found that with modified Langmuir equation fitting, adsorption $Q_{max}$ of $AFB_1$ on Li-, Na-, K-, Cs-, Mg-, Ca-, Sr-, Ba-smectite were 0.20, 0.38, 0.59, 0.36, 0.48, 0.52, 0.55, and 0.63 mol/kg, respectively (Deng et al., 2012). Divalent cation sat-

Table 2.3. Adsorption isotherm fit parameters for ZEN adsorption on 37GR saturated with different cations.

| Exchange cation on 37GR | Modified Langmuir QKLM | | | |
| --- | --- | --- | --- | --- |
| | $Q_{max}$ (mol/kg) | $K_d$ ($\mu M^{-1}$) | b | $\eta^2$ |
| Li | 0.20 | 0.118 | -6.26 | 0.96 |
| Na | 0.45 | 0.075 | -1.99 | 0.92 |
| K | 0.53 | 0.054 | -1.88 | 0.99 |
| Cs | 0.24 | 0.048 | -4.77 | 0.97 |
| Mg | 0.29 | 0.077 | -2.41 | 0.95 |
| Ca | 0.31 | 0.112 | -0.95 | 0.97 |
| Sr | 0.34 | 0.088 | 0.00 | 0.87 |
| Ba | 0.23 | 0.056 | -5.84 | 0.82 |

urated smectites had not only higher $Q_{max}$ also higher adsorption affinities ($K_d$) for $AFB_1$ than for ZEN. The $K_d$ values of $AFB_1$ on Li-, Na-, K-, Cs-, Mg-, Ca-, Sr-, Ba-smectite were 0.021, 0.018, 0.127, 0.088, 0.224, 0.201, 0.096, 0.275 $\mu M^{-1}$, respectively. A concave shape isotherm at low concentration and then adsorption increased as ZEN concentration rose with an adsorption maximum is classified as an S2 isotherm by Giles and Smith (1974). The S-type adsorption isotherms of all the samples in the studied concentration range indicated their low affinities for ZEN at low concentration and a higher energy barrier for ZEN to overcome to be adsorbed by the smectites.

A size-matching hypothesis between $AFB_1$ and adsorbed smectite was proposed and further affirmed by Deng et al. (2012). To enhance the adsorption capacity and affinity of $AFB_1$, divalent cations saturated smectites were higher preferred than monovalent cations due to the remaining unoccupied surface area they created were better matching with $AFB_1$'s molecule size. However, experiments conducted with same cations did not show the same trends in ZEN despite that ZEN and $AFB_1$ were highly similar in polarity, solubility, molecular weight, and structure.
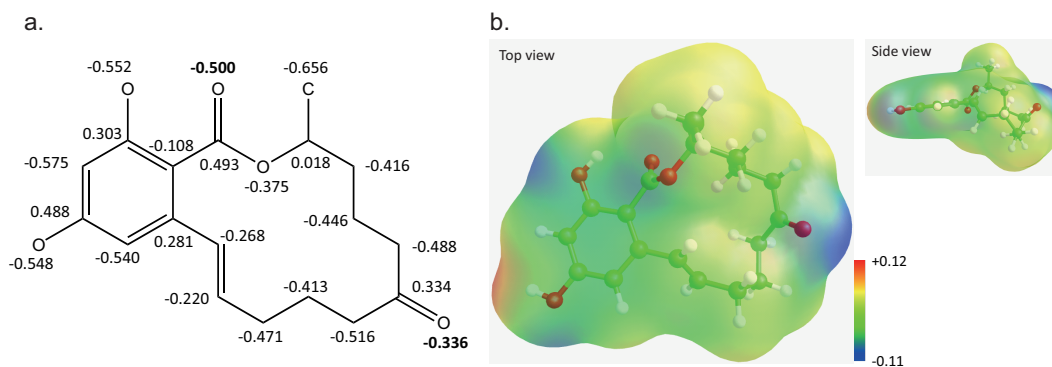
Figure 2.7. Net atomic charge (a) of non-hydrogen atoms and surface electrostatic potential (b) of zearalenone (Unit: elementary charge, e).

At low ZEN concentration (single point adsorption), smectite with monovalent cations showed higher adsorption capacities than those with divalent cations, which is in contradiction to the aflstoxin $B_1$'s adsorption and Deng *et al.*'s size-matching theory. This result can be attributed to the surface electrostatic potential difference between ZEN and $AFB_1$. A highly negative charge (-0.22 atomic charge units) sites closed to two adjoining carbonyl oxygen on $AFB_1$ formed a hydrophobic part in which coordinated with cations on smectite through van der Waals interactions (Deng et al., 2012). Yet on ZEN, the most negative surface electrostatic potential site was about -0.11 atomic charge units which located at one carbonyl oxygen, and the other carbonyl oxygen was less negative although itself had high negative charge(Figure 2.7).

Without such highly negative part on ZEN, interaction with interlayer cations was more restricted compared to $AFB_1$. The two $(-CH_2-)_3$ chains made the ZEN structure flexibto a planer -similar structure in the interlayer of smectite. However, it is less flat than AfB1, thus it is more difficult to form hydrophobic interactions with smectite surface. A size-matching between ZEN and hydrophobic nonpolar sites on smectite was not observed.

The strength of an ion attracting water molecules is described by hydration potential, which is cor-

Table 2.4. Selected properties of cations.

| Ion | Ionic radius[a] (nm) | Hydrated radius[a] (nm) | $Z^2/r$ (1/nm) | $Q_{max}$ (mol/kg) |
|-----|------|------|------|------|
| $Li^+$ | 0.060 | 0.382 | 16.67 | 0.20 |
| $Na^+$ | 0.095 | 0.358 | 10.53 | 0.45 |
| $K^+$ | 0.133 | 0.331 | 7.52 | 0.53 |
| $Cs^+$ | 0.169 | 0.329 | 5.92 | 0.24 |
| $Mg^{2+}$ | 0.065 | 0.428 | 61.54 | 0.29 |
| $Ca^{2+}$ | 0.099 | 0.412 | 40.40 | 0.31 |
| $Sr^{2+}$ | 0.113 | 0.412 | 35.40 | 0.34 |
| $Ba^{2+}$ | 0.135 | 0.404 | 29.63 | 0.23 |

[a] Nightingale (1959).

related to the ratio of square of the ionic charge (Z) to the radius (*r*), $Z^2/r$ (Tansel, 2012). Higher $Z^2/r$ values suggested water molecules in the interlayer of divalent cation saturated smectites were held more tightly in which were unfavoured for hydrophobic ZEN to be adsorbed, thus, resulting in lower adsorption capacities. In general, ZEN adsorption capacities were increasing with decreasing of the $Z^2/r$ value with the exceptions of $Cs^+$ and $Ba^{2+}$ (Table 2.4).

### 2.3.4 Mycotoxin adsorption on BDTDA-6TX

Adsorption isotherms of the cationic surfactant modified smectite for ZEN and OTA suggested that BDTDA-6TX was a good adsorbent for ZEN as the $Q_{max}$ was estimated about 1.19 mol/kg (Table 2.5). The isotherms were fitted well ($\eta^2$=0.95 for ZEN; 0.90 for OTA) to the Langmuir equation (Figure 2.8). The comparatively steep slope and unsaturated adsorption in the experimental concentration range indicated higher affinity and capacity of the BDTDA-6TX to remove ZEN from aqueous solution.

BDTDA is a quaternary ammonium compound with a long hydrophobic aliphatic chain which con-

Table 2.5. Langmuir isotherm parameters for zearalenone and ochratoxin A on BDTDA-6TX.

| Adsorbent | Mycotoxin | Langmuir | | |
|-----------|-----------|-----------|---------|----------|
| | | $Q_{max}$ (mol/kg) | $K_d$ | $\eta^2$ |
| BDTDA-6TX | ZEN | 1.19 | 0.154 | 0.95 |
| | OTA | 0.24 | 0.024 | 0.90 |

tributes its hydrophobicity. Studies of cationic surfactant modified materials on adsorbing organic molecules such as phenol, chlorophenol, polycyclic aromatic hydrocarbons, and nonionic organic contaminants suggested the adsorption can be greatly improved by increasing the hydrophobicity of the adsorbent (Akbal, 2005; Chen and Zhu, 2001; Koh and Dixon, 2001; Rai et al., 2007). However, adsorption capacity of OTA onto this organo-clay was not significantly enhanced despite its low water solubility (Figure 2.8).

In adsorption isotherm, pH of all the aqueous solution was unadjusted and measured at pH=6.9 for ZEN and pH=6.5 for OTA. The pH value of adsorption system can affect the degree of ionization of mycotoxins. The estimated $pK_a$ of 7.62 was reported for ZEN (Table 2.1), therefore, ZEN in solution was mainly nonionic, however, a mixture of organic and inorganic adsorbents used to adsorption ZEN at various pH condition (3.0, 4.5, and 6.0) showed the solution pH effects were insignificant (Bordini et al., 2015). Yiannikouris et al. (2013) evaluated the abilities of yeast cell wall and hydrated sodium calcium aluminosilicate (HSCAS) on sequestrating ZEN at pH ranging from 2.5 to 8.0. The percentages of bounding ZEN were 53.76 % to 60.40 % on yeast cell wall and 46.87 % to 63.13 % on HSCAS within the pH range, suggesting little pH influence. The OTA has two $pK_a$ values of 3.5 and 7.0 for a carboxyl group on the phenylalanine moiety and a phenol group on the dihydroisocoumarin portion, respectively (Table 2.1). This means the OTA molecules present in aqueous solution are mainly in anionic form (both monoanion and dianion) at neutral pH and in uncharged form at pH < 3.5. In vitro studies showed OTA adsorption on organic adsorbents
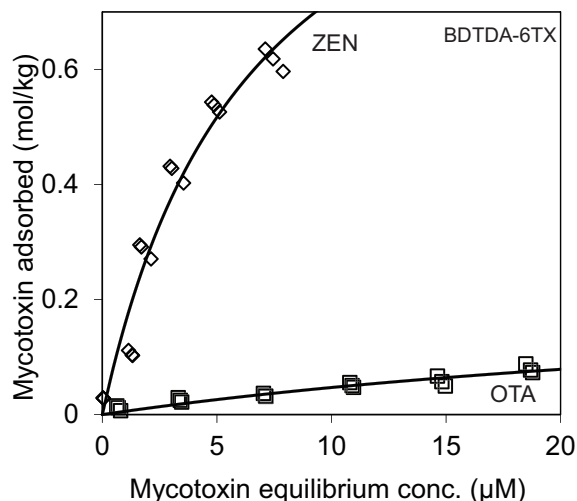
Figure 2.8. Adsorption isotherms of zearalenone and ochratoxin A by BDTDA-6TX.

and organically modified adsorbents were pH-dependant and significantly higher at pH <4.0 than those at pH > 4.0, thus in this tested pH value, the OTA adsorption on organo-clay was not significantly increased (Marković et al., 2017; Faucet-Marquis et al., 2014; Avantaggiato et al., 2014).

### 2.3.5   Adsorption and desorption of zearalenone on ZEN-smectite complexes

During the synthesis of ZEN-K-Smectite complex, 40% of the ZEN adsorption occurred in the first treatment of smectite with ZEN solution (Table 2.6). The increasing ZEN adsorption in the second treatment suggested that the smectite was not saturated with ZEN. Desorption of ZEN from the smectite was observed after the ZEN-K-Sm was either washed with deionized water (77.8%) or with a 0.1 M $Cu^{2+}$ solution (92.6%), which implied the instability of the adsorbed ZEN on the complexes.

### 2.3.6   Characterization of ZEN-K-Sm and ZEN-Cu-Sm complexes

The X-ray diffraction analysis indicated that the interlayer of smectite was not fully occupied by ZEN. In a preliminary test, the d-spacing of a K-smectite increased from 11.7 Å to 12.2 Å at room

Table 2.6. Adsorption and desorption of zearalenone during synthesis of ZEN-K-Sm and ZEN-Cu-Sm complexes.

| ZEN treatment | Adsorption (mol/kg) | Desorption (mol/kg) | |
|---|---|---|---|
| | ZEN-K-Sm | DI water wash | Cu solution replaced |
| 1st | 0.11 | 0.14 | 0.12 |
| 2nd | 0.16 | 0.07 | 0.13 |
| Total (mol/kg) | 0.27 | 0.21 | 0.25 |

temperature after treated with ZEN and collapsed to 10.2 Å after heated in furnace at 300°C for 2 hours (Figure 2.9a). Although the interlayer of the K-smectite itself collapsed to the same extent after heating, an increasing d-spacing before heating and a small shoulder (arrow in Figure 2.9a) appeared after heating indicated the ZEN molecule entered at least part of the interlayer of smectite.

To investigate the effect of exchange cation on bonding strength, $Cu^{2+}$ was chosen to replace the interlayer $K^+$ in ZEN-K-smectite complex due to the valence and size differences between $K^+$ and $Cu^{2+}$. The variable temperature XRD results of ZEN-K-Sm, ZEN-Cu-Sm, and pure K-smectite were consistent with preliminary X-ray diffraction analysis: d-spacing was increased from 12.1 Å to 12.6 Å at room temperature and collapsed to 10.2 Å after heated (Figure 2.9b). The preliminary and variable temperature XRD results suggested the ZEN molecule was able to enter the interlayer of smectite, however, the weak peak increasing indicated the adsorption was unstable after washing/$Cu^{2+}$ replacing, which was consistent with the desorption result (Table 2.6).

The ZEN characteristic bands were 1709, 1695, and 1644 $cm^{-1}$ attributed to the carbonyl groups, 1611 and 1578 $cm^{-1}$ corresponding to ring C=C stretching, 1436 $cm^{-1}$ arose from bending of the hydroxyl group and ring deformation. The bands in the range between 1456 and 1102 $cm^{-1}$ not assigned above were derived from -$CH_2$ bending vibration (Figure 2.10, top) (Movasaghi et al., 2008;
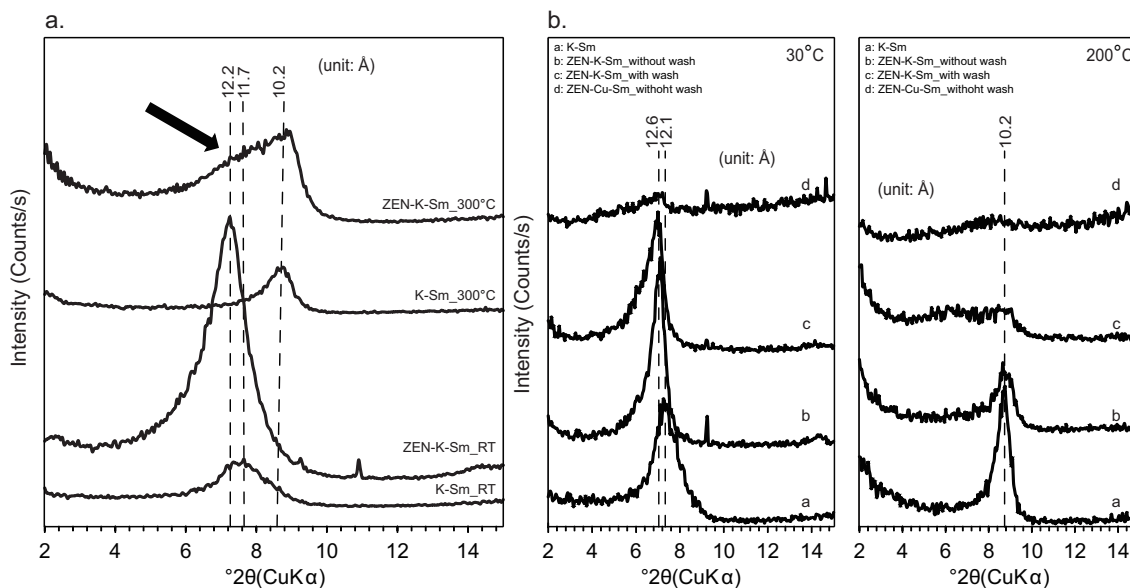
Figure 2.9. X-ray diffraction patterns of K-smectite and ZEN-K-smectite complexes (a) and ZEN-Cu-Sm complexes (b) at room temperature and heated at 300/200°C (a: K-smectite, b: ZEN-K-smectite without wash, c: ZEN-K-smectite with wash, d: ZEN-Cu-smectite without wash).

Krol et al., 2018). Despite the fact that most of the adsorbed ZEN on ZEN-K-Sm were desorbed after washed or saturated with the $CuCl_2$ solution, identical ZEN IR band positions were observed on the ZEN-Smectite complexes; moreover, most of the IR bands remained in the same position (indicated by the dotted lines in Figure 2.10). When recorded at 0% humidity, the FTIR bands of adsorbed ZEN in the three ZEN-Smectite complexes were same and were very close to those bands of free ZEN. FTIR band shifting of adsorbed ZEN was not observed in ZEN-Cu-Sm when ZEN-K-Sm was treated with $CuCl_2$. Moreover, unlike the interaction between carbonyl oxygen on $AFB_1$ and hydration shell water of exchange cation(Deng et al., 2010, 2012; Deng and Tenorio Arvide, 2011), most of the FTIR bands showed no shift when the humidity change from 0% to 100%. No band shift with humidity change suggested the water molecule did not affect in the bonding of ZEN on smectite. The absence of IR band shifts when the interlayer cation was replaced, and water content was varied was largely due to the low adsorption of ZEN on the smectite. It seemed that other than $-CH_2$ band changed at 1404, 1311, 1267, and 1258 cm$^{-1}$, only small bands changes in the carbonyl group (1690, 1635, and 1614 cm$^{-1}$) occurred, indicating that only carbonyl (C=O)
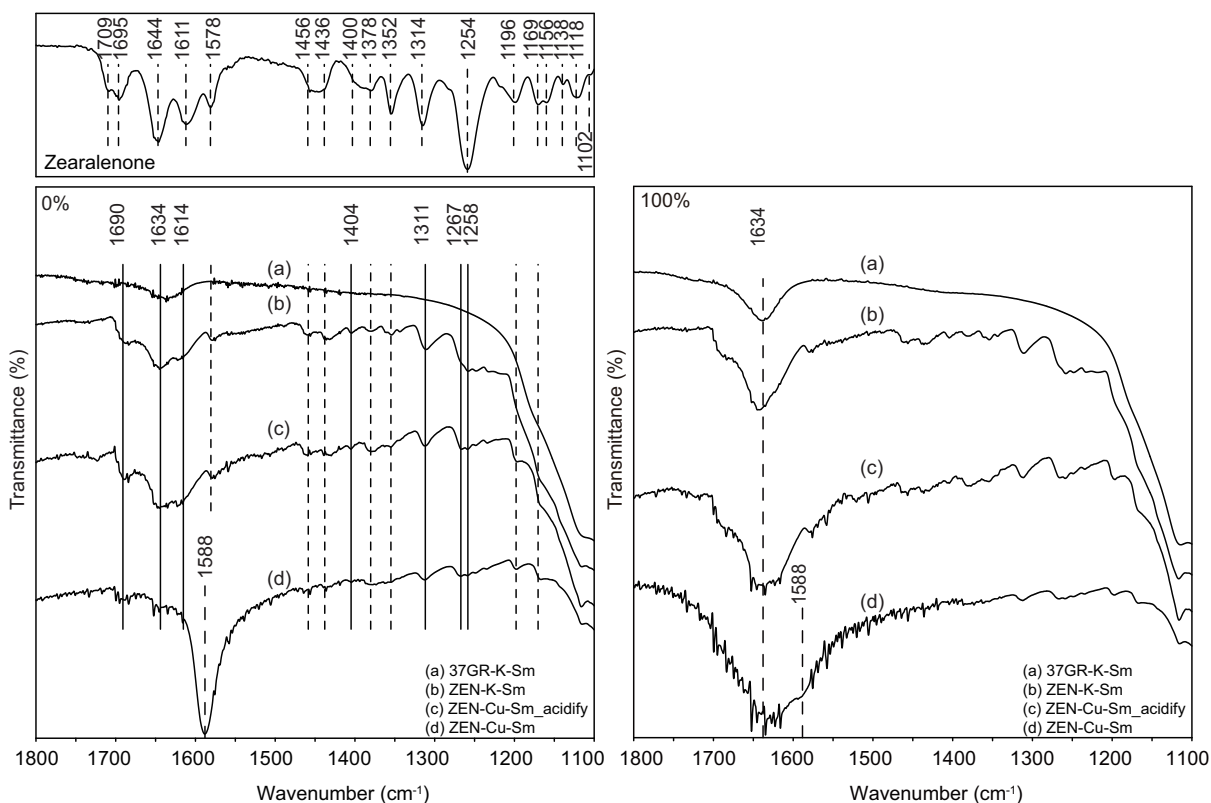
Figure 2.10. Infrared spectra of free zearalenone (upper left) and of zearalenone-smectite complexes saturated with $K^+$ and $Cu^{2+}$ at nearly 0% humidity by $N_2$ purge (lower left) and 100% humidity (right).

groups were involved in the ZEN binding process. Most likely, the ZEN molecule was adsorbed on hydrophobic sites of smectite without interacting with the cation and its hydrated water.

## 2.4    Conclusion

Comparing to the reported adsorption of $AFB_1$ by smectites, all tested smectites, with or without modification with cation exchange or charge reduction, showed much lower adsorption for ZEN, OTA, and DON. The cation exchange or charge reduction did not exert the same effects on the adsorption of ZEN, OTA, and DON as they did on $AFB_1$.

The best CEC range for ZEN adsorption on natural smectite in this study was between 107

41

and 136 cmol/kg. The smectite showed highest adsorption capacity for DON and OTA was 1MS (CEC=107.7 col/kg). The charge reduced smectite, 5OK, did not exert obviously increase or decrease in the OTA adsorption. However, the ZEN and DON exhibited different response to charge reduction. The ZEN adsorption increased with charge reduced, and the DON adsorption reduced with charge reduced. The smectites with monovalent exchangeable interlayer cation had higher adsorption capacity for OTA, DON, and ZEN. The isothermal adsorption of ZEN suggested smectites with monovalent cation had higher affinity and $Q_{max}$ than with divalent cation. The result was attributed to the tightly held water around divalent cation, and thus unfavoured the adsorption of hydrophobic ZEN. A cationic surfactant modified smectite showed an enhancement of ZEN adsorption, however, it did not improve the OTA adsorption. The FTIR and XRD results suggested the interlayer adsorption of ZEN. The IR pattern indicated the ZEN was adsorbed on hydrophobic sites of smectite and did not interact with the interlayer cation and its hydrated water.

# 3.  ADSORPTION OF FUMONISIN $B_1$ ON SMECTITES

## 3.1  Introduction

Mycotoxins are toxic, relatively small (molecular weight $< 700$ g mol$^{-1}$) secondary metabolites produced by fungi (Turner et al., 2009). Fungi such as *Fusarium proliferatum* and *Fusarium Liseola*, i.e. *F. moniliforme* (as known as *F. verticillioides Sacc.*), are the most prevalent fungi associated with corn (Zea mays L.). These fungi produce fumonisins (Marasas et al., 1984; Soriano and Dragacci, 2004; Voss et al., 2007). The genus *Fusarium* was first established by Link in 1809, and Sheldon recognized that *F. moniliforme* was implicated in moldy corn toxicosis in farm animals in USA (Link, 1809; Sheldon, 1904; Marasas, 1996). Nevertheless, it was until 1988, fumonisins were formally identified and introduced by Gelderblom et al. (1988) from *F. moniliforme* infected corn, and at the same time, Bezuidenhout et al. (1988) explained the sturctures of fumonisin $A_1$, $A_2$, $B_1$ and $B_2$. The structure of fumonisins consists of a long hydroxylated hydrocarbon chain with added two propane-1,2,3,-tricarboxylic acids, methyl and amino groups (Figure 3.1). More than 28 different fumonisins have been identified and further classified into four groups, A, B, C, and P, based on their structural similarities (Gelderblom et al., 2007). The most prevalent fumonisins are fumonisin $B_1$, $B_2$, and $B_3$. The most abundant and most toxic is fumonisin $B_1$ (FB$_1$) (Wild and Gong, 2010; Abbas et al., 2006; Caloni et al., 2000; Wilkes et al., 1995). About 70 % total fumonisins found in naturally contaminated foods and feeds are FB$_1$ (Krska et al., 2007).

The fungi contamination occurs worldwide and is determinant by location, climate, and susceptibility of the plants to the fungal invasion, insect damage, and crop stress (Wild and Gong, 2010). According to the International Agency for Research on Cancer (IARC), the FB$_1$ is considered as a carcinogen to human and is classified as a Group 2B carcinogen in 1992 (IARC, 2002). The toxicity of fumonisins to animals is animal dependent; cattle are considered less susceptible to fumonisin toxicity, but other animals can have symptoms with varying severity: leukoencephalomalacia

| | R1 | R2 | R3 |
|---|---|---|---|
| Fumonisin B₁ | OH | OH | H |
| Fumonisin B₂ | H | OH | H |
| Fumonisin B₃ | OH | H | H |
| Fumonisin A₁ | OH | OH | COCH₃ |
| Fumonisin A₂ | H | OH | COCH₃ |
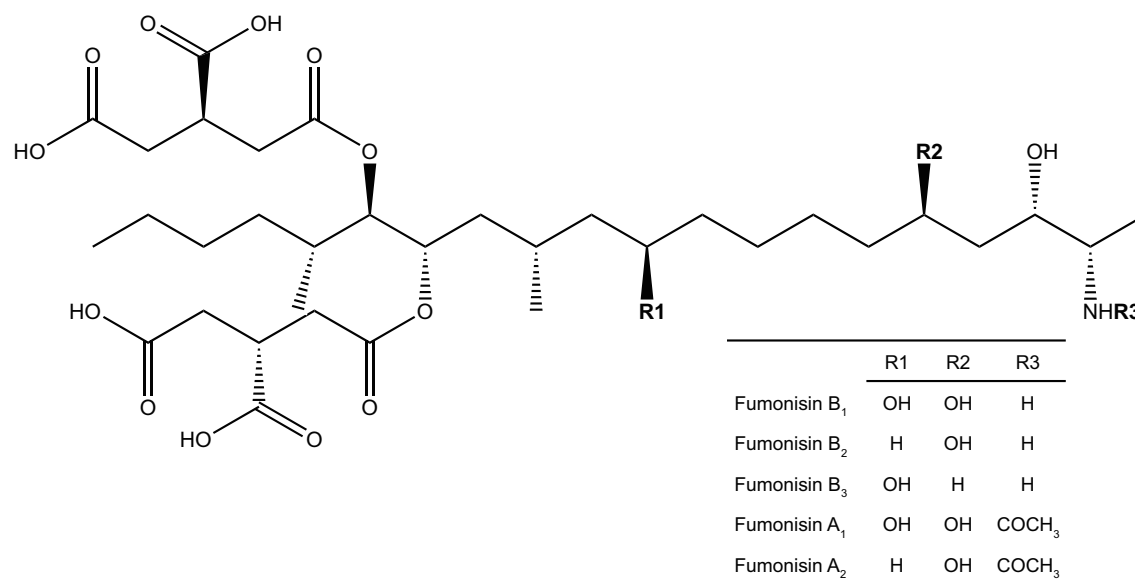
Figure 3.1. Chemical structures of fumonisins.

(LEM) in horses, immunosuppression in poultry, pulmonary edema in pigs, hepatocarcinogenic and nephrotoxic in rats, atherogenic effects in vervet monkey, medial hypertrophy of pulmonary arteries in swine, and brain hemorrhage in rabbits (Soriano and Dragacci, 2004; Voss et al., 2007; Gelderblom et al., 1988; Caloni et al., 2000).

One possibility for mycotoxin detoxification is the use of adsorbent materials. The efficiency of those materials depends on the chemical structure and physical properties of both the adsorbent and the mycotoxin, moreover the features of the adsorbate molecules, like polarity, solubility, shape, and charge distribution (Avantaggiato et al., 2005). Activated carbon, zeolites, and various natural and modified materials have been tested to inactivate fumonisins and thus to reduce their bioavailability(Galvano et al., 1997; Avantaggiato et al., 2005, 2014). They are seldom used in practice due to uncertainty on the selectivity, efficiency, and potential adverse health effects of the materials. Bentonite, a natural clay, is used as anti-caking agents in animal feeds. Certain bentonites have shown the capability to bind other mycotoxins such as aflatoxins (Deng et al., 2012; Barrientos-Velazquez et al., 2016). Fumonisins have a positive charge on its amino group and possess net
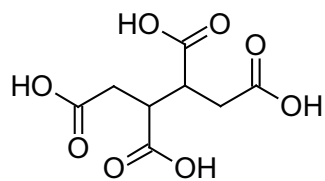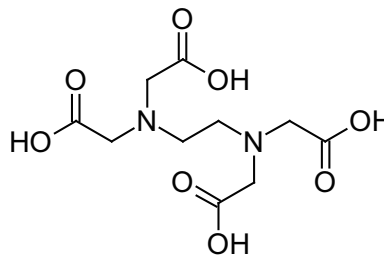
1,2,3,4-butanetetracarboxylic acid (BTCA)    Ethylenediaminetetraacetic acid (EDTA)

Figure 3.2. Chemical structures of 1,2,3,4-butanetetracarboxylic acid (BTCA) and ethylenedi-aminetetraacetic acid (EDTA).

positive charge at low pH, and bentonites should be able to adsorb fumonisins by cation exchange reaction at the low pH found in the stomach. These molecules might be adsorbed at neutral pH if they exist as zwitterions. This study was aimed to find the controlling factors in $FB_1$ adsorption on smectite and to investigate the adsorption site and stability of fumonin $B_1$ on smectite.

## 3.2   Materials and methods

### 3.2.1   Reagents and clay sample

The smectite sample used in this study was a bentonite (4TX) from Gonzales, Texas, supplied by Southern Clay Product. Only the $< 2$ µm clay fraction was used in this study and the size fractionation procedure was as described in Section 2.2.1.1. This clay sample was saturated with $Na^+$ after size fractionation by flocculated the clay suspension with NaCl. The cation exchange capacity (CEC) of the clay was 81.2 cmol $kg^{-1}$, and the organic carbon was equal to 0.07 %.

Fumonisin $B_1$ was obtained from Sigma-Aldrich Inc. A 1000 mg/L stock solution was prepared by dissolving 10 mg of $FB_1$ powder in 10 mL mixture of acetonitrile:water (1:1, v/v) in a 10-mL volumetric flask. This stock solution was wrapped with aluminum foil and stored at 4°C. To prepare the working solution, an aliquot of the 1000 mg/L stock solution was diluted with a mixture of acetonitrile:water (1:1, v/v) to the desired concentration.

The pH of $FB_1$ solution was adjusted with HCl and NaOH solutions. Three different concentration (1 mM, 0.1 mM, and 0.01 mM) HCl solutions were prepared by diluting from an adequate amount of 0.1 M HCl solution to 100 mL to obtain HCl blank solutions with pH= 3, 4, and 5. The HCl blank solutions with pH= 6 was prepared by diluting from 0.1 M HCl solution and then adjusting with NaOH solution.

### 3.2.2   Estimation of chemical species of fumonisin $B_1$ at different pH

As electrostatic attraction and repulsion between positive part of $FB_1$ and negative sites on smectite dominate the interaction of $FB_1$ with smectite, the species change of $FB_1$ at different pH need to be calculated to predict their interaction. Unfortunately, the dissociate constants of fumonisins are not available in the literature. Two compounds 1,2,3,4-butanetetracarboxylic acid (BTCA) and ethylenediaminetetraacetic acid (EDTA), which have four carboxylic acid groups as $FB_1$ does (Figure 3.2), were used to estimate the acid dissociation constant (Ka) values of four carboxylic acid groups on $FB_1$ (Table 3.1). The $pKa_0$ of the amino group on $FB_1$ was 9.46, obtained from the chemical properties function on ChemDraw Professional 17.0 (Perkin-Elmer, Inc.). The simplified chemical equations of acid dissociation on $FB_1$ were

$$NH_3^+AH_4 \rightleftharpoons NH_3^+AH_3^- + H^+ \qquad Ka_1 = \frac{(H^+)(NH_3^+AH_3^-)}{(NH_3^+AH_4)}$$

$$NH_3^+AH_3^- \rightleftharpoons NH_3^+AH_2^{2-} + H^+ \qquad Ka_2 = \frac{(H^+)(NH_3^+AH_2^{2-})}{(NH_3^+AH_3^-)}$$

$$NH_3^+AH_2^{2-} \rightleftharpoons NH_3^+AH^{3-} + H^+ \qquad Ka_3 = \frac{(H^+)(NH_3^+AH^{3-})}{(NH_3^+AH_2^{2-})}$$

$$NH_3^+AH^{3-} \rightleftharpoons NH_3^+A^{4-} + H^+ \qquad Ka_4 = \frac{(H^+)(NH_3^+A^{4-})}{(NH_3^+AH^{3-})}$$

$$NH_3^+A^{4-} \rightleftharpoons NH_2A^{4-} + H^+ \qquad Ka_0 = \frac{(H^+)(NH_2A^{4-})}{(NH_3^+A^{4-})}$$
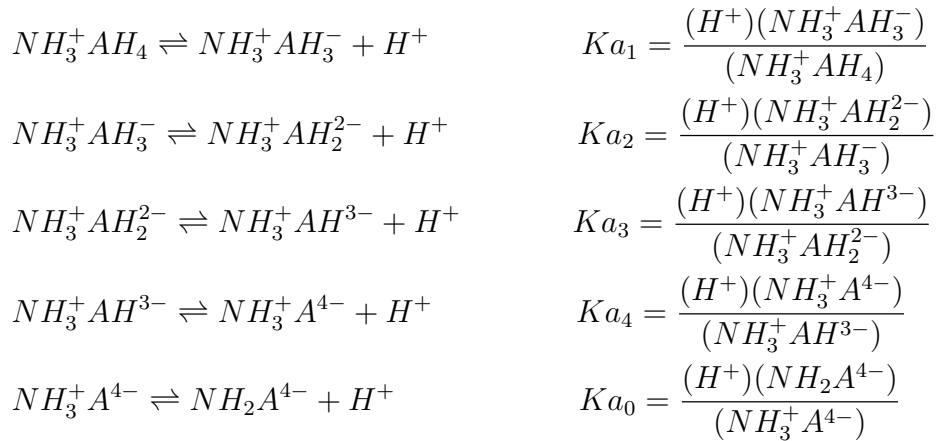
where the $NH_3^+AH_4$ represented the amino group-protonated $FB_1$, and $NH_3^+AH_3^-$, $NH_3^+AH_2^{2-}$, $NH_3^+AH^{3-}$, $NH_3^+A^{4-}$, and $NH_2A^{4-}$ represented $FB_1$ with one to four of the carboxylic acid groups and the amino group dissociated. The concentration of each species are

$$(NH_3^+AH_4) = \frac{(H^+)(NH_3^+AH_3^-)}{Ka_1}$$

$$(NH_3^+AH_3^-) = \frac{(H^+)(NH_3^+AH_2^{2-})}{Ka_2}$$

$$(NH_3^+AH_2^{2-}) = \frac{(H^+)(NH_3^+AH^{3-})}{Ka_3}$$

$$(NH_3^+AH^{3-}) = \frac{(H^+)(NH_3^+A^{4-})}{Ka_4}$$

$$(NH_3^+A^{4-}) = \frac{(H^+)(NH_2A^{4-})}{Ka_0}$$

Rearrangements of the equations give

$$(NH_3^+AH_3^-) = \frac{(NH_3^+AH_4)(Ka_1)}{(H^+)} \tag{3.1}$$

$$(NH_3^+AH_2^{2-}) = \frac{(NH_3^+AH_4)(Ka_1)(Ka_2)}{(H^+)^2} \tag{3.2}$$

$$(NH_3^+AH^{3-}) = \frac{(NH_3^+AH_4)(Ka_1)(Ka_2)(Ka_3)}{(H^+)^3} \tag{3.3}$$

$$(NH_3^+A^{4-}) = \frac{(NH_3^+AH_4)(Ka_1)(Ka_2)(Ka_3)(Ka_4)}{(H^+)^4} \tag{3.4}$$

$$(NH_2A^{4-}) = \frac{(NH_3^+AH_4)(Ka_1)(Ka_2)(Ka_3)(Ka_4)(Ka_0)}{(H^+)^5} \tag{3.5}$$

Table 3.1. The pKa values of 1,2,3,4-butanetetracarboxylic acid (BTCA) and ethylenediaminetetraacetic acid (EDTA).

| Chemical | Acid dissociation constants | | | |
|---|---|---|---|---|
| | pKa$_1$ | pKa$_2$ | pKa$_3$ | pKa$_4$ |
| 1,2,3,4-butanetetracarboxylic acid (BTCA)[a] | 3.25 | 4.51 | 5.02 | 6.54 |
| ethylenediaminetetraacetic acid (EDTA)[b] | 2.0 | 2.7 | 6.2 | 10.3 |

[a] Jolly and Bonizzoni (2014).
[b] Dawson et al. (1986).

The FB$_1$ concentration in the solution is the concentration sum of all the species, which can be displayed as

$$(FB_1) = (NH_3^+AH_4) + (NH_3^+AH_3^-) + (NH_3^+AH_2^{2-}) + (NH_3^+AH^{3-}) + (NH_3^+A^{4-})$$

$$+ (NH_2A^{4-})$$

$$= (NH_3^+AH_4) + \frac{(NH_3^+AH_4)(Ka_1)}{(H^+)} + \frac{(NH_3^+AH_4)(Ka_1)(Ka_2)}{(H^+)^2}$$

$$+ \frac{(NH_3^+AH_4)(Ka_1)(Ka_2)(Ka_3)}{(H^+)^3} + \frac{(NH_3^+AH_4)(Ka_1)(Ka_2)(Ka_3)(Ka_4)}{(H^+)^4}$$

$$+ \frac{(NH_3^+AH_4)(Ka_1)(Ka_2)(Ka_3)(Ka_4)(Ka_0)}{(H^+)^5}$$

The concentration of NH$_3^+$AH$_4$ species at different pH value can be calculated with the Ka values of BTCA or EDTA (Table 3.1), and the other species can be derived with equations (3.1) to (3.5).

$$log(NH_3^+AH_4) = log(FB_1) - log\left(1 + \frac{(Ka_1)}{(H^+)} + \frac{(Ka_1)(Ka_2)}{(H^+)^2} + \frac{(Ka_1)(Ka_2)(Ka_3)}{(H^+)^3}\right.$$

$$\left. + \frac{(Ka_1)(Ka_2)(Ka_3)(Ka_4)}{(H^+)^4} + \frac{(Ka_1)(Ka_2)(Ka_3)(Ka_4)(Ka_0)}{(H^+)^5}\right)$$

The fraction of each species was calculated at pH value between 2.5 to 9.5. The FB$_1$ concentration used to estimate the NH$_3^+$AH$_4$ species was $1.11 \times 10^{-5}$ M (8 mg/L).

### 3.2.3 Synthesis of fumonisin B$_1$-smectite complexes at different pH

The smectite was mixed with FB$_1$ in an equivalent of 20 % of the clay mass at pH 3, 4, 5, and 6 and washed twice with blank solutions at the same pH. To synthesize 20% FB$_1$-Sm complexes, 100 μL of 1000 mg/L FB$_1$ solution was mixed with 5 mL HCl blank solution at desired pH value in 15-mL centrifuge tubes containing 0.5 mg of 4TX smectite sample. The mixture in centrifuge tubes was shaken overnight at 200 rpm. After centrifuging at 3000 rpm for 5 min, the supernatant was collected for pH value measurement, and the solid residues were washed twice (5 mL and 2 mL) with respective HCl blank solution at the same pH value. These FB$_1$-smectite complexes were used for further XRD and FTIR analysis.

### 3.2.4 Characterization of fumonisin B$_1$-smectite complexes

Each FB$_1$-smectite sample was investigated using X-ray diffraction (XRD). The XRD analysis was performed on a Bruker D8 Advance (Bruker, Madison, WI), using X-ray diffractometer with a CuK$\alpha$ source operated at 35 kV and 45 mA, and a SolX (Bruker, Madison, WI) energy dispersive detector. The XRD patterns were recorded at 30°C under room humidity ($\sim$ 61 %) and 0 % humidity (N$_2$ purged). The samples saturated with FB$_1$ at pH 3 and without FB$_1$ were also investigated with variable temperature XRD using the XRK 900 reactor chamber. The XRD pattern of the samples was recorded at each 25°C interval when they were heated from 100 to 300°C; but with a 50°C interval from 350 to 500°C . The purpose of heating treatments was to remove the interlayer water, therefore, to determine the interlayer accessibility of smectite to FB$_1$.

The infrared patterns of FB$_1$-smectite samples at different pH were recorded with Fourier-transform infrared (FTIR) spectroscopy using the attenuated total reflectance (ATR) accessory. The FB$_1$-smectite suspension was air-dried on the diamond crystal, and the FTIR spectra were recorded with a resolution of 1 cm$^{-1}$ and 64 scans using a Spectrum 100 Fourier transform infrared spectrometer (Perkin-Elmer, Inc.).

### 3.2.5  Effects of pH on fumonisin B$_1$ adsorption

The effects of pH on FB$_1$ adsorption on smectite, 4TX, was conducted in the range of pH from 3 to 7. A series of solutions with pH 3, 4, 5, 5.2, 5.4, 5.6, 5.8, 6, and 7 was prepared from 1 mM HCl solution and adjusted with NaOH solution. FB$_1$ working solutions (8 mg/L) were diluted from 1000 mg/L stock solution with respective pH solution. Fifty microliters of Na-4TX dispersion containing 0.1 mg of smectite was mixed with 5 mL of 8 mg/L FB$_1$ solution in 15-mL centrifuge tubes. After shaking overnight at 200 rpm, the supernatant was filtered through 0.2 μm pore size membrane filters, and the concentration of FB$_1$ was quantified by reversed-phase high-performance liquid chromatography (HPLC). The final pH of the filtrate were measured after overnight adsorption. All experiments were conducted in triplicate.

### 3.2.6  Adsorption isotherm of fumonisin B$_1$ at different pH values

Three different pH, 4, 5.5, and 7, were selected to test the pH effects on FB$_1$ adsorption isotherm. The adsorption isotherm procedures were described in Kannewischer et al. (2006). Dilutions from 1000 mg/L stock solution were made to prepare 8 mg/L FB$_1$ solutions in deionized water with respective pH values. The concentrations were 0.0, 0.4, 1.6, 3.2, 4.8, 6.4, and 8.0 mg/L with a total volume of 5 mL and a volume of 50 μL of the 4TX smectite dispersion containing 0.1 mg of smectite sample was added into each isotherm point. After overnight shaking at 200 rpm and room temperature, the samples were filtered through 0.2 μm pore size membrane filters, and the FB$_1$ concentration in the supernatant was quantified using an HPLC. The adsorbed FB$_1$ was plotted against the equilibrium concentration to fit the Langmuir model (LM). This adsorption experiment conducted in triplicate.

### 3.2.7   Quantification of fumonisin $B_1$ by high-performance liquid chromatography (HPLC)

Reversed-phase HPLC (Agilent Technologies 1200 Series) (Agilent Technologies, Santa Clara, CA) was used to quantify $FB_1$ remaining in the supernatant after adsorption. $FB_1$ was separated on a C18 analytical column (2.6 μm particle size, 100 Å pore diameter, and $100{\times}4.6$ mm dimensions) fitted with a guard column (Model: AJ0-9000) (Phenomenex, Torrance, CA). The $FB_1$ analysis was performed based on a reference AOAC official analytical method 995.15 with minor modification (AOAC, 2000). The mobile phase was a mixture of methanol: 0.1 M $NaH_2PO_4$ (77:23, v/v) with the pH value adjusted to 3.3 with $H_3PO_4$ and the flow rate set at 1 mL/min. Fluorescence was detected by excitation at 335 nm and emission at 440 nm. The $FB_1$ solutions were derivatized with *o*-phthaldialdehyde (OPA) reagent (Sigma-Aldrich Inc., St. Louis, MO) before injected into HPLC: 100 μL of OPA reagent was mixed with 100 μL $FB_1$ solution, and 20 μL of the mixture was injected into HPLC within 2 min after adding OPA reagent.

### 3.3   Results

### 3.3.1   Estimation of chemical species of fumonisin $B_1$ at different pH

There are four carboxylic acid groups and one amino group on the $FB_1$ molecule (Figure 3.1). Unfortunately, the dissociation constants of fumonisins are unknown. The estimated $pKa_0$ of the amino group should be in the range of 9 to 11 according to known pKa values of other amino compounds. The pKa values of butane-1,2,3,4-tetracarboxylic acid (BTCA) and ethylenediaminetetraacetic acid (EDTA) were used as the estimated values of $FB_1$ (Table 3.1).

Despite the uncertainty of the pKa values, the estimation using the values of BTCA and EDTA suggested that the $FB_1$ should exist predominantly as a cationic species at pH 3.3 or lower pH and an anionic species with one to four carboxylic groups dissociated above pH 3.3 (Figure 3.3). The amino group deprotonates and at a very high pH value. It can be expected that the cationic species will be adsorbed by the negatively charged smectite and the anionic species will be repulsed.
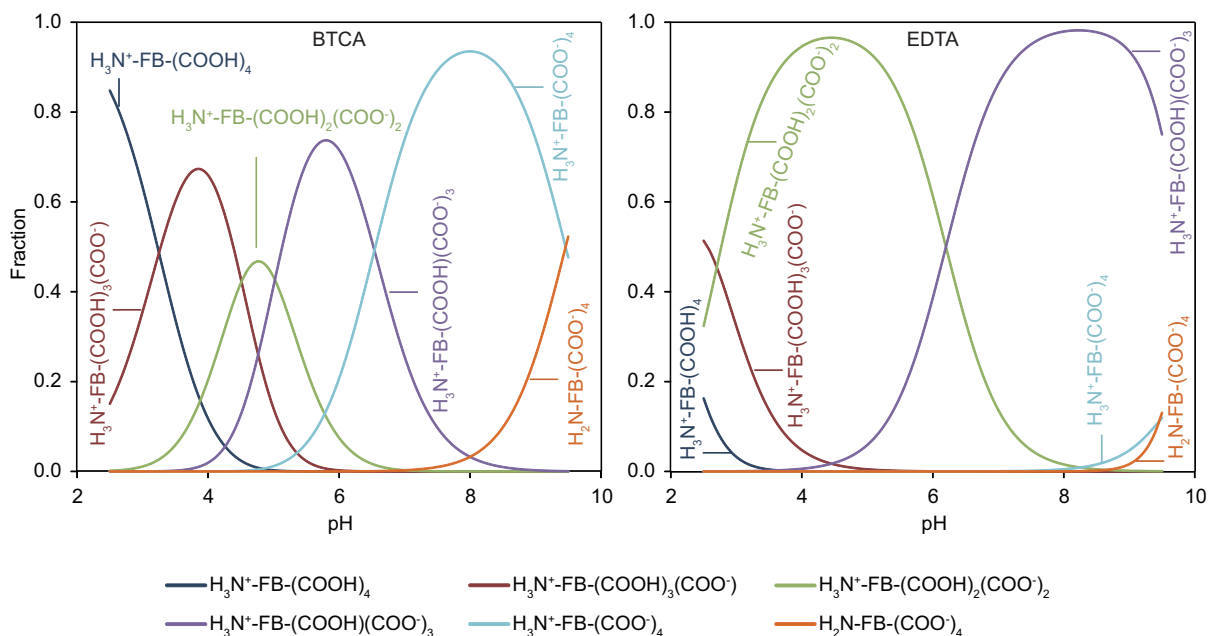
Figure 3.3. Speciation estimation of FB$_1$ using pKa vales of butane-1,2,3,4-tetracarboxylic acid (BTCA) and ethylenediaminetetraacetic acid (EDTA).

### 3.3.2  Evidence of interlayer adsorption of FB$_1$ on smectite at low pH

The basal spacing of Na-4TX smectite was 11.4 Å at room humidity and was expanded to ~14 Å after adsorbing FB$_1$ (Figure 3.4). Heating this FB$_1$-smectite complex at higher temperatures resulted in the gradual reduction of the basal spacing to about 12 Å at 400°C  and to about 9.9 Å at 500°C. On the contrary, the smectite without adsorbing FB$_1$ collapsed to 9.7 Å at 100°C  or higher temperatures. The higher basal spacing of FB$_1$-smectite at elevated temperatures suggested that FB$_1$ can access the interlayer space of smectite at low pH. The basal space response to heating indicated a ~13 Å d-spacing after dehydration between 100-250°C. The 3Å d-spacing increase suggested there was only one layer of FB$_1$ in the interlayer of smectite.
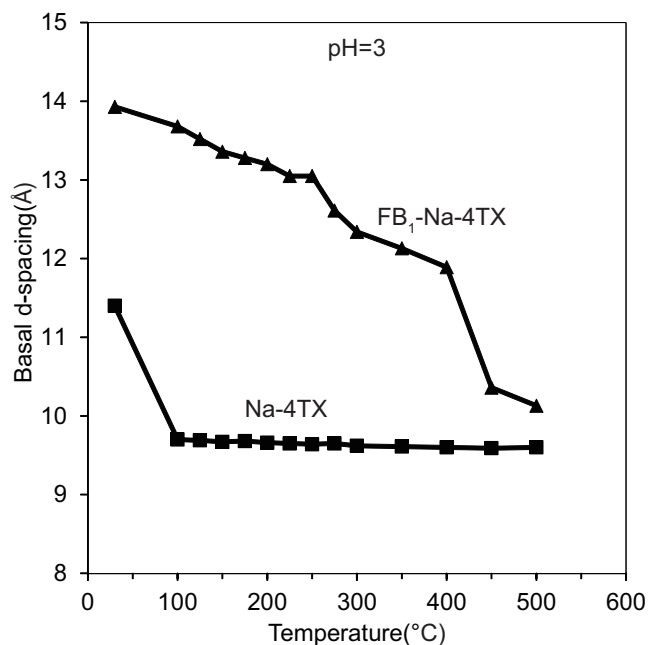
Figure 3.4. The basal d-spacing of smectite (Na-4TX) and $FB_1$-smectite ($FB_1$-Na-4TX) complex at pH 3 after heating at elevated temperatures.

### 3.3.3 Effects of solution pH on the interlayer access of $FB_1$ in smectite

Without adsorbing $FB_1$, the smectites had basal spacings of greater than 12 Å at room humidity and reduced to 9.8 Å at 0 % humidity with $N_2$ purge. After adsorbing $FB_1$, the highest expansion of the smectite was observed as 14.4 Å basal spacing at pH 3 (room humidity). This basal spacing was not reduced after $N_2$ purged, suggesting interlayer adsorption. After adsorbing $FB_1$, the basal spacing of smectite was still about 14 Å with slightly decreased with an increase in pH from 3 to 5 at 0 % humidity as observed on the XRD patterns (Figure 3.5 left), suggesting the interlayer adsorption of $FB_1$ persisted up to pH 5. At pH 6, the basal spacing collapsed to about 10 Å. The decreased adsorption is most likely due to the formation of anionic fumonisin species from dissociation.

The presence of $FB_1$ in the interlayer of smectite 4TX was also detected by the new absorption bands corresponding to $FB_1$. Infrared analysis (Figure 3.6) suggested some band changes on smec-

53
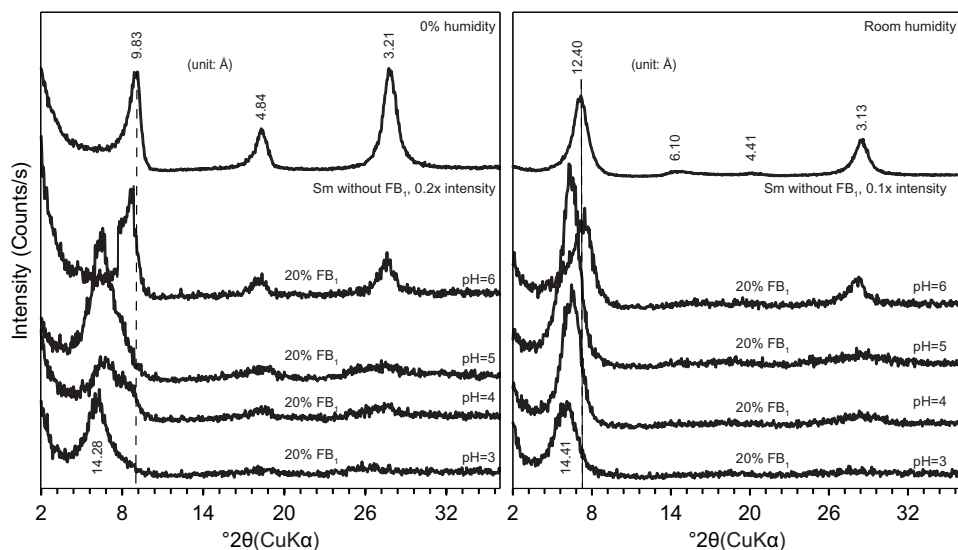
Figure 3.5. XRD patterns of smectites at 0 % humidity (left) and room humidity (right) after adsorbing $FB_1$ at different pH values.

tite after adsorbing $FB_1$. The adsorbed $FB_1$ in smectite 4TX interlayer induced an emergence of new bands at 2937, 2859, 1732, and broad bands between 1300 to 1500 $cm^{-1}$ assigned to the asymmetric stretching of $-CH_2$, symmetric stretching of $-CH_2$, carboxyl group (C=O), and bending of $-CH_2$, respectively. The intensity changes of $FB_1$ bands with pH were consistent with the XRD patterns (Figure 3.5). The intensity of 2937 and 2859 $cm^{-1}$ bands decreased when pH increased from 3 to 6. The same phenomenon can be observed from the three bands at 1436, 1396, and 1376 $cm^{-1}$. The infrared bands of $FB_1$ were broad and showed shifts from 1732 $cm^{-1}$ to 1718 $cm^{-1}$ (14 $cm^{-1}$ redshifts) when the $FB_1$ was adsorbed to smectite 4TX. As the samples were washed two times with respective blank HCl solution, the persistence of $FB_1$ infrared bands indicated the resistance of adsorbed $FB_1$.

### 3.3.4 Effects of pH on fumonisin $B_1$ adsorption

Figure 3.7 shows $FB_1$ adsorption on 4TX as a function of $FB_1$ solution pH. Adsorption of $FB_1$ decreased linearly with increase in solution pH. The decreased trend of the curve indicated that the
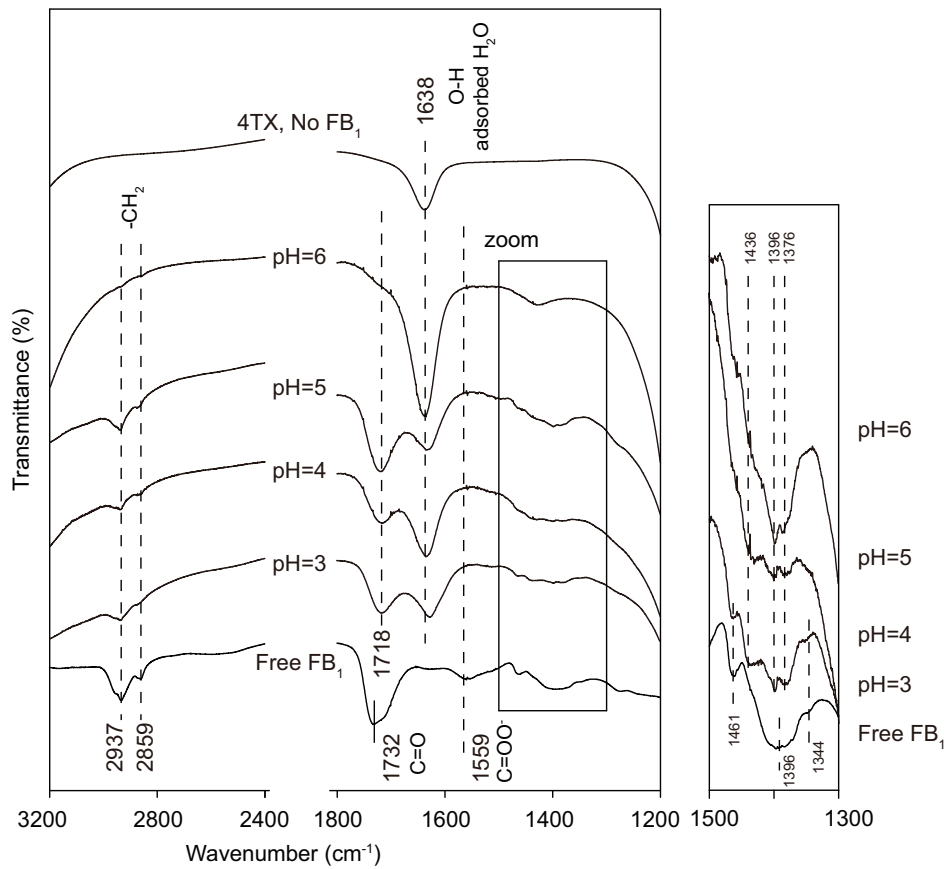
Figure 3.6. Infrared spectra of $FB_1$ (bottom), smectite before (top) and after adsorbing $FB_1$ at different pH.
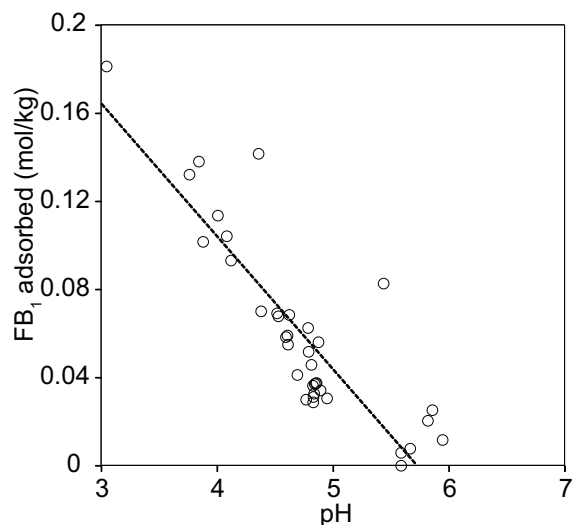
Figure 3.7. $FB_1$ adsorption on 4TX at different pH.

cationic species of $FB_1$ existed in the lower range of pH value. The rapidly decreased adsorption of $FB_1$ at pH>3.7 suggested the $pKa_0$ value of $FB_1$ should occur below pH 3.7, which was consistent with the estimated pKa value of 3.3 by BTCA compound and of 3.3 by ChemDraw Professional 17.0 (Perkin-Elmer, Inc.).

Figure 3.8 shows the $FB_1$ adsorption isotherm on 4TX carried out at three pH values. The adsorption data were fitted to the Langmuir equation to evaluate the pH effects on adsorption capacity and affinity parameter ($K_d$) for $FB_1$. The estimated $Q_{max}$ values of adsorbed $FB_1$ by Langmuir equation were 0.33 mol/kg at pH 4, 0.06 mol/kg at pH 5.5, and 304.5 mol/kg at pH 7. At higher pH, i.e. pH 7, smectite 4TX showed an unreality $Q_{max}$ value due to the adsorption data points was linear and too far away from the L-shape. The pH value of $FB_1$ solution strongly influenced the affinity of $FB_1$ adsorbed to smectite 4TX. A significantly increase in adsorption affinity ($K_d$= 0.99 $\mu M^{-1}$) was observed at pH 4 compared to at solution pH 5.5 ($K_d$= 0.38 $\mu M^{-1}$) and 7 ($K_d$= $8.3 \times 10^{-6} \mu M^{-1}$). The adsorption isotherms at different pH showed that the adsorbed $FB_1$ was electrostatically bound to the negative charge of smectite 4TX. Thus, $FB_1$ with lower pH value showed higher affinity and adsorption capacity.
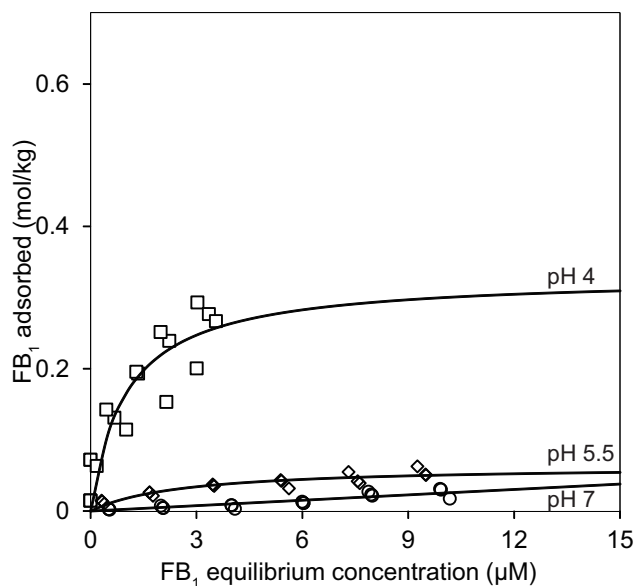
Figure 3.8. Adsorption isotherm of $FB_1$ at different pH.

## 3.4 Discussion

$FB_1$, with four carboxylic acid groups and one amino group, can be present in zwitterionic, cationic, or anionic forms depend on the pH of the solution. The pH value had profound effects on the adsorption of amphiphilic molecules by adsorbents (active carbon, montmorillonite, palygorskite, etc.) (Brown et al., 2014; Monge et al., 2016; Zermane et al., 2005; Hajjaji and Alami, 2009; Berhane et al., 2016). However, the effects of solution pH varied with the properties of adsorbed compounds. The adsorption of methylene blue by smectite-rich clay was enhanced with increasing pH through increasing the amount of monomers and dimers of methylene blue to be adsorbed (Hajjaji and Alami, 2009). Changing pH might not affect the adsorption capacity when the pH was below the pKa value of a zwitterionic compound. Two substantial adsorption drops were observed at pH values corresponding to $pKa_1$ and $pKa_2$ of ciprofloxacin on a palygorskite-montmorillonite mixture, suggested a repulsion between the deprotonation part of the compound and the adsorbent. At pH values between $pKa_1$ and $pKa_2$, a relatively slow adsorption decrease

57

was due to the formation of zwitterion from deprotonation of the carboxylic group and protonation of the secondary amine group (Berhane et al., 2016). In this study, however, the formation of zwitterion resulted in dramatical adsorption decreased with pH increasing. The decrease of adsorption with pH increase can be attributed to deprotonation of $FB_1$. $FB_1$ speciated as a function of pH and existed predominantly as cationic in the lower pH up to 3.3 through protonation of the amine group and no dissociation of the carboxyl group (Figure 3.1), thus, increasing the adsorption capacity. The estimated $Q_{max}$ of $FB_1$ at pH 4 were 0.33 mol/kg, equalling to 60% of added $FB_1$. On the other hand, the cation exchange capacity of Na-4TX was 81.2 cmol/kg, suggesting the maximum adsorption capacity would be 0.812 mol/kg if all cation in the interlayer were replaced by $FB_1$ (the $AH_5^+$ species). This result implied at pH 4, $FB_1$ can only replace 40% of the interlayer cation ($Na^+$).

Infrared analysis helps the understanding of structural features of molecules such as functional groups and chemical bonds and gives more information to identify the bonding mechanism. In the range of 1350 to 1450 $cm^{-1}$, the broad band might form due to overlap, corresponding to -$CH_2$ scissoring and combination of C-O bending and stretching of the carboxylate ion (-$COO^-$) (Gautier et al., 2009; Max and Chapados, 2004). For instance, a value of $1397\pm36$ $cm^{-1}$ for -$CH_2$ deformation scissoring and $1406\pm12$ $cm^{-1}$ for -$CO_2$ symmetric stretching of 22 species of 9 carboxylic acids were reported. However, three distinct bands, 1436, 1396, 1376 $cm^{-1}$, were split and seen after the $FB_1$ was adsorbed onto smectite 4TX, suggesting same adsorption mechanism might occur between $FB_1$ and smectite from pH 3 to 6. This implied the adsorption of $FB_1$ might drove by the electrostatically force between the protonated amino group of $FB_1$ and negative charge of smectite in the test pH range. Furthermore, the decrease in adsorption of $FB_1$ was attributed to the increasing amount of dissociated carboxyl group, resulting in the higher repulsion force between $FB_1$ and smectite. However, fully dissociation of the four carboxyl groups on $FB_1$ was not achieved up to pH 7 by indication of 1718 $cm^{-1}$ band presence.

## 3.5 Conclusion

Smectite 4TX was able to adsorb $FB_1$ in its interlayer at low pH. The adsorption capacity had an inverse relationship with the solution pH. The theoretical estimation suggested $FB_1$ exists as anionic form at pH above 4.4, and the adsorption of $FB_1$ at pH value beyond this point will greatly decrease due to more repulsion interaction. Isothermal adsorption data indicated at pH 7, adsorption of $FB_1$ can still be observed. The XRD and FTIR results confirmed the interlayer accessibility of smectite by $FB_1$ up to pH 6.

# 4. SYNTHESIZED LAYERED DOUBLE HYDROXIDES (LDHS) AS FUMONISIN $B_1$ BINDERS

## 4.1 Introduction

Fumonisins are a group of aliphatic mycotoxins identified in 1980's, and they are mainly produced by *Fusarium moniliform* and *F. proliferatum*. There are 28 distinct fumonisins. They are categorized as fumonisin A, B, C, and P. Fumonosin $B_1$ (FB$_1$) is the most toxic and the most abundant fumonisin (Gelderblom et al., 2007). Fumonosin $B_1$ is a common contaminant of cereal grains worldwide, particularly in maize. The FB$_1$ has been linked to leukoencephalomalacia (LEM) in horses, and human esophageal cancer (Marasas et al., 1988).

One of the promising technologies to inactivate mycotoxins in feed and food is adsorption approach. Numerous materials such as bentonite, zeolite, activated carbon, and processed bentonite NovaSil (NS) clay have been proposed and proved to be effective mycotoxins binders (Galvano et al., 1997; Marroquín-Cardona et al., 2009; Wang et al., 2008; Dakovic et al., 2010; Kubena et al., 1991). The binding efficiency of the adsorbents for mycotoxins is determined by the structure, physical, and chemical properties of both adsorbent and the adsorbed mycotoxin.

Layered double hydroxides (LDHs) are hydrotalcite-like compounds with the ability of intercalation of anionic compounds. They are widely used as anionic adsorbents, catalysts and catalyst supports, photo-catalysts, anion exchangers, drug delivery, and bonding materials (Gu et al., 2018; Cavani et al., 1991; Khan and O'Hare, 2002; Wang and O'Hare, 2012). LDHs have high specific surface area (20-120 m$^2$/g) and high anion exchange capacity (200-500 cmol(-)/kg) and are widely used as anionic pollutant adsorbents (Miyata, 1980, 1983).

The isomorphic substitution of divalent cations by trivalent cations in the layered double hydrox-

ides (LDHs) results in excess positive charges within the layers, which are balanced by the inter-layer anions. The chemical composition of LDHs is generally expressed as

$$[M^{2+}_{1-x}M^{3+}_x(OH)_2]^{x+}X^{m-}_{x/m} \cdot nH_2O$$
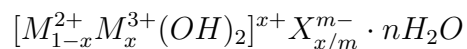
where $M^{2+}= Ca^{2+}$, $Mg^{2+}$, $Ni^{2+}$, $Mn^{2+}$, $Fe^{2+}$; $M^{3+}= Al^{3+}$, $Fe^{3+}$, $Mn^{3+}$, $Cr^{3+}$; and $X^-= Cl^-$, $Br^-$, $NO_3^-$, $SO_4^{2-}$, $PO_4^{2-}$, $CO_3^{2-}$.

Numerous studies on adsorption of anionic organic and inorganic contaminants by LDHs have demonstrated their effectiveness in removing both inorganic and organic anions, such as phosphate, chromate, arsenate, arsenic, arsenite, selenate, and phthalocyanines (Chibwe and Jones, 1989; Carrado et al., 1993; Rhee et al., 1997; Goswamee et al., 1998; You et al., 2001; Wang et al., 2006; Yang et al., 2005; Seida and Nakano, 2002). The adsorption efficiency of LDHs depends on synthesis condition, solution pH, and types of contaminant. Layer charge density and interlayer anion type of LDHs are two factors affected their adsorption capacity (You et al., 2001; Kooli et al., 1995; Parker et al., 1995).

FB$_1$ is a long hydrocarbon chain containing hydroxyl, amino, and carboxyl groups (Figure 4.1). With amino and carboxyl groups in its structure, FB$_1$ can be protonated at low pH and exist as an anion when pH increased (Chapter 3). Smectite in bentonite, as an adsorbent, has the negative charge from substitutions to adsorb cationic FB$_1$ at low pH, while at higher pH, no adsorption of FB$_1$ is expected. The aims of this study were to synthesize LDHs as a potential FB$_1$ binder in alkaline solution and to investigate layer charge density effects of LDHs on FB$_1$ adsorption.
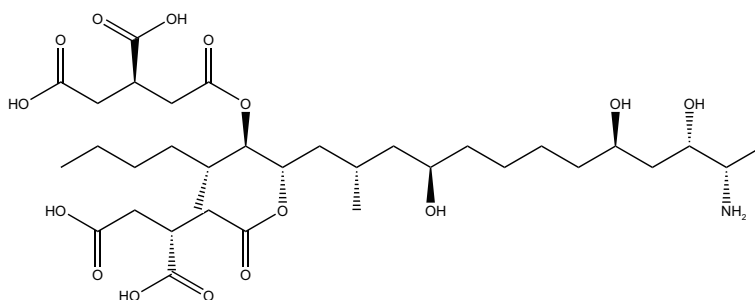
Figure 4.1. Chemical structure of fumonisin $B_1$.

## 4.2 Materials and methods

### 4.2.1 Preparation of layered double hydroxides

The Mg/Al-LDHs were synthesized by using a constant pH co-precipitation method (Chao et al., 2008; He et al., 2006). Mixed metal solutions containing magnesium nitrate and aluminium nitrate were prepared by dissolving $Mg(NO_3)_2 \cdot 6H_2O$ and $Al(NO_3)_3 \cdot 9H_2O$ in deionized water with a total concentration of 1.0 M. The $Al^{3+}/Mg^{2+}$ ratio of LDH3, LDH4, and LDH5 were 0.33/0.67, 0.25/0.75, and 0.2/0.8 to achieve the $Al^{3+}/(Al^{3+}+Mg^{2+})$ molar ratios at 1/3, 1/4, and 1/5.

One hundred mL of each ratio of mixed nitrate salt solution was added dropwise into 200 mL of deionized water with 5 ml/min flow rate. The pH of the mixture was maintained at 10±0.2 by addition of 2 M NaOH. Upon the addition of the nitrate salt solution was complete, the LDH suspension was aged for 1 hour at room temperature following by 18 hours at 65°C. After centrifugation, the supernatant was decanted, and the precipitate was washed with deionized water to remove any excess salts. Afterward, part of the collected solid was drying in an oven at 95°C for further chemical composition analysis and the rest were dispersed in deionized water for adsorption experiments. All the experiments were conducted with carbonate-free deionized water and with $N_2$ gas purging during the synthesis process to avoid interlayer $CO_3^{-2}$ combination with hydroxide layer.
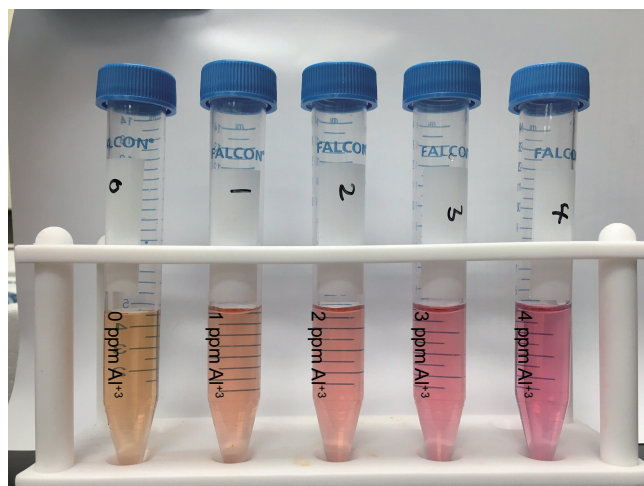
Figure 4.2. Color changes of $Al^{3+}$ solution at different concentration with addition of Eriochrome cyanine R dye.

### 4.2.2 Layered double hydroxides characterization

#### 4.2.2.1 Chemical composition

The synthesized layered double hydroxides were digested in an acid solution to quantify the $Mg^{2+}$ and $Al^{3+}$ contents. Ten mg samples were dissolved in 10 mL of 8 N HCl. The digestion solution was brought to 100 mL with deionized water after overnight shaking at 200 rpm. The dissolved $Mg^{2+}$ in digestion solutions was determined by using ion chromatography (Dionex DX-500, Sunnycale, CA, USA), and the content of $Al^{3+}$ in digestion solution was determined by a colorimetric method with the Eriochrome cyanine R dye (APHA et al., 1998). The mixture of Eriochrome cyanine R dye and diluted aluminum solutions produced a red to pink complex (Figure 4.2) which exhibited a maximum absorption at 535 nm. The carbon and nitrogen contents of the LDH powder samples were obtained with a Thermo Finnigan Flash EA 1112 elemental analyzer.

#### 4.2.2.2 X-ray diffraction

The three LDH, LDH3, LDH4, and LDH5, were air dried on glass discs to form thin films and investigated using X-ray diffraction by a Bruker D8 Advance X-ray diffractometer (Bruker, Madi-

son, WI). The diffractometer was operated at 40 kV and 40 mA using CuK$\alpha$ radiation source and SolX energy dispersive detector with step a size of 0.05°2$\theta$ and a dwell time of 5 seconds per step.

### 4.2.2.3  *Fourier-transform infrared spectroscopy analysis*

Each LDH sample was air dried as a film on a ZnS window with diameter of 25 mm and thickness of 2 mm (ClearTran, International Crystal Labs, Garfield, New Jersey, USA) for FTIR study. The FTIR spectra were recorded in the transmission mode with a resolution of 2 cm$^{-1}$, and a total of 32 scans were collected on a Spectrum 100 Fourier transform infrared spectrometer (Perkin-Elmer).

## 4.2.3   Fumonisin B$_1$ adsorption on LDHs

### 4.2.3.1  *Effects of layer charge density of LDH on FB$_1$ adsorption*

Fumonisin B$_1$ was obtained from Sigma-Aldrich Inc. (St. Louis, MO). The solvent used to prepare the 1000 mg/L FB$_1$ stock solution was a mixture of acetonitrile: water (1:1, v/v). Ten milligrams of FB$_1$ powder was dissolved in 10 mL of solvent in 10-mL volumetric flask and then diluted to 200 mg/L with deionized water. The volumetric flasks of 200 mg/L stock solution were wrapped with aluminum foil and stored at 4 °C for further uses.

A dilution was made to prepare an 8 mg/L FB$_1$ working solution in deionized water. To add the small amount of LDHs into each concentration, the LDHs dispersions were diluted in deionized water to make 2 mg/mL clay suspensions. Afterward, 50 μL of LDH3, LDH4, or LDH5 suspension was added into each test tube containing 5 mL of 8 mg/L mycotoxin solution. The mixtures were shaken overnight at 200 rpm on a rotary shaker and filtered through 0.2 μm filters. Quantification of FB$_1$ in clear filtrates was performed by reversed-phase high-performance liquid chromatography (HPLC). All experiments were conducted in triplicate.

*4.2.3.2   Fumonisin B₁ adsorption isotherm on LDH3*

The adsorption isotherms were conducted with batch experiment (Kannewischer et al., 2006). To prepare the working solution for isotherms, an aliquot of the stock solution was diluted with deionized water to 8 mg/L. The isotherm experiments were conducted by adding 0.1 mg LDH3 powder to each 5 mL of 0.0, 0.4, 1.6, 3.2, 4.8, 6.4, and 8.0 mg/L $FB_1$ solution. After shaking for 24 hours at 200 rpm, the samples were filtered through 0.2 μm pore size membrane filters. The adsorption of $FB_1$ was calculated from the difference between the initial and final concentrations, and the data were applied to the Langmuir equation. This study was conducted in triplicate and then averaged.

*4.2.3.3   Effects of solution pH on FB₁ adsorption on LDH3*

Fumonisin $B_1$ adsorption on LDH3 was conducted at 5 different pHs. To obtain $FB_1$ solution in different pH, 50 mL of 8 mg/L $FB_1$ working solutions were diluted from 200 mg/L stock solution with addition of different amounts of 2.5 mM NaOH solution (50, 25, 5, 2.5, and 1 mL). Each adsorption point had a total volume of 5 mL. A volume of 50 μL of the LDHs dispersion containing 0.1 mg of LDH was used for each pH adsorption. After shaking overnight at 200 rpm, the supernatant was filtered through 0.2 μm pore size membrane filters, and the concentration of $FB_1$ was quantified by reversed-phase high-performance liquid chromatography (HPLC). The final pH values of the filtrate were measured after overnight adsorption. The experiments were conducted in duplicate.

### 4.2.4   Quantification of fumonisin B₁

Fumonisin $B_1$ was quantified by reversed-phase high-performance liquid chromatography (HPLC) with Agilent Technologies 1200 Series pump and fluorescence detector (Agilent Technologies, Santa Clara, CA). The separation was carried out on a C18 analytical column with a particle size of 2.6 μm, a pore diameter of 100 Å, and dimensions of 100×4.6 mm (Phenomenex, Torrance, CA).

Fumonisin $B_1$ analysis was performed based on a reference AOAC official analytical method 995.15 with minor modification (AOAC, 2000). A mixture of methanol: 0.1 M $NaH_2PO_4$ (77:23, v/v) with the pH value adjusted to 3.3 with $H_3PO_4$ was used as the mobile phase at a flow rate of 1 mL/min. The excitation and emission wavelengths were 335 nm and 440 nm, respectively, and the retention time was around 2 min. For the standard curve, $FB_1$ solutions concentration at 0.0, 0.4, 0.8, 1.6, 2.4, 3.2, 4.0, 4.8, 5.6, 6.4, 7.2 and 8.0 mg/L were measured. $FB_1$ solutions were derivatized with $o$-phthaldialdehyde (OPA) reagent (Sigma-Aldrich Inc., St. Louis, MO) before injecting into HPLC. One hundred μL of OPA reagent was transferred into 100 μL $FB_1$ solution, and 20 μL was injected within 2 min after adding OPA reagent.

The $o$-phthaldialdehyde reagent was prepared by dissolved 40 mg of OPA in 1 mL methanol and diluted with 5 mL of 0.1 M disodium tetraborate. A 2-mercaptoethanol solution (50 μl) was then added into the reagent and thoroughly mixed. This OPA reagent was stored in an aluminum foil wrapped vial for up to 1 week.

### 4.2.5 Synthesis of fumonisin $B_1$-LDH complexes at different pH

The LDH3, LDH4, and LHD5 were mixed with $FB_1$ in an equivalent of 20 % of the clay mass at an alkaline high pH and a neutral pH. To synthesize $FB_1$-LDH complexes, 1 mL of 200 mg/L $FB_1$ solution was mixed with 4 mL of 3.125 mM NaOH or deionized water in 15-mL centrifuge tubes containing 1 mg of LDH3, LDH4, or LDH5. The mixture in centrifuge tubes was shaken overnight at 200 rpm. After centrifuging at 4300 rpm for 10 min, the supernatant was collected for pH value measurement and the solid residues were washed twice (5 mL and 2 mL) with respective pH solution (2.5 mM NaOH or deionized water). These $FB_1$-LDH complexes were used for further XRD and FTIR analysis.

66

### 4.2.6   Characterization of fumonisin $B_1$-LDH complexes

The $FB_1$-LDH complexes were air dried on the polished side of silicon plates (0.407 mm$\times$130 mm$\times$150mm) cut from a (100) silicon wafer (University Wafers, Boston, Massachusetts, USA) for X-ray diffraction analysis. A Bruker D8 Advance diffractometer with a CuK$\alpha$ radiation source and a Sol-X detector was used to record the diffraction patterns. The diffractometer was operated at 40 kV and 40 mA with a step size of 0.05°2$\theta$ and a dwell time of 5 seconds per step. A portion of the $FB_1$-LDH complex was air dried on a ZnS window for FTIR analysis. The spectra were recorded in transmission mode with 32 scans and a resolution of 2 cm$^{-1}$.

### 4.3   Results

### 4.3.1   LDHs characterization

#### 4.3.1.1   Chemical composition

The $Al^{3+}/(Mg^{2+}+Al^{3+})$ molar ratios of synthesized LDHs were determined to be 0.32, 0.22, and 0.17, which were similar to the initial molar concentration of the starting mixed metal solutions (Table 4.1). Since the positive charges of LDHs resulted from the isomorphous substitution of aluminum for magnesium, the interlayer counterbalanced nitrate was increased as the amount of aluminum increased. Even though nitrogen gas purge and carbonate-free deionized water were used in the synthesis process, a small amount of carbonate contamination was detected.

#### 4.3.1.2   X-ray diffraction

Figure 4.3 gives the powder XRD patterns and their corresponding basal spacing values for the three Mg/Al-NO$_3$ LDHs with different starting $Al^{3+}/(Al^{3+}+Mg^{2+})$ ratios in solution: (a) LDH3, $Al^{3+}/(Al^{3+}+Mg^{2+})$=1/3, (b) LDH4, $Al^{3+}/(Al^{3+}+Mg^{2+})$=1/4, and (c) LDH5, $Al^{3+}/(Al^{3+}+Mg^{2+})$=1/5. Compared with LDH3 and LDH4, the sharper reflections of LDH5 indicated a larger crystallite. The $d_{003}$ values of LDH3, LDH4, and LDH5 corresponding to the basal spacing of two consecu-

Table 4.1. Chemical composition of LDHs.

| LDHs | Structural composition (mmol/g) | | | | Molar ratio $Al^{3+}/(Mg^{2+}+Al^{3+})$ | | $AEC^a$ (mol/kg) | Structural formula |
|---|---|---|---|---|---|---|---|---|
| | Al | Mg | N | C | initial | experimental | | |
| LDH3 | 3.73 | 8.07 | 1.94 | 0.53 | 0.33 | 0.32 | 4.23 | $Mg_{0.68}Al_{0.32}(OH)_2(NO_3)_{0.22}(CO_3)_{0.05}$ |
| LDH4 | 2.66 | 9.23 | 1.81 | 0.57 | 0.25 | 0.22 | 3.15 | $Mg_{0.78}Al_{0.22}(OH)_2(NO_3)_{0.14}(CO_3)_{0.04}$ |
| LDH5 | 1.99 | 9.79 | 1.77 | 0.4 | 0.20 | 0.17 | 2.53 | $Mg_{0.83}Al_{0.17}(OH)_2(NO_3)_{0.11}(CO_3)_{0.03}$ |

[a] Anion exchange capacity was calculated based on molecular weight and corresponding $Al^{3+}$ content.

Table 4.2. Interlayer spacing of Mg/Al-$NO_3$ layered double hydroxides.

| Sample | Thickness of the hydroxide layer (Å) | $d_{003}$ | Interlayer spacing (Å) | Interlayer nitrate orientation |
|--------|--------------------------------------|-----------|------------------------|-------------------------------|
| LDH3   |       | 8.28 | 3.51 | tilted     |
| LDH4   | 4.77  | 7.94 | 3.17 | horizontal |
| LDH5   |       | 7.93 | 3.16 | horizontal |

tive hydroxide layers were 8.28, 7.94, and 7.93 Å, respectively. As basal spacing increased with layer charge density, the configuration of interlayer nitrate changed from single layer to multiple layers was proposed (Xu and Zeng, 2001). The height of the interlayer spacing was calculated by subtracting the thickness of the hydroxide layer (4.77 Å) from the $d_{003}$ (Zigan and Rothbauer, 1967) and showed in Table 4.2. The interlayer spacing of LDHs were 3.51 Å for LDH3, 3.17Å for LDH4, and 3.16 Å for LDH5, which are smaller than the estimated diameter of nitrate (3.66 Å) (Figure 4.4). Wang and Wang (2007) proposed a different configuration of interlayer nitrate in the LDHs by using X-ray diffraction and polarized ATR-FTIR spectroscopy. Consequently, the larger basal spacing of LDH3 is likely the result of the tilted orientation of interlayer nitrate. On the other hand, the smaller basal spacing of LDH4 and LDH5 might be due to the horizontal orientation of the interlayer nitrate (Figure 4.4).

### 4.3.1.3   *Infrared spectroscopic analysis*

The strong and broad features in the regions of 3800-2500 cm$^{-1}$ and 1200-700 were stretching and vibration of water (Figure 4.5). In the 3800-2500 cm$^{-1}$ region, the bands at 3666 and 3469 cm$^{-1}$ indicated the $\nu_{OH}$ vibrations of the O-H in hydroxide layers. Another band corresponding to interlayer water was assigned at 1645 cm$^{-1}$ ($\delta_{H_2O}$). The N-O vibration bands at 1360 cm$^{-1}$ and 823 cm$^{-1}$ were Raman- and IR-active degenerate stretching ($\nu_3$, *E'* type) and IR-active N-O out-of-plane bending ($\nu_2$, $A_2''$ type), respectively. The weak shoulder at 1052 cm$^{-1}$ for LDH3 and
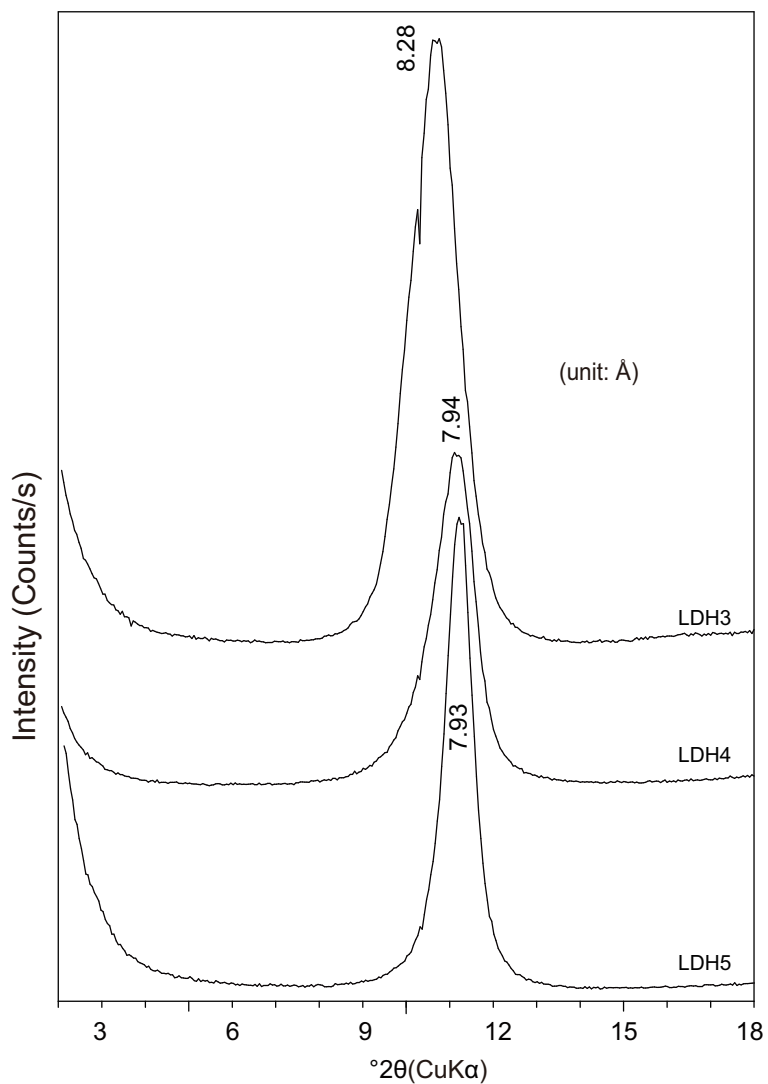
Figure 4.3. Powder X-ray diffraction patterns of Mg/Al-NO$_3$ layered double hydroxides, LDH3, LDH4, and LDH5.
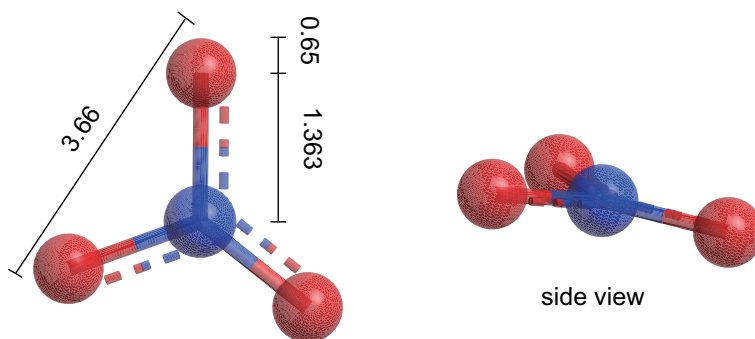


Figure 4.4. Estimated nitrate size by the bond length of N-O and the diameter of oxygen. (unit: Å)

1039 cm$^{-1}$ for LDH4 and LDH5 were attributed to the N-O stretching ($\nu_1$, $A_1$' type) of a free nitrate. It's notable that this band is not IR-active in a planar triangular nitrate molecule with D$_{3h}$ symmetry, but appears when this symmetry is distorted (Chouillet et al., 2004). A small shoulder at 1433 cm$^{-1}$ was observed with the identical band at 1360 cm$^{-1}$ for LDH3. With the increase of charge density, i.e., increase of Al$^{3+}$ ratio, the shoulder decreased and the band sharpened. An undisturbed free nitrate ion is a planar molecule has N-O stretching at 1051 cm$^{-1}$ (Rosenthal, 1973), however, the nitrate in the interlayer of the hydroxide layers was expected to be influenced by the vibration symmetry. The interlayer nitrate of LDH3 was considered lay in a tilted direction, two of the N-O bonds, thus, interact with each side of the hydroxide layer and the third N-O bond was less affected by the hydroxide layer. Therefore, this third N-O bond might react with interlayer water through H-bond and exhibited a similar band position at 1052 cm$^{-1}$ as that of free nitrate in water (Figure 4.5) (Wang and Wang, 2007). Although $CO_3^{-2}$ was detected in the composition analysis, no obvious $CO_3^{-2}$ absorbing band was found in FTIR and the contribution of $CO_3^{2-}$ to the structural property was considered negligible.

### 4.3.2 Effects of layer charge density of LDHs on FB$_1$ adsorption

A single FB$_1$ concentration experiment was conducted to evaluate the adsorption efficiency of Mg/Al-LDHs. With this simple evaluation, the loading capacity of LDHs for FB$_1$ can be concisely revealed and compared. The three LDHs exhibited significantly different FB$_1$ adsorption capacities with different Al$^{3+}$/Mg$^{2+}$ ratios, namely, with different charge densities (Figure 4.6). The amount of adsorbed FB$_1$ was positively correlated with the layer charge density. The LDH3, which has the highest layer charge density showed highest FB$_1$ adsorption (Figure 4.6). The decrease in FB$_1$ adsorption with anion exchange capacity (AEC) reduced indicated the FB$_1$ might be adsorbed by ion exchange. However, a disproportionate decreasing amount of AEC to adsorbed FB$_1$ implied FB$_1$ – NO$_3^-$ ion exchange was not the only reaction. Surface adsorption of FB$_1$ might occur on LDH and will be further elucidated later. As the species of FB$_1$ are pH-dependent, the pH values of the FB$_1$ solution were determined after adsorption. The pH of FB$_1$ on LDH3 was one unit lower than the

71
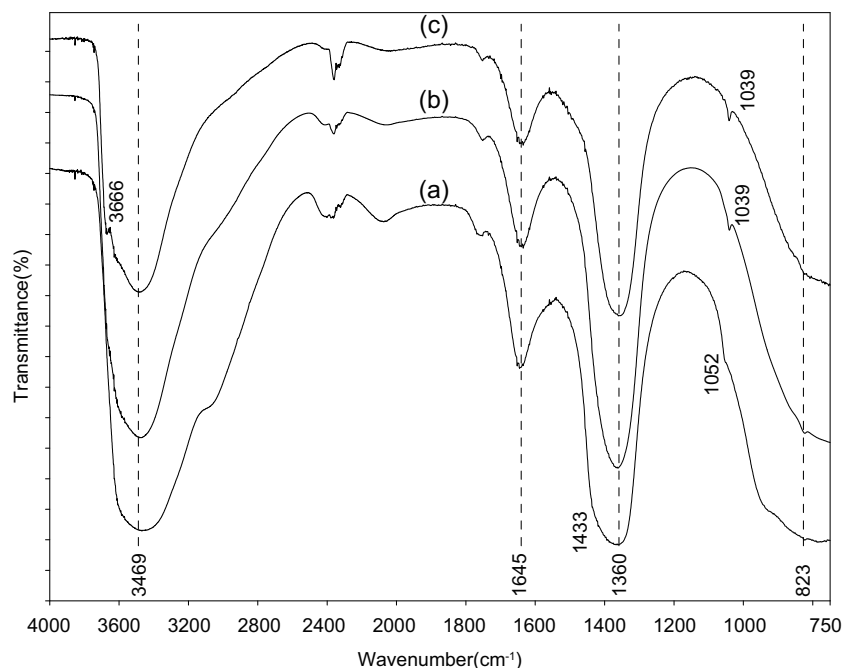
Figure 4.5. FTIR spectra of Mg/Al-NO$_3$ layered double hydroxides, (a) LDH3, (b) LDH4, and (c) LDH5.

values of FB$_1$ on LDH4 and LDH5, suggested the high adsorption of FB$_1$ on LDH3 might attribute to the effects of solution pH. Yet, the similar pH values of FB$_1$ on LDH4 and LDH5 indicated the layer charge density was the major determining factor.

### 4.3.3 Fumonisin B$_1$ adsorption isotherm on LDH3

The isothermal adsorption (Figure 4.7) was conducted with LDH3 only as it had the highest adsorption capacity for FB$_1$. The adsorbed amount of FB$_1$ gradually increased upon increasing concentration of FB$_1$ until a relative flat plateau was reached. This adsorption isotherm was classified as L-type by Giles and Smith (1974), indicating a high affinity between LDH3 and FB$_1$ and a minimum competition from NO$_3^-$ for the adsorption sites. The estimated maximum FB$_1$ adsorption was determined to be 0.30 mol/kg, corresponding to 7% of the anion exchange capacity (Table 4.1). In adsorption isotherm, the LDH3 was incorporated in the form of suspension prepared from
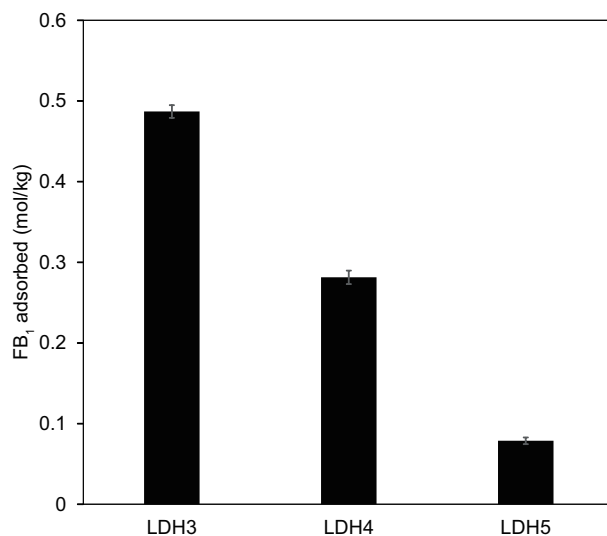
Figure 4.6. Effects of layer charge density of LDHs on $FB_1$ adsorption. (Final pH value after 24 hr: LDH3: pH 4.4; LDH4: pH 5.3; LDH5: pH 5.5).

re-dispersion of oven-dried LDH3 powder, which was different from the suspension used in the study of layer charge density effect (Section 4.3.2). The re-dispersion powder was not as homogeneous as the original dispersion acquired after co-precipitation, and thus, some off data points were observed through a thoroughly stir was performed before each adsorbent addition.

### 4.3.4    Effects of solution pH on $FB_1$ adsorption on LDH3

The amount of adsorbed $FB_1$ by LDH3 against the solution pH (Figure 4.8) indicated that the $FB_1$ adsorption capacity decreased from 0.49 to 0.11 mol/kg when final solution pH was increased from 4.3 to 10.7. As the positive charge on LDHs can be considered as permanent , and more negatively charged species of $FB_1$ should be developed at high pH, an increase in adsorption of $FB_1$ with pH increased was expected. However, the adsorption results indicated the increasing adsorption trend with pH was not observed here; one probable cause is the competition of solution $OH^-$ with $FB_1$ for active sites on the adsorbent.
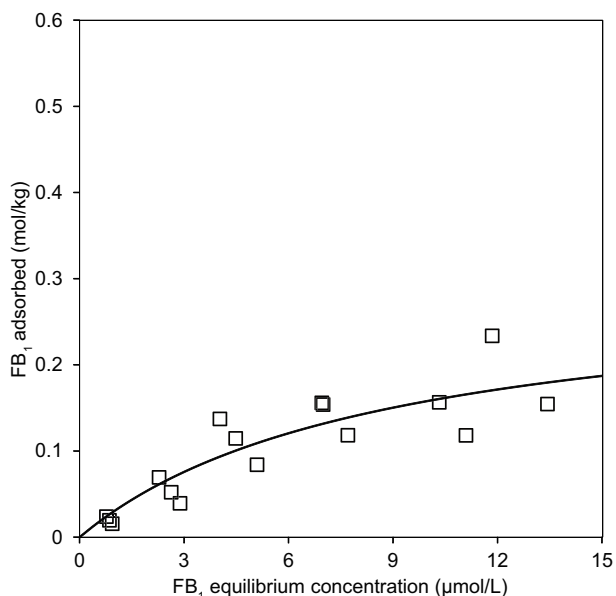
Figure 4.7. Adsorption isotherm of $FB_1$ by LDH3.

### 4.3.5  $FB_1$-LDH characterization

To clarify the structure implications to the pH effects on $FB_1$ adsorption of LDH with various charge density, the FTIR spectra and XRD patterns of the LDHs after incorporating with $FB_1$ in an equivalent of 40% of the LDH mass were investigated (Figure 4.9 and 4.10). The presence of $FB_1$ in complex was indicated by the new characteristic bands of $FB_1$ at 2960 $cm^{-1}$, 2937 $cm^{-1}$, 2862 $cm^{-1}$, 1732 $cm^{-1}$, 1568 $cm^{-1}$, and between 1300 to 1100 $cm^{-1}$ corresponding to asymmetric -$CH_3$ stretching, asymmetric -$CH_2$ stretching, symmetric -$CH_2$ stretching, symmetric C=OOH stretching, asymmetric C=OO$^-$ stretching, and -$CH_2$ bending, respectively.

Bands associated with C=OOH and C=OO$^-$ at 1732 and 1568 $cm^{-1}$ decreased in intensity with increasing pH, indicating the decrease in adsorption, which was in accord with the adsorption results (Figure 4.8). It is noticeable in Figure 4.9 that only intensity change occurred with pH change. Lack of band shifts suggested that the dissociated carboxyl groups, i.e., carboxylate, was not involved in the $FB_1$ adsorption on LDHs.
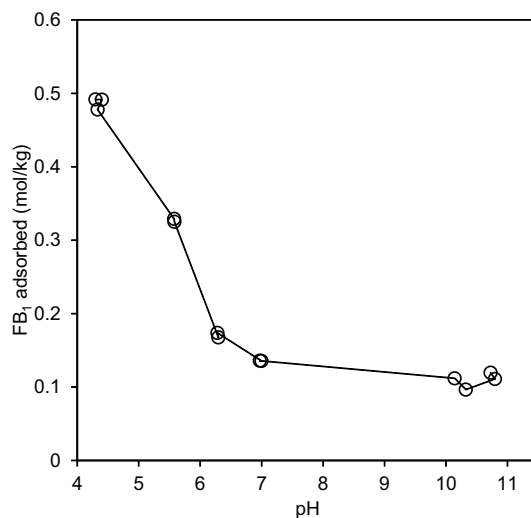
Figure 4.8. Effects of FB$_1$ solution pH on adsorption to LDH3.

The charge density of LDHs affected the bonding nitrate and the amount of interlayer water after adsorbing FB$_1$. The interlayer water indicated by 1645 cm$^{-1}$ was observed in LDH5 after incorporating FB$_1$. When charge density increased, this band appeared as a shoulder in LDH4 and then disappeared in LDH3. The same observation can be found by less strong and broad feature in the range of 3700 to 3200 cm$^{-1}$ (stretching of interlayer water) and 1200 to 700 cm$^{-1}$ (vibration of interlayer water). These results suggested the removal of interlayer water after adsorbing FB$_1$, especially in LDH3. Blue shifts were observed on nitrate band at 1360 cm$^{-1}$ after adsorbing FB$_1$. When LDHs were intercalated with FB$_1$, the N-O stretching band at 1360 cm$^{-1}$ shifted to 1368 cm$^{-1}$, 1370 cm$^{-1}$ and 1386 cm$^{-1}$ with the observation of the different amount of interlayer water removal indicated by the band at 1645 cm$^{-1}$ ($\delta_{H_2O}$). The blue shift of N-O stretching might imply that the distortions had occurred during the intercalation by FB$_1$ with the presence of interlayer water. Another nitrate band at 1052 cm$^{-1}$ in LDH3 which affirmed the tilted orientation of nitrate disappeared when FB$_1$ was adsorbed by LDH3, indicating the orientation of interlayer nitrate might change.
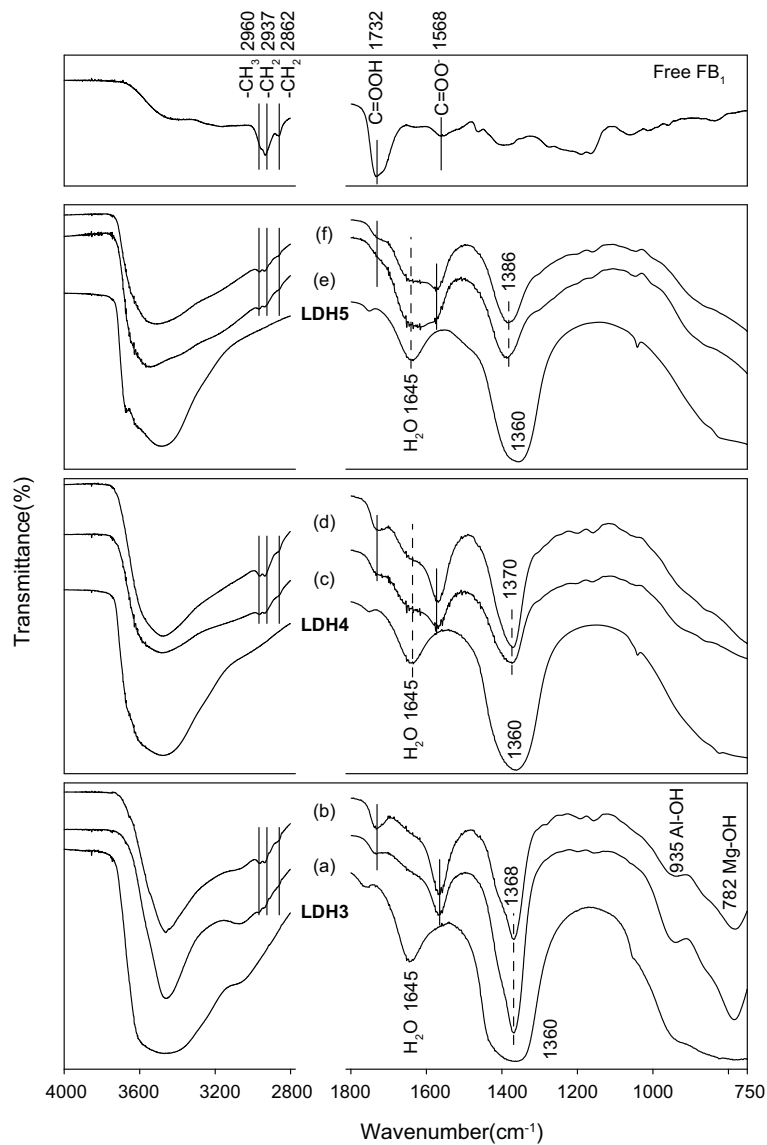
Figure 4.9. FTIR spectra of $FB_1$ and Mg/Al-LDHs interacting with $FB_1$ at different pH: LDH3 at pH 10.4 (a) and 6.0 (b), LDH4 at pH 10.4 (c) and 6.0 (d), and LDH5 at pH 10.4 (e) and 5.6 (f). $FB_1$ characteristic bands are marked with solid vertical lines.
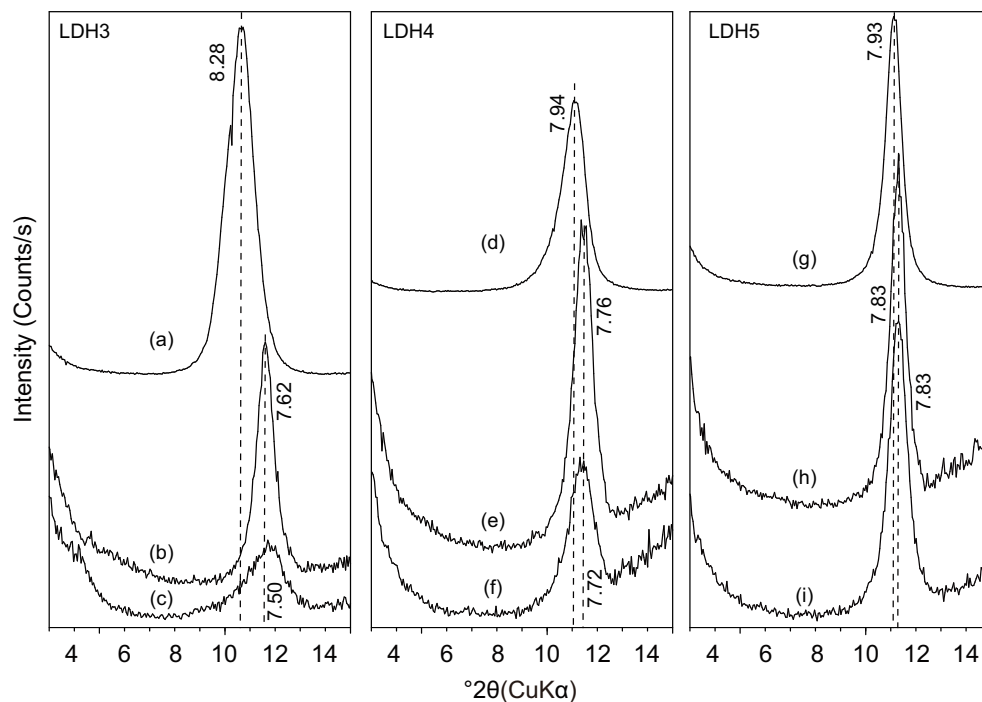
Figure 4.10. XRD patterns of LDHs before and after $FB_1$ adsorption: LDH3 (a), $FB_1$-LDH3 at pH 10.4 (b) and pH 6.0 (c), LDH4 (d), $FB_1$-LDH3 at pH 10.4 (e) and pH 6.0 (f), LDH5 (g), $FB_1$-LDH5 at pH 10.4 (h) and pH 5.6 (i).

Increasing of basal spacing is an indication of interlayer adsorption by materials with layer structure. The FTIR spectra showed that $FB_1$ was in the complex and resistant to wash, the d-spacing of LDHs, however, were decreased after adsorbing $FB_1$ (Figure 4.10). After interacting with $FB_1$, the decrease of basal spacing was LDH3 > LDH4 > LDH5, suggested that with higher $FB_1$ adsorption, basal spacing decreased more. The greater decrement in basal spacing with more $FB_1$ incorporation was in accord with the adsorption result with pH change. For instance, LDH3 showed higher adsorption capacity at lower pH, and thus, more basal spacing decrease (Figure 4.10, (c)) was observed compared to the basal spacing at higher pH (Figure 4.10, (b)). The d-spacing change in LDH3 indicated that $FB_1$ did go into the interlayer of LDH. However, the presence of strong $NO_3^-$ bands on the IR pattern suggested the interlayer anion exchange was incomplete.

## 4.4 Discussion

Fumonisin $B_1$ is a large molecule containing four carboxyl groups and one amino group, suggesting that $FB_1$ can exist in cationic, zwitterionic, or anionic form depending on the solution pH. The previous study showed that $FB_1$ was able to be adsorbed in the interlayer of smectite at low pH through electrostatic interactions between the negative charge of smectite and the protonated amino group of cationic $FB_1$. Due to the positive charge, regardless of pH, LDHs can adsorb anionic molecules. High adsorption of $FB_1$ by LDH3 at pH 4 suggested the electrostatic interactions between the dissociated carboxyl group and positively charge of LDH. Increasing $FB_1$ adsorption with pH was expected as the amount of anionic $FB_1$ species increased at higher pH. However, when the pH was increased, a competition between the co-existing anion, $OH^-$, and anionic $FB_1$ for the positive charge sites on LDHs resulted in a decrease in $FB_1$ adsorption on LDHs. For instance, the $OH^-$ concentration in pH 11 solution equalled to 1 mM, which was one hundred times greater than that of $FB_1$ (0.01 mM) in solution and thus became a competitor for adsorbing site.

The anion exchange capacity of LDH3, LDH4, and LDH5 were 4.23, 3.15, and 2.53 mol/kg, respectively. The estimated $FB_1$ adsorption was 76% by LDH3, 57% by LDH4, and 46% by LDH5 ($FB_1$/LDH, w/w) if assuming only one carboxyl group was involved in adsorption. With starting $FB_1$ quantity equal to 40% of LDH mass, 87.8%, 50.7%, and 14.2% of $FB_1$ in solution were adsorbed on LDH3, LDH4, and LDH5, respectively, at neutral pH solution. Even at pH as high as 10.7, 21.5% of $FB_1$ removal was achieved by LDH3. The difference between estimated and experimental adsorption amount in LDH3 implied other than interlayer adsorption, adsorption on the external surface of LDHs might occur.

The affinity of various anions on Mg/Al-LDH was reported in the order of $SO_4^{2-} > F^- > HPO_4^{2-} > Cl^- > B(OH)_4^- > NO_3^-$ (Parker et al., 1995), which was similar to the order $OH^- > F^- > Cl^- > Br^- > NO_3^- > I^-$ for monovalent anions and $CO_3^{2-} > SO_4^{2-}$ for divalent anions reported in another study (Miyata, 1983). The adsorption of herbicide MCPA (4-chloro-2-methylphenoxyacetic acid)

on Mg/Al-LDH with different starting interlayer anion suggested that higher adsorption capacity was observed on LDH with lower affinity interlayer anion. For instance, the adsorption capacity of MCPA on LDH was in the order of Mg/Al-$NO_3$-LDH > Mg/Al-Cl-LDH > Mg/Al-$CO_3$-LDH (Inacio et al., 2001). The $FB_1$ adsorption on LDHs might be enhanced by selecting interlayer anions which have low affinity to LDHs and can be easily replaced by $FB_1$ through anion exchange reaction.

## 4.5   Conclusion

Mg/Al LDHs synthesized with different $Al^{3+}$/$Mg^{2+}$ ratio exhibited the significant difference in $FB_1$ adsorption due to the different charge density. The $FB_1$ adsorption was primarily driven by the electrostatic interactions between the anionic part on $FB_1$ and the positive charge sites on LDHs. $FB_1$ can be adsorbed in the interlayer of LDHs with incomplete anion exchange with $NO_3^-$ or $CO_3^{2-}$ in this experiment. Competition between anionic $FB_1$ and $OH^-$ for adsorbing site resulted in $FB_1$ adsorption reduced with increasing solution pH. FTIR and XRD results suggested that $FB_1$ was adsorbed into the interlayer of LDHs.

# 5. CONCLUSIONS

Comparing to the reported adsorption of $AFB_1$ by smectites, all tested smectites, with or without modifications with cation exchange or charge reduction, showed much less adsorption for ZEN, OTA, and DON. The cation exchange or charge reduction did not exert the same effects on the adsorption of ZEN, OTA, and DON as they did on $AFB_1$. The results indicated the size-matching theory between adsorbed $AFB_1$ and smectites was not applicable on ZEN despite this theory well explained the determinative roles of layer charge density and type of exchange cation of smectites on adsorbing $AFB_1$, a mycotoxin shared high similarities in polarity, solubility, molecular weight, and structure with ZEN. The determinative factor of ZEN adsorption was the hydrophobicity of the adsorbent, which can be indicated by the charge density of smectites and $Z^2/r$ value of exchange cations. Lacking a highly negative surface charge carbonyl oxygen and less planar structure of ZEN made the hydrophobic interaction between carbonyl oxygen and smectite more difficult than $AFB_1$. Water-soluble DON showed inverse responses to exchange cation and layer charge density of smectite on adsorption compared to hydrophobic ZEN. The very little OTA adsorption at neutral pH in aqueous solution was attributed to the extent of protonation of the two hydroxyl groups on OTA molecule.

The $FB_1$ can be adsorbed into interlayer of smectite at low pH. The affinity between $FB_1$ and smectite decreased with solution pH. The chemical speciation of $FB_1$ at different pH was the main determinative factor influenced the adsorption of $FB_1$ on smectite. Increasing the amount of anionic $FB_1$ species at high pH resulted in lower adsorption capacity of smectite for $FB_1$.

The LDH3 with higher charge density showed highest adsorption capacity for $FB_1$ due to more exchangeable sites. The $FB_1$ adsorption on Mg/Al LDHs was primarily driven by the electrostatic interactions between the anionic part on $FB_1$ and the positive charge sites on LDHs. Anion exchange of $NO_3^-$ or $CO_3^{2-}$ by $FB_1$ was the major adsorption mechanism. Competition between

anionic $FB_1$ and $OH^-$ for exchangeable sites at higher pH resulted in a decrease in $FB_1$ adsorption despite the number of negatively charged carboxylate group $FB_1$ increased.

REFERENCES

H. K. Abbas, R. D. Cartwright, W. P. Xie, and W. T. Shier. Aflatoxin and fumonisin contamination of corn (maize, Zea mays) hybrids in Arkansas. *Crop Protection*, 25(1):1–9, 2006.

M. A. Abdel-Wahhab, A. A. El-Kady, A. M. Hassan, O. M. Abdel-Moneim, and S. H. Abdel-Aziem. Effectiveness of activated carbon and Egyptian montmorillonite in the protection against deoxynivalenol-induced cytotoxicity and genotoxicity in rats. *Food and Chemical Toxicology*, 83:174–182, 2015.

P. W. Abrahams. Involuntary soil ingestion and geophagia: A source and sink of mineral nutrients and potentially harmful elements to consumers of earth materials. *Applied Geochemistry*, 27(5): 954–968, 2012.

A. F. Afifi, M. A. Foaad, and E. M. Fawzi. Effect of gamma irradiation on elimination of aflatoxins produced by apple mycoflora in apple fruits. *Acta Microbiologica Polonica*, 52(4):379–386, 2003.

C. G. Afolabi, R. Bandyopadhyay, J. F. Leslie, and E. J. A. Ekpo. Effect of sorting on incidence and occurrence of fumonisins and Fusarium verticillioides on maize from Nigeria. *Journal of Food Protection*, 69(8):2019–2023, 2006.

F. Akbal. Sorption of phenol and 4-chlorophenol onto pumice treated with cationic surfactant. *Journal of Environmental Management*, 74(3):239–244, 2005.

AOAC. AOAC official method 995.15. Fumonisins B1, B2, and B3 in corn. Liquid chromatographic method. In *AOAC Office Methods Analysis*. 2000.

APHA, AWWA, and WEF. *Standard methods for the examination of water and wastewater*. American Public Health Association, American Water Works Association, Water Environment Federation, Washington DC, 20th edition, 1998.

J. W. ApSimon, B. A. Blackwell, and O. E. Edwards. Relative configuration of the C-1 to C-5 fragment of fumonisin B1. *Tetrahedrom Letters*, 35(2):7703–7706, 1994.

M. M. Atalla, N. M. Hassanein, A. A. El-Beih, and Y. A. G. Youssef. Mycotoxin production

in wheat grains by different Aspergilli in relation to different relative humidities and storage periods. *Nahrung-Food*, 47(1):6–10, 2003.

H. Autrup, K. A. Bradley, A. K. M. Shamsuddin, J. Wakhisi, and A. Wasunna. Detection of putative adduct with fluorescence characteristics identical to 2,3-dihydro-2-(7'-guanyl)-3-hydroxyaflatoxin-B-1 in human-urine collected in Murang'a district, Kenya. *Carcinogenesis*, 4(9):1193–1195, 1983.

G. Avantaggiato, R. Havenaar, and A. Visconti. Evaluation of the intestinal absorption of deoxynivalenol and nivalenol by an in vitro gastrointestinal model, and the binding efficacy of activated carbon and other adsorbent materials. *Food and Chemical Toxicology*, 42(5):817–824, 2004.

G. Avantaggiato, M. Solfrizzo, and A. Visconti. Recent advances on the use of adsorbent materials for detoxification of Fusarium mycotoxins. *Food Additives and Contaminants*, 22(4):379–388, 2005.

G. Avantaggiato, D. Greco, A. Damascelli, M. Solfrizzo, and A. Visconti. Assessment of multi-mycotoxin adsorption efficacy of grape pomace. *Journal of Agricultural and Food Chemistry*, 62(2):497–507, 2014.

A. L. Barrientos-Velazquez, A. M. Cardona, L. Liu, T. Phillips, and Y. Deng. Influence of layer charge origin and layer charge density of smectites on their aflatoxin adsorption. *Applied Clay Science*, 132:281–289, 2016.

J. Bauer and M. Gareis. Ochratoxin A in der nahrungsmittelkette. *Journal of Veterinary Medicine, Series B*, 34:613–627, 1987.

A. D. Becke. Density-functional thermochemistry. III. The role of exact exchange. *Journal of Chemical Physics*, 98(7):5648–5652, 1993.

T. M. Berhane, J. Levy, M. P. S. Krekeler, and N. D. Danielson. Adsorption of bisphenol A and ciprofloxacin by palygorskite-montmorillonite: Effect of granule size, solution chemistry and temperature. *Applied Clay Science*, 132(SI):518–527, 2016.

S. C. Bezuidenhout, W. C. A. Gelderblom, C. P. Gorstallman, R. M. Horak, W. F. O. Marasas, G. Spiteller, and R. Vleggaar. Structure elucidation of the fumonisins, mycotoxins from

Fusarium-Moniliforme. *Journal of The Chemical Society-Chemical Communications*, (11):743–745, 1988.

D. Bhatnagar, P. J. Cotty, and T. E. Cleveland. Preharvest aflatoxin contamination - molecular strategies for its control. *ACS Symposium Series*, 528:272–292, 1993.

D. Bhatnagar, G. A. Payne, T. E. Cleveland, and J. F. Robens. Mycotoxins: Current issues in USA. In D. Barug, H. P. van Egmond, R. López-Garcí, W. A. van Osenbruggen, and A. Visconti, editors, *Meeting the mycotoxin menace*, pages 275–280. Wageningen Academic, Wageningen, 2004.

S. A. Bhatti, M. Z. Khan, M. K. Saleemi, and M. Saqib. Aflatoxicosis and ochratoxicosis in broiler chicks and their amelioration with locally available bentonite clay. *Pakistan Veterinary Journal*, 36(1):68–72, 2016.

J. G. Bordini, D. Borsato, A. S. Oliveira, M. A. Ono, T. H. Zaninelli, E. Y. Hirooka, and E. Y. S. Ono. In vitro zearalenone adsorption by a mixture of organic and inorganic adsorbents: Application of the Box Behnken approach. *World Mycotoxin Journal*, 8(3):291–299, 2015.

S. A. Boyd, M. M. Mortland, and C. T. Chiou. Sorption characteristics of organic-compounds on hexadecyltrimethylammonium-smectite. *Soil Science Society of America Journal*, 52(3):652–657, 1988.

K. A. Brown, T. Mays, A. Romoser, A. Marroquin-Cardona, N. J. Mitchell, S. E. Elmore, and T. D. Phillips. Modified hydra bioassay to evaluate the toxicity of multiple mycotoxins and predict the detoxification efficacy of a clay-based sorbent. *Journal of Applied Toxicology*, 34(1):40–48, 2014.

W. Bryden. Mycotoxins in the food chain: human health implications. *Asia Pacific journal of clinical nutrition*, 16 Suppl 1:95–101, 2007.

T. Calado, A. Venâncio, and L. Abrunhosa. Irradiation for mold and mycotoxin control: A review. *Comprehensive Reviews in Food Science and Food Safety*, 13, 2014.

F. Caloni, M. Spotti, H. Auerbach, H. den Camp, J. F. Gremmels, and G. Pompa. In vitro metabolism of fumonisin B1 by ruminal microflora. *Veterinary Research Communications*, 24

(6):379–387, 2000.

K. W. Campbell and D. G. White. Evaluation of corn genotypes for resistance to aspergillus ear rot, kernel infection, and aflatoxin production. *Plant Disease*, 79(10):1039–1045, 1995.

K. A. Carrado, J. E. Forman, R. E. Botto, and R. E. Winans. Incorporation of phthalocyanines by cationic and anionic clays via ion-exchange and direct synthesis. *Chemistry of Materials*, 5(4): 472–478, 1993.

F. Cavani, F. Trifiro, and A. Vaccari. Hydrotalcite-type anionic clays: Preparation, properties and applications. *Catalysis Today*, 11(2):173–301, 1991.

Y. F. Chao, P. C. Chen, and S. L. Wang. Adsorption of 2,4-D on Mg/Al-NO3 layered double hydroxides with varying layer charge density. *Applied Clay Science*, 40(1-4):193–200, 2008.

B. L. Chen and L. Z. Zhu. Partition of polycyclic aromatic hydrocarbons on organobentonites from water. *Journal of Environmental Sciences*, 13(2):129–136, 2001.

K. Chibwe and W. Jones. Intercalation of organic and inorganic anions into layered double hydroxides. *Journal of The Chemical Society-Chemical Communications*, (14):926–927, 1989.

C. Chouillet, J. M. Krafft, C. Louis, and H. Lauron-Pernot. Characterization of zinc hydroxynitrates by diffuse reflectance infrared spectroscopy - structural modifications during thermal treatment. *Spectrochimica Acta Part A-Molecular and Biomolecular Spectroscopy*, 60(3):505–511, 2004.

H. A. Clark and S. M. Snedeker. Ochratoxin A: Its cancer risk and potential for exposure. *Journal of Toxicology and Environmental Health-Part B-Critical Reviews*, 9(2-3):265–296, 2006.

T. E. Cleveland, P. F. Dowd, A. E. Desjardins, D. Bhatnagar, and P. J. Cotty. United States Department of Agriculture - Agricultural Research Service research on pre-harvest prevention of mycotoxins and mycotoxigenic fungi in US crops. *Pest Management Science*, 59(6-7):629–642, 2003.

Codex Alimentarius. *Code of practice for the prevention and reduction of mycotoxin contamination in cereals*. CAC/RCP 51-2003, 2003.

R. J. Cole and R. H. Cox. Handbook of toxic fungal metabolites. Academic Press, New York, NY,

1981.

Council for Agricultural Science and Technology (CAST). *Mycotoxins : Risks in plant, animal, and human systems.* Task force report: no. 139. Ames, IA : Council for Agricultural Science and Technology, 2003.

A. Dakovic, M. Kragovic, G. E. Rottinghaus, Z. Sekulic, S. Milicevic, S. K. Milonjic, and S. Zaric. Influence of natural zeolitic tuff and organozeolites surface charge on sorption of ionizable fumonisin B1. *Colloids and Surfaces B: Biointerfaces*, 76(1):272–278, 2010.

R. M. C. Dawson, D. C. Elliott, W. H. Elliott, and K. M. Jones. *Data for biochemical research.* Oxford : Clarendon Press, 1986., 3rd edition, 1986.

R. de la Campa, J. D. Miller, and K. Hendricks. Fumonisin in tortillas produced in small-scale facilities and effect of traditional masa production methods on this mycotoxin. *Journal of Agricultural and Food Chemistry*, 52(14):4432–4437, 2004.

Y. Deng and M. G. Tenorio Arvide. Automation of size fractionation to extract clays and silts. *Clay Minerals*, 46(3):515–523, 2011.

Y. Deng, A. L. Barrientos-Velazquez, F. Billes, and J. B. Dixon. Bonding mechanisms between aflatoxin B1 and smectite. *Applied Clay Science*, 50(1):92–98, 2010.

Y. Deng, L. Liu, A. L. Barrientos-Velazquez, and J. B. Dixon. The determinative role of the exchange cation and layer-charge density of smectite on aflatoxin adsorption. *Clays and Clay Minerals*, 60(4):374–386, 2012.

Y. J. Deng and M. Szczerba. Computational evaluation of bonding between aflatoxin B-1 and smectite. *Applied Clay Science*, 54(1):26–33, 2011.

J. B. Dixon, D. G. Schulze, and Soil Science Society of America. *Soil mineralogy with environmental applications*. Number 7. Soil Science Society of America, Madison, Wis., USA, 2002.

J. W. Dorner, R. J. Cole, and P. D. Blankenship. Effect of inoculum rate of biological control agents on preharvest aflatoxin contamination of peanuts. *Biological Control*, 12(3):171–176, 1998.

J. W. Dorner, R. J. Cole, and D. T. Wicklow. Aflatoxin reduction in corn through field application of competitive fungi. *Journal of Food Protection*, 62(6):650–656, 1999.

S. C. Duarte, C. M. Lino, and A. Pena. Ochratoxin A in feed of food-producing animals: An undesirable mycotoxin with health and performance effects. *Veterinary Microbiology*, 154(1-2): 1–13, 2011.

J. M. Essigmann, R. G. Croy, A. M. Nadzan, W. F. Busby, V. N. Reinhold, G. Büchi, and G. N. Wogan. Structural identification of the major DNA adduct formed by aflatoxin B1 in vitro. *Proceedings of the National Academy of Sciences of the United States of America*, 74(5):1870–1874, 1977.

V. Faucet-Marquis, C. Joannis-Cassan, K. Hadjeba-Medjdoub, N. Ballet, and A. Pfohl-Leszkowicz. Development of an in vitro method for the prediction of mycotoxin binding on yeast-based products: case of aflatoxin B-1, zearalenone and ochratoxin A. *Applied Microbiology and Biotechnology*, 98(17):7583–7596, 2014.

R. E. Ferrell Jr. Medicinal clay and spiritual healing. *Clays and Clay Minerals*, 56(6):751–760, 2008.

M. J. Frisch, G. W. Trucks, H. B. Schlegel, P. M. W. Gill, B. G. Johnson, M. A. Robb, J. R. Cheeseman, T. A. Keith, G. A. Petersson, J. A. Montgomery Jr., K. Raghavachari, M. A. Al-Laham, V. G. Zakrzewski, J. V. Ortiz, J. B. Foresman, J. Cioslowski, B. B. Stefanov, A. Nanayakkara, M. Challacombe, C. Y. Peng, P. Y. Ayala, W. Chen, M. W. Wong, J. L. Andres, E. S. Replogle, R. Gomperts, R. L. Martin, D. J. Fox, J. S. Binkley, D. J. Defrees, J. Baker, J. P. Stewart, M. Head-Gordon, C. Gonzalez, and J. A. Pople. *Gaussian 94, Revision, C.3*. Gaussian, Inc., Pittsburgh, PA, 1995.

F. Galvano, A. Pietri, T. Bertuzzi, M. Bognanno, L. Chies, A. De Angelis, and M. Galvano. Activated carbons: in vitro affinity for fumonisin B1 and relation of adsorption ability to physicochemical parameters. *Journal of Food Protection*, 60:985–991, 1997.

M. Gareis and J. Ceynowa. Influence of the fungicide matador (tebuconazole triadimenol) on mycotoxin production by Fusarium-Culmorum. *Zeitschrift für Lebensmittel-Untersuchung und -Forschung*, 198(3):244–248, 1994.

M. Gautier, F. Muller, J. M. Beny, L. Le Forestier, P. Alberic, and P. Baillif. Interactions of

ammonium smectite with low-molecular-weight carboxylic acids. *Clay Minerals*, 44(2):207–219, 2009.

W. C. A. Gelderblom, K. Jaskiewicz, W. F. O. Marasas, P. G. Thiel, R. M. Horak, R. Vleggaar, and N. P. J. Kriek. Fumonisins - novel mycotoxins with cancer-promoting activity produced by Fusarium-moniliforme. *Applied and Environmental Microbiology*, 54(7):1806–1811, 1988.

W. C. A. Gelderblom, V. Sewram, G. S. Shephard, P. W. Snijman, K. Tenza, L. van der Westhuizen, and R. Vleggaar. Structure and natural occurrence of stereoisomers of the fumonisin B series mycotoxins. *Journal of Agricultural and Food Chemistry*, 55(11):4388–4394, 2007.

M. Ghadiri, W. Chrzanowski, and R. Rohanizadeh. Biomedical applications of cationic clay minerals. *RSC Advance*, 5(37):29467–29481, 2015.

C. H. Giles and D. Smith. A general treatment and classification of the solute adsorption isotherm. I. Theoretical. *Journal of Colloid and Interface Science*, 47(3):766–778, 1974.

R. L. Goswamee, P. Sengupta, K. G. Bhattacharyya, and D. K. Dutta. Adsorption of Cr(VI) in layered double hydroxides. *Applied Clay Science*, 13(1):21–34, 1998.

Z. Gu, S. Yan, S. Cheong, Z. Cao, H. Zuo, A. C. Thomas, B. E. Rolfe, and Z. P. Xu. Layered double hydroxide nanoparticles: Impact on vascular cells, blood cells and the complement system. *Journal of Colloid and Interface Science*, 512:404–410, 2018.

M. Haidukowski, M. Pascale, G. Perrone, D. Pancaldi, C. Campagna, and A. Visconti. Effect of fungicides on the development of Fusarium head blight, yield and deoxynivalenol accumulation in wheat inoculated under field conditions with Fusarium graminearum and Fusarium culmorum. *Journal of the Science of Food and Agriculture*, 85(2):191–198, 2005.

M. Hajjaji and A. Alami. Influence of operating conditions on methylene blue uptake by a smectite rich clay fraction. *Applied Clay Science*, 44(1-2):127–129, 2009.

A. M. Hamblin and D. G. White. Inheritance of resistance to aspergillus ear rot and aflatoxin production of corn from Tex6. *Phytopathology*, 90(3):292–296, 2000.

J. He, M. Wei, B. Li, Y. Kang, D. G. Evans, and X. Duan. Preparation of layered double hydroxides. In *Layered Double Hydroxides*, volume 119, pages 89–119. 2006.

J. G. Heathcote and J. R. Hibbert. *Aflatoxins: chemical and biological aspects.* Elsevier Scientific Publishing Co., Amsterdam, Netherlands, 1978.

R. A. Hill, P. D. Blankenship, R. J. Cole, and T. H. Sanders. Effects of soil-moisture and temperature on preharvest invasion of peanuts by the Aspergillus flavus group and subsequent aflatoxin development. *Applied and Environmental Microbiology*, 45(2):628–633, 1983.

U. Hofmann and R. Klemen. Verlust der austauschfähigkeit von lithiumionen an bentonit durch erhitzung. *Zeitschrift für anorganische Chemie*, 262(15):95–99, 1950.

D. Hormisch, D. Hormisch, I. Brost, G. W. Kohring, F. Giffhorn, R. M. Kroppestedt, E. Stackebradt, P. Färber, and W. H. Holzapfel. Mycobacterium fluoranthenivorans sp. nov., a fluoranthene and aflatoxin-B1 degrading bacterium from contaminated soil of a former coal gas plant. *Systematic and Applied Microbiology*, 27(6):653–660, 2004.

H. U. Humpf and K. A. Voss. Effects of thermal food processing on the chemical structure and toxicity of fumonisin mycotoxins. *Molecular Nutrition & Food Research*, 48(4):255–269, 2004.

H. S. Hussein and J. M. Brasel. Toxicity, metabolism, and impact of mycotoxins on humans and animals. *Toxicology*, 167(2):101–134, 2001.

A. Huwig, S. Freimund, O. Käppeli, and H. Dutler. Mycotoxin detoxication of animal feed by different adsorbents. *Toxicology Letters*, 122(2):179–188, 2001.

IARC. Some naturally occurring substances: Food items and constituents, heterocyclic aromatic amines and mycotoxins. *IARC Monographs on the Evaluation of Carcinogenic Risks to Humans*, 56:245–395, 1993.

IARC. Some traditional herbal medicines, some mycotoxins, naphthalene and styrene. *IARC Monographs on the Evaluation of Carcinogenic Risks to Humans*, 82:301–366, 2002.

J. Inacio, C. Taviot-Gueho, C. Forano, and J. P. Besse. Adsorption of MCPA pesticide by MgAl-layered double hydroxides. *Applied Clay Science*, 18(5-6, SI):255–264, 2001.

S. Z. Iqbal, I. A. Bhatti, M. R. Asi, M. Zuber, M. Shahid, and I. Parveen. Effect of $\gamma$ irradiation on fungal load and aflatoxins reduction in red chillies. *Radiation Physics and Chemistry*, 82:80–84, 2013.

W. F. Jaynes and J. M. Bigham. Charge reduction, octahedral charge, and lithium retention in heated, Li-saturated smectites. *Clays and Clay Minerals*, 35(6):440–448, 1987.

W. F. Jaynes, S. J. Traina, J. M. Bigham, and C. T. Johnston. Preparation and characterization of reduced-charge hectorites. *Clays and Clay Minerals*, 40(4):397–404, 1992.

A. M. Jolly and M. Bonizzoni. Intermolecular forces driving encapsulation of small molecules by PAMAM dendrimers in water. *Macromolecules*, 47(18):6281–6288, 2014.

I. Kannewischer, M. G. Tenorio Arvide, G. N. White, and J. B. Dixon. Smectite clays as adsorbents of aflatoxin B1: Initial steps. *Clay Science*, 12(Supplement2):199–204, 2006.

J. I. Keenan and G. P. Savage. Mycotoxins in groundnuts, with special reference to aflatoxin. In J. Smartt, editor, *The Groundnut Crop : A scientific basis for improvement*, pages 509–551. Chapman and Hall, London, 1994.

A. I. Khan and D. O'Hare. Intercalation chemistry of layered double hydroxides: Recent developments and applications. *Journal of Materials Science*, 12(11):3191–3198, 2002.

R. R. King, R. E. McQueen, D. Levesque, and R. Greenhalgh. Transformation of deoxynivalenol (vomitoxin) by rumen microorganisms. *Journal of Agricultural and Food Chemistry*, 32(5): 1181–1183, 1984.

S. M. Koh and J. B. Dixon. Preparation and application of organo-minerals as sorbents of phenol, benzene and toluene. *Applied Clay Science*, 18(3):111–122, 2001.

F. Kooli, V. Rives, M. A. Ulibarri, and W. Jones. Pillaring of layered double hydroxides possessing variable layer charge with vanadium polyoxoanions. In S. Komarneni, D. M. Smith, and J. S. Beck, editors, *Advances in Porous Materials*, volume 371 of *Materials Research Society Symposium Proceedings*, pages 143–149. Mat Res Soc; Gas Res Inst; Los Alamos Natl Lab; Lawrence Livermore Natl Lab; Sandia Natl Labs; Millipore Corp; Aluminum Co Amer; Cabot Sorp; Air Prod & Chem Inc, 1995.

P. Krogh. Ochratoxins. In J. V. Rodricks, C. W. Hesseltine, and M. A. Mehlman, editors, *Mycotoxins in human and animal health*, pages 489–498. Pathotox Publishers, Inc., Park Forest South, IL, 1977.

A. Krol, P. Pomastowski, K. Rafinska, V. Railean-Plugaru, J. Walczak, and B. Buszewski. Microbiology neutralization of zearalenone using Lactococcus lactis and Bifidobacterium sp. *Analytical and Bioanalytical Chemistry*, 410(3):943–952, 2018.

R. Krska, E. Szente, M. Freudenschuss, C. Hametner, and P. Zöllner. Purity assessment of commercially available crystalline deoxynivalenol. *Journal of AOAC International*, 87:909–919, 2004.

R. Krska, E. Welzig, and H. Boudra. Analysis of Fusarium toxins in feed. *Animal Feed Science and Technology*, 137(3-4):241–264, 2007.

L. F. Kubena, W. E. Huff, R. B. Harvey, A. G. Yersin, M. H. Elissalde, D. A. Witzel, L. E. Giroir, T. D. Phillips, and H. D. Petersen. Effects of a hydrated sodium calcium aluminosilicate on growing turkey poults during aflatoxicosis. *Poultry Science*, 70(8):1823–1830, 1991.

T. Kuiper-Goodman, P. M. Scott, and H. Watanabe. Risk assessment of the mycotoxin zearalenone. *Regulatory Toxicology and Pharmacology*, 7(3):253–306, 1987.

H. M. Kurtbay, Z. Bekci, M. Merdivan, and K. Yurdakoc. Reduction of ochratoxin A levels in red wine by bentonite, modified bentonites, and chitosan. *Journal of Agricultural and Food Chemistry*, 56(7):2541–2545, 2008.

C. T. Lee, W. T. Yang, and R. G. Parr. Development of the Colle-Salvetti correlation-energy formula into a functional of the electron-density. *Physical Review B*, 37(2):785–789, 1988.

S. L. Lemke, P. G. Grant, and T. D. Phillips. Adsorption of zearalenone by organophilic montmorillonite clay. *Journal of Agricultural and Food Chemistry*, 46(9):3789–3796, 1998.

S. L. Lemke, S. E. Ottinger, C. L. Ake, K. Mayura, and T. D. Phillips. Deamination of fumonisin B1 and biological assessment of reaction product toxicity. *Chemical Research in Toxicology*, 14 (1):11–15, 2001.

M. Lesnik, A. Cencic, S. Vajs, and A. Simoncic. Milling and bread baking techniques significantly affect the mycotoxin (deoxynivalenol and nivalenol) level in bread. *Acta Alimentaria*, 37(4): 471–483, 2008.

C. D. Liao, L. C. Chiueh, and D. Y. C. Shih. Determination of zearalenone in cereals by high-

performance liquid chromatography and liquid chromatography-electrospray tandem mass spectrometry. *Journal of Food and Drug Analysis*, 17(1):52–58, 2009.

C. H. Lim and M. L. Jackson. Expandable phyllosilicate reactions with lithium on heating. *Clays and Clay Minerals*, 34(3):346–352, 1986.

M. Lindemann, D. J Blodgett, E. T Kornegay, and G. Schurig. Potential ameliorators of aflatoxicosis in weaning growing swine. *Journal of animal science*, 71:171–178, 1993.

H. F. Link. Observationes in ordines plantarum naturals, Dissetatio I. *Mag. Ges. Naturf. Freunde Berlin*, 3:3–42, 1809.

J. Lovett, R. G. Thompson, and B. K Boutin. Trimming as a means of removing patulin from fungus-rotted apples. *Journal - Association of Official Analytical Chemists*, 58:909–911, 1975.

J. Mannon and E. Johnson. Fungi down on the farm. *New Scientist*, 105:12–16, 1985.

W. F. O. Marasas. *Fumonisins: history, world-wide occurrence and impact*, pages 1–17. Springer US, Boston, MA, 1996.

W. F. O. Marasas, T. A. Toussoun, and P. E. Nelson. Toxigenic Fusarium species, identity and mycotoxicology, 1984.

W. F. O. Marasas, T. S. Kellerman, W. C. A. Gelderblom, J. A.W. Coetzer, P. G. Thiel, and J. J. Vanderlugt. Leukoencephalomalacia in a horse induced by fumonisin-B1 isolated from Fusarium-moniliforme. *Onderstepoort Journal of Veterinary Research*, 55(4):197–203, 1988.

M. Marković, A. Daković, G. E. Rottinghaus, A. Petković, M. Kragović, D. Krajišnik, and J. Milić. Ochratoxin A and zearalenone adsorption by the natural zeolite treated with benzalkonium chloride. *Colloids and Surfaces A: Physicochemical and Engineering Aspects*, 529(Supplement C): 7–17, 2017.

A. Marroquín-Cardona, Y. Deng, J. F. Taylor, C. T. Hallmark, N. M. Johnson, and T. D. Phillips. In vitro and in vivo characterization of mycotoxin-binding additives used for animal feeds in Mexico. *Food Additives & Contaminants: Part A*, 26(5):733–743, 2009.

N. Masimango, J. Remacle, and J. L. Ramaut. Role of adsorption in elimination of aflatoxin-B1 from contaminated media. *European Journal of Applied Microbiology and Biotechnology*, 6(1):

101–105, 1978.

F. Massart and G. Saggese. Oestrogenic mycotoxin exposures and precocious pubertal development. *International Journal of Andrology*, 33(2):369–376, 2010.

F. Massart, V. Meucci, G. Saggese, and G. Soldani. High growth rate of girls with precocious puberty exposed to estrogenic mycotoxins. *Journal of Pediatrics*, 152(5):690–695, 2008.

J. J. Max and C. Chapados. Infrared spectroscopy of aqueous carboxylic acids: Comparison between different acids and their salts. *Journal of Physical Chemistry A*, 108(16):3324–3337, 2004.

K. S. McKenzie, A. B. Sarr, K. Mayura, R. H. Bailey, D. R. Miller, T. D. Rogers, W. P. Norred, K. A. Voss, R. D. Plattner, L. F. Kubena, and T. D. Phillips. Oxidative degradation and detoxification of mycotoxins using a novel source of ozone. *Food and Chemical Toxicology*, 35(8): 807–820, 1997.

K. S. McKenzie, L. F. Kubena, A. J. Denvir, T. D. Rogers, G. D. Hitchens, R. H. Bailey, R. B. Harvey, S. A. Buckley, and T. D. Phillips. Aflatoxicosis in turkey poults is prevented by treatment of naturally contaminated corn with ozone generated by electrolysis. *Poultry Science*, 77 (8):1094–1102, 1998.

S. Miertus, E. Scrocco, and J. Tomasi. Electrostatic interaction of a solute with a continuum. A direct utilization of ab initio molecular potentials for the prevision of solvent effects. *Chemical Physics*, 55(1):117–129, 1981.

S. Miyata. Physico-chemical properties of synthetic hydrotalcites in relation to composition. *Clays and Clay Minerals*, 28(1):50–56, 1980.

S. Miyata. Anion-exchange properties of hydrotalcite-like compounds. *Clays and Clay Minerals*, 31(4):305–311, 1983.

F. A. Momany and M. A. Dombrink-Kurtzman. Molecular dynamics simulations on the mycotoxin fumonisin B1. *Agricultural and food chemistry*, 49:1056–1061, 2001.

M. del P. Monge, A. P. Magnoli, M. V. Bergesio, N. Tancredi, C. E. Magnoli, and S. M. Chiacchiera. Activated carbons as potentially useful non-nutritive additives to prevent the effect of

fumonisin B-1 on sodium bentonite activity against chronic aflatoxicosis. *Food Additives and Contaminants Part A-Chemistry Analysis Control Exposure & Risk Assessment*, 33(6):1043–1052, 2016.

Z. Movasaghi, S. Rehman, and I. U. Rehman. Fourier transform infrared (FTIR) spectroscopy of biological tissues. *Applied Spectroscopy Reviews*, 43(2):134–179, 2008.

K. Neme and A. Mohammed. Mycotoxin occurrence in grains and the role of postharvest management as a mitigation strategies. A review. *Food Control*, 78:412–425, 2017.

E. R. Nightingale. Phenomenological theory of ion solvation - effective radii of hydrated ions. *Journal of Physical Chemistry*, 63(9):1381–1387, 1959.

L. M. Parker, N. B. Milestone, and R. H. Newman. The use of hydrotalcite as an anion absorbent. *Industrial & Engineering Chemistry Research*, 34(4):1196–1202, 1995.

S. S. Parlat, A. Ö. Yildiz, and H. Oguz. Effect of clinoptilolite on performance of Japanese quail (Coturnix coturnix Japonica) during experimental aflatoxicosis. *British poultry science*, 40: 495–500, 1999.

A. Pedretti, L. Villa, and G. Vistoli. VEGA - An open platform to develop chemo-bio-informatics applications, using plug-in architecture and script programming. *Journal of computer-aided molecular design*, 18:167–173, 2004.

P. B. Rai, S. S. Banerjee, and R. V. Jayaram. Removal of disperse dyes from aqueous solution using sawdust and BDTDA-Sawdust. *Journal of Dispersion Science and Technology*, 28(7): 1066–1071, 2007.

E. Razzazi-Fazeli, J. Böhm, K. E. Ahmed, B. Cecon, and B. Rabus. Investigation on the biodegradability of mycotoxins nivalenol (NIV) and deoxynivalenol (DON) in a rusitec fermentor and their monitoring by HPLC/MS. *Mycotoxin research*, 16:9–14, 2000.

S. W. Rhee, M. J. Kang, H. Kim, and C. H. Moon. Removal of aquatic chromate ion involving rehydration reaction of calcined layered double hydroxide (Mg-Al-CO3). *Environmental Technology*, 18(2):231–236, 1997.

J. L. Richard. Some major mycotoxins and their mycotoxicoses - An overview. *International*

*Journal of Food Microbiology*, 119(1-2):3–10, 2007.

M. R. Rosenthal. The myth of the non-coordinating anion. *Journal of Chemical Education*, 50(5): 331–335, 1973.

I. Y. S. Rustom. Aflatoxin in food and feed: occurrence, legislation and inactivation by physical methods. *Food Chemistry*, 59(1):57–67, 1997.

G. Schatzmayr, D. Schatzmayr, E. Fuchs, S. Nitsch, M. Mohnl, M. Täubel, A. Loibner, R. Braun, and E. M Binder. Investigation of different yeast strains for the detoxification of ochratoxin A. *Mycotoxin research*, 19:124–128, 2003.

G. Schatzmayr, F. Zehner, M. Taubel, D. Schatzmayr, A. Klimitsch, A. P. Loibner, and E. M. Binder. Microbiologicals for deactivating mycotoxins. *Molecular Nutrition & Food Research*, 50(6):543–551, 2006.

Y. Seida and Y. Nakano. Removal of phosphate by layered double hydroxides containing iron. *Water Research*, 36(5):1306–1312, 2002.

J. L. Sheldon. A corn mold (Fusarium moniliforme n. sp.). *17th Annual report - Nebraska Agricultural Experiment Station*, pages 23–32, 1904.

C. N. Shih and E. H. Marth. Aflatoxin can be degraded by the mycelium of Aspergillus parasiticus. *Zeitschrift für Lebensmittel-Untersuchung und Forschung*, 158(6):361–362, 1975.

Sigma-Aldrich. Safety datasheet: Deoxynivalenol. Technical report, 2016. URL `https://www.sigmaaldrich.com/catalog/product/sigma/d0156?lang=en{&}region=US`.

J. M. Soriano and S. Dragacci. Occurrence of fumonisins in foods. *Food Research International*, 37(10):985–1000, 2004.

M. Spotti, M. L. Fracchiolla, F. Arioli, F. Caloni, and G. Pompa. Aflatoxin B1 binding to sorbents in bovine ruminal fluid. *Veterinary Research Communications*, 29(6):507–515, 2005.

M. J. Sweeney and A. D. W. Dobson. Mycotoxin production by Aspergillus, Fusarium and Penicillium species. *International Journalo Food Microbiology*, 43(3):141–158, 1998.

E. W. Sydenham, L. van der Westhuizen, S. Stockenstrom, G. S. Shephard, and P. G. Thiel.

Fumonisin-contaminated maize: physical treatment for the partial decontamination of bulk shipments. *Food Additives and Contaminants*, 11(1):25–32, 1994.

E. W. Sydenham, S. Stockenstrom, P. G. Thiel, G. S. Shephard, K. R. Koch, and W. F. O. Marasas. Potential of alkaline-hydrolysis for the removal of fumonisins from contaminated corn. *Journal of Agricultural and Food Chemistry*, 43(5):1198–1201, 1995.

B. Tansel. Significance of thermodynamic and physical characteristics on permeation of ions during membrane separation: Hydrated radius, hydration free energy and viscous effects. *Separation and Purification Technology*, 86:119–126, 2012.

P. G. Thiel, W. F. O. Marasas, E. W. Sydenham, G. S. Shephard, and W. C. A. Gelderblom. The implications of naturally-occurring levels of fumonisins in corn for human and animal health. *Mycopathologia*, 117(1-2):3–9, 1992.

C. S. Tibola, J. M. C. Fernandes, and E. M. Guarienti. Effect of cleaning, sorting and milling processes in wheat mycotoxin content. *Food Control*, 60(Supplement C):174–179, 2016.

A. M. Torres, M. M. Reynoso, F. G. Rojo, and S. N. Chulze. Fusarium species (section Liseola) and its mycotoxins in maize harvested in northern Argentina. *Food additives and Contaminants*, 18(9):836–843, 2001.

N. W. Turner, S. Subrahmanyam, and S. A. Piletsky. Analytical methods for determination of mycotoxins: A review. *Analytica Chimica Acta*, 632(2):168–180, 2009.

I. Var, B. Kabak, and Z. Erginkaya. Reduction in ochratoxin A levels in white wine, following treatment with activated carbon and sodium bentonite. *Food Control*, 19(6):592–598, 2008.

E. Vekiru, C. Hametner, R. Mitterbauer, J. Rechthaler, G. Adam, G. Schatzmayr, R. Krska, and R. Schuhmacher. Cleavage of zearalenone by trichosporon mycotoxinivorans to a novel nonestrogenic metabolite. *Applied and Environmental Microbiology*, 76(7):2353–2359, 2010.

K. A. Voss, G. W. Smith, and W. M. Haschek. Fumonisins: Toxicokinetics, mechanism of action and toxicity. *Animal Feed Science and Technology*, 137(3-4):299–325, 2007.

R. D. Walker and D. G. White. Inheritance of resistance to aspergillus ear rot and aflatoxin production of corn from CI2. *Plant Disease*, 85(3):322–327, 2001.

J. S. Wang, H. Luo, M. Billam, Z. Wang, H. Guan, L. Tang, T. Goldston, E. Afriyie-Gyawu, C. Lovett, J. Griswold, B. Brattin, R. J. Taylor, H. J. Huebner, and T. D. Phillips. Short-term safety evaluation of processed calcium montmorillonite clay (NovaSil) in humans. *Food Additives and Contaminants*, 22(3):270–279, 2005.

P. Wang, E. Afriyie-Gyawu, Y. Tang, N. M. Johnson, L. Xu, L. Tang, H. J. Huebner, N. A. Ankrah, D. Ofori-Adjei, W. Ellis, P. E. Jolly, J. H. Williams, J. S. Wang, and T. D. Phillips. NovaSil clay intervention in Ghanaians at high risk for aflatoxicosis: II. Reduction in biomarkers of aflatoxin exposure in blood and urine. *Food Additives and Contaminants*, 25(5):622–634, 2008.

Q. Wang and D. O'Hare. Recent advances in the synthesis and application of layered double hydroxide (LDH) nanosheets. *Chemical Reviews*, 112(7):4124–4155, 2012.

S. L. Wang and P. C. Wang. In situ XRD and ATR-FTIR study on the molecular orientation of interlayer nitrate in Mg/Al-layered double hydroxides in water. *Colloids and Surfaces a-Physicochemical and Engineering Aspects*, 292(2-3):131–138, 2007.

S. L. Wang, R. J. Hseu, R. R. Chang, P. N. Chiang, J. H. Chen, and Y. M. Tzou. Adsorption and thermal desorption of Cr(VI) on Li/Al layered double hydroxide. *Colloids and Surfaces A-Physicochemical and Engineering Aspects*, 277(1-3):8–14, 2006.

C. P. Wild and Y. Y. Gong. Mycotoxins and human disease: A largely ignored global health issue. *Carcinogenesis*, 31(1):71–82, 2010.

J. G. Wilkes, J. B. Sutherland, M. I. Churchwell, and A. J. Williams. Determination of fumonisins B1, B2, B3 and B4 by high-performance liquid chromatography with evaporative light-scattering detection. *Journal of chromatography. A*, 695:319–323, 1995.

K. C. Williams, B. J. Blaney, and R. T. Peters. Pigs fed fusarium-infected maize containing zearalenone and nivalenol with sweeteners and bentonite. *Livestock Production Science*, 39(3): 275–281, 1994.

H. Xiao, S. Madhyastha, R. R. Marquardt, S. Z. Li, J. K. Vodela, A. A. Frohlich, and B. W. Kemppainen. Toxicity of ochratoxin A, its opened lactone form and several of its analogs: Structure-activity relationships. *Toxicology and Applied Pharmacology*, 137(2):182–192, 1996.

Z. P. Xu and H. C. Zeng. Abrupt structural transformation in hydrotalcite-like compounds Mg1-xAlx(OH)2(NO3)x·nH2O as a continuous function of nitrate anions. *Journal of Physical Chemistry B*, 105(9):1743–1749, 2001.

L. Yang, Z. Shahrivari, P. K. T. Liu, M. Sahimi, and T. T. Tsotsis. Removal of trace levels of arsenic and selenium from aqueous solutions by calcined and uncalcined layered double hydroxides (LDH). *Industrial & Engineering Chemistry Research*, 44(17):6804–6815, 2005.

A. Yiannikouris, H. Kettunen, J. Apajalahti, E. Pennala, and C. A. Moran. Comparison of the sequestering properties of yeast cell wall extract and hydrated sodium calcium aluminosilicate in three in vitro models accounting for the animal physiological bioavailability of zearalenone. *Food Additives and Contaminants Part A-Chemistry Analysis Control Exposure & Risk Assessment*, 30(9):1641–1650, 2013.

T. Yoshizawa, A. Yamashita, and Y. Luo. Fumonisin occurrence in corn from high-risk and low-risk areas for human esophageal cancer in China. *Applied and Environmental Microbiology*, 60 (5):1626–1629, 1994.

Y. W. You, G. F. Vance, and H. T. Zhao. Selenium adsorption on Mg-Al and Zn-Al layered double hydroxides. *Applied Clay Science*, 20(1-2):13–25, 2001.

F. Zermane, M. W. Naceur, B. Cheknane, and N. A. Messaoudene. Adsorption of humic acids by a modified Algerian montmorillonite in synthesized seawater. *Desalination*, 179(1-3):375–380, 2005.

F. Zigan and R. Rothbauer. Neutronenbeugungsmessungen am brucit. *Neues Jahrbuch fuer Mineralogie, Monatshefte*, 4:137–143, 1967.

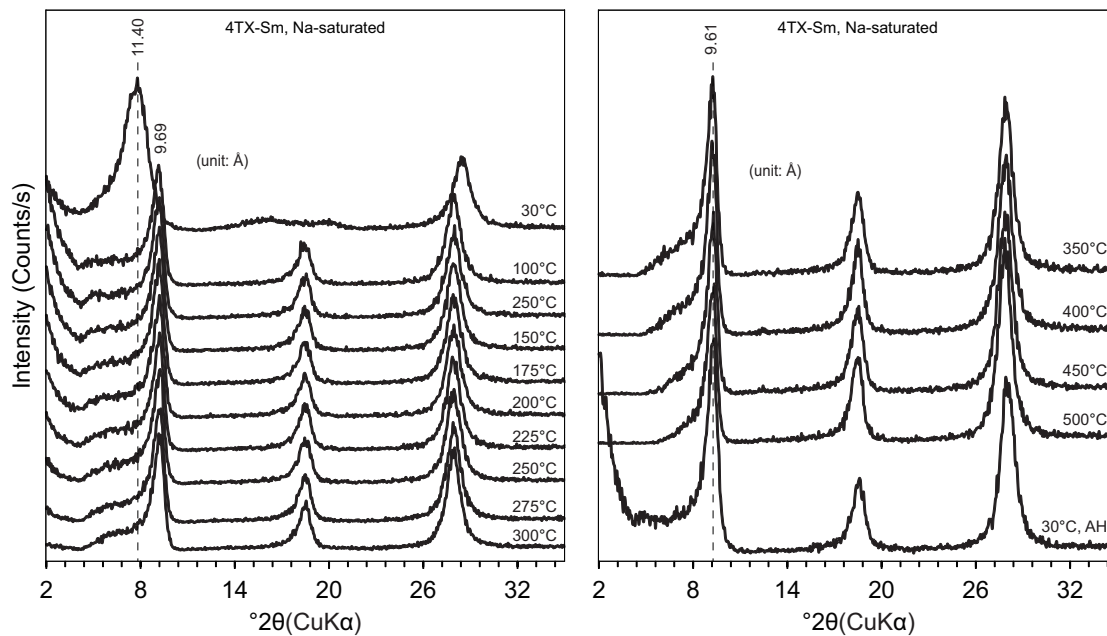XRD PATTERNS OF SMECTITE 4TX BEFORE AND AFTER ADSORBED FUMONISIN B$_1$

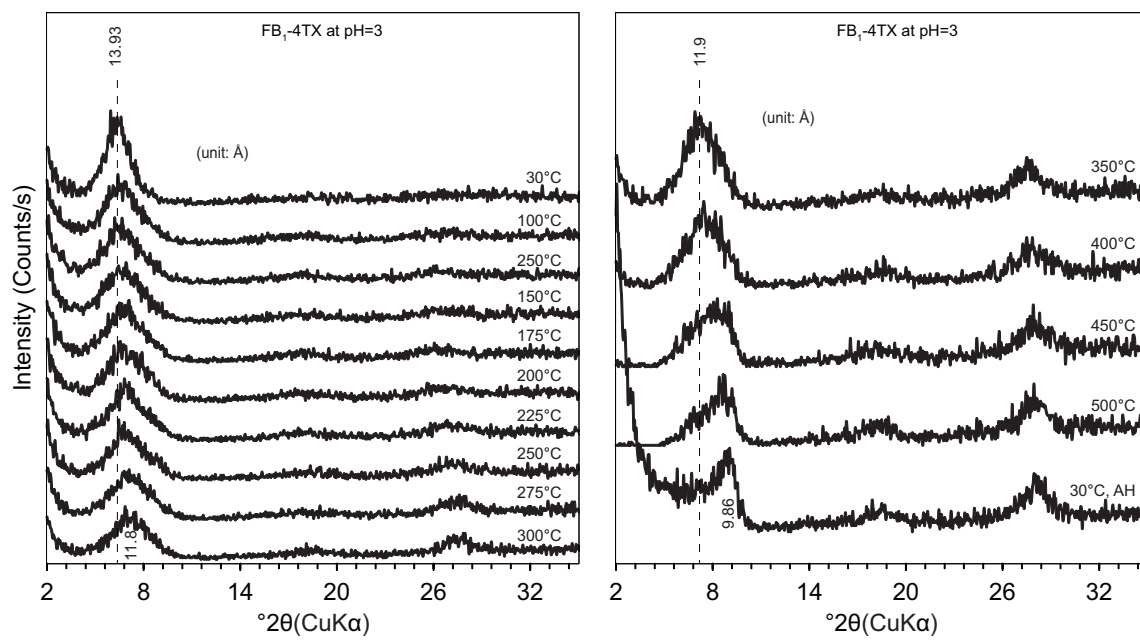Figure A.1. XRD patterns of smectite Na-4TX at different temperatures.

Figure A.2. XRD patterns of smectite Na-4TX after adsorbed FB$_1$ at pH 3 treated with different temperatures.